Dissertation

Investigating the Stress-Resistance of the Cancer Cell Secretory Pathway

submitted by

Thomas RAUTER, BSc MSc MSc

for the Academic Degree of

Doctor of Philosophy (PhD)

at the

Medical University of Graz

Gottfried Schatz Research Center

Molecular Biology and Biochemistry

under the Supervision of

Assoz. Prof. Priv.-Doz. Mag. pharm. Dr. rer. nat. Roland Malli

2021

Declaration

I hereby declare that this thesis is my own original work and that I have fully acknowledged by name all of those individuals and organisations that have contributed to the research for this thesis. Due acknowledgement has been made in the text to all other material used. Throughout this thesis and in all related publications I followed the “Standards of Good Scientific Practice and Ombuds Committee at the Medical University of Graz“.

Graz, February 27th, 2021 *Thomas Rauter*

Disclosures

Part of this thesis has been published in:

Rauter, T.; Burgstaller, S.; Gottschalk, B.; Ramadani-Muja, J.; Bischof, H.; Hay, J.C.; Graier, W.F.; Malli, R. ER-to-Golgi Transport in HeLa Cells Displays High Resilience to Ca^{2+} and Energy Stresses. *Cells* **2020**, *9*, 2311. https://doi.org/10.3390/cells9102311 (1)

Co-authors who contributed to the publication:

- **Sandra Burgstaller**
  Interfaculty Institute of Cell Biology, University of Tuebingen
  Auf der Morgenstelle 15, 72076 Tuebingen, GERMANY

- **Benjamin Gottschalk**
  Molecular Biology and Biochemistry, Gottfried Schatz Research Center, Medical University of Graz
  Neue Stiftingtalstraße 6/6, 8010 Graz, AUSTRIA

- **Jeta Ramadani-Muja**
  Molecular Biology and Biochemistry, Gottfried Schatz Research Center, Medical University of Graz
  Neue Stiftingtalstraße 6/6, 8010 Graz, AUSTRIA

- **Helmut Bischof**
  Department of Pharmacology, Toxicology and Clinical Pharmacy, Institute of Pharmacy, University of Tuebingen
  Auf der Morgenstelle 8, 72076 Tuebingen, GERMANY

- **Jesse C. Hay**
  Division of Biological Sciences and Center for Structural and Functional Neuroscience, The University of Montana
  32 Campus Drive, HS 302A, Missoula, MT 59812-4824, USA

- **Wolfgang F. Graier**
  Molecular Biology and Biochemistry, Gottfried Schatz Research Center, Medical University of Graz
  Neue Stiftingtalstraße 6/6, 8010 Graz, AUSTRIA

- **Roland Malli**
  Molecular Biology and Biochemistry, Gottfried Schatz Research Center, Medical University of Graz
  Neue Stiftingtalstraße 6/6, 8010 Graz, AUSTRIA

I confirm that all co-authors have agreed to use their data in my thesis. I have obtained permission from *Cells* to reproduce figures published in Rauter et al. 2020 (1).

Cells is an international peer-reviewed open access journal and published monthly online by MDPI, which allows the reuse of published data in a PhD thesis at any time after publication.

Please visit the following websites for rights and permission statements:

https://creativecommons.org/licenses/by/4.0/
https://creativecommons.org/licenses/by/4.0/legalcode

During my PhD studies I also contributed to the following publications:

- Bacsa, B; Graziani, A; Krivic, D; Wiedner, P; Malli, R; Rauter, T; Tiapko, O; Groschner, K. Pharmaco-Optogenetic Targeting of TRPC Activity Allows for Precise Control Over Mast Cell NFAT Signaling. Frontiers in Immunology. 2020.

- Bischof, H; Burgstaller, S; Waldeck-Weiermair, M; Rauter, T; Schinagl, M; Ramadani-Muja, J; Graier, WF; Malli, R; Live-Cell Imaging of Physiologically Relevant Metal Ions Using Genetically Encoded FRET-Based Probes. Cells. 2019.

- Depaoli, MR; Bischof, H; Eroglu, E; Burgstaller, S; Ramadani-Muja, J; Rauter, T; Schinagl, M; Waldeck-Weiermair, M; Hay, JC; Graier, WF; Malli, R; Live cell imaging of signaling and metabolic activities. Pharmacology and Therapeutics. 2019.

- Hurný, A; Cuesta, C; Cavallari, N; Ötvös, K; Duclercq, J; Dokládal, L; Montesinos, JC; Gallemí, M; Semerádová, H; Rauter, T; Stenzel, I; Persiau, G; Benade, F; Bhalearo, R; Sýkorová, E; Gorzsás, A; Sechet, J; Mouille, G; Heilmann, I; De Jaeger, G; Ludwig-Müller, J; Benková, E; SYNERGISTIC ON AUXIN AND CYTOKININ 1 positively regulates growth and attenuates soil pathogen resistance. Nature Communications. 2020.

- Ramadani-Muja, J; Gottschalk, B; Pfeil, K; Burgstaller, S; Rauter, T; Bischof, H; Waldeck-Weiermair, M; Bugger, H; Graier, WF; Malli, R; Visualization of Sirtuin 4 Distribution between Mitochondria and the Nucleus, Based on Bimolecular Fluorescence Self-Complementation. Cells. 2019.

- Rauter, T; Depaoli, MR; Bischof, H; Graier, WF; Malli, R; Metabolic Profiling of Single Cancer Cells Using Mitochondrial ATP Probes. STAR Protocols. 2020.

Dedication

To all the young, curious minds that will shape the future of science. Collective efforts will ensure the wellbeing of humanity in an increasingly competitive scientific world.

“Jeder Versuch eines Einzelnen, für sich zu lösen, was alle angeht, muß scheitern.”

aus *Die Physiker* von Friedrich Dürrenmatt, 1962.

Acknowledgements

As a PhD student I received funding from the Medical University of Graz through the PhD program Molecular Medicine (MOLMED) and from the Austrian Science Fund (FWF, P28529 and I3716 to Roland Malli).

Completing a PhD mainly requires three things: intrinsic curiosity for the miracles of nature, hard work coupled with a certain element of sacrifice and the immense support of your professional and personal environment. While the first two things have been up to me, the whole experience would never have been possible without a healthy support system. And besides the Medical University of Graz and the Austrian Science Fund, which made my research work possible through their financial support, I would also like to thank a few people who significantly contributed to the completion of this thesis.

First, I would like to thank my supervisor Roland Malli, who has been a tremendous supporter of my work as a scientist and has always provided me with an open ear for my struggles and a helping hand to steer me into the right direction. I also would like to thank the other members of my thesis committee, Wolfgang F. Graier, head of this fine institute where you find a huge number of amazing scientists I had the chance to meet during my years at the MedUni, and Jesse C. Hay, who always brought a different perspective into the project strengthening the foundation of my research.

This journey would not have been possible without the support of my dear colleagues that became close friends of mine over the years: A big thanks to Sandra Burgstaller, Helmut Bischof, Jeta Muja, Benjamin Gottschalk, Maria R. Depaoli, René Rost, Sandra Blass and Anna Schreilechner as well as all the other smart people I had the opportunity to meet and work with in the Graier/Malli lab and the MedUni Graz in general. A big thanks also to all the great co-authors of the publications I was lucky to work on – I am very proud to find my name next to such outstanding researchers!

Last, but certainly not least, I want to thank my whole family: My parents, Waltraud and Andreas Rauter, my brother, Mattias Rauter, and my amazing girlfriend Christiane Gruber, who have all made this possible by providing me with their infinite support and love, for which I will always be grateful!

Table of Contents

Abbreviations

Important abbreviations that are used more than once in the text are defined here:

2-DG 2-deoxy-D-glucose
ACLSM..... Array confocal laser scanning microscope
AMPK..... 5’ adenosine monophosphate-activated protein kinase
ATP ..... Adenosine-5’-triphosphate
BiFC ..... Bimolecular fluorescence complementation
Ca^{2+} ..... Calcium ion
CAD ..... Conditional aggregation domain
ER..... Endoplasmic reticulum
ERAD ..... ER-associated protein degradation
FF ..... Form factor
FP ..... Fluorescent protein
FFT ..... Fast fourier transform
FRET..... Förster resonance energy transfer
GH, hGH ..... (human) growth hormone
GPI..... Glycosylphosphatidylinositol
GTP..... Guanosine-5’-triphosphate
IP_3 ..... Inositol 1,4,5-triphosphate
MMP..... Matrix metalloproteinases
MT..... Microtubules
Noc..... Nocodazole
ROS ..... Reactive oxygen species
SERCA..... (sarco)endoplasmic reticulum Ca^{2+} ATPase
SNARE..... SNAP receptor
TI..... Transport index
TM..... transmembrane
TRAPT ..... Transport reporter for analysis of protein trafficking
VEGF ..... Vascular endothelial growth factor
VSVG ..... Vesicular stomatitis virus G protein

Abstract

Secretory proteins are a large and important part of the human proteome. They are either membrane-associated or soluble proteins and most of them first target the endoplasmic reticulum (ER) to enter the classical secretory pathway. Cargo proteins start their journey through this pathway from the ER to the Golgi via vesicular structures, representing the initial step in this process. Modern, high-resolution imaging techniques in combination with innovative genetically encoded, fluorescent protein (FP)-based tools allow the synchronization and real-time visualization of such trafficking events. It has been shown that many tumor cells rely heavily on protein secretion to maintain cancer-specific hallmarks like high growth and proliferation rates and also enable metastasis. Despite this knowledge about the role of the secretory pathway in cancer cells, not a lot is known about its general energy supply and specifically its resistance to stress. In this thesis, we applied state-of-the-art techniques to allow a closer look into the complex interrelation between metabolic activity and early secretory trafficking events in cancer cells as well as test the sensitivity of ER-to-Golgi transport to energy and Ca^{2+} stresses. The experiments revealed a yet unseen stability of secretory transport under significant energy stress by nutrient starvation, mimicking a situation tumor cells might encounter during their life. Surprisingly, the cancer cell model also displayed high efficiency in ER-to-Golgi trafficking upon short-term Ca^{2+} stress induction. However, treatment with the antimetabolite 2-deoxy-D-glucose (2-DG) effectively and almost completely abolished secretory transport of luminal and transmembrane cargo constructs, underlining the importance of the glycolysis-based energy supply to maintain effective protein trafficking in cells exhibiting the Warburg effect. We further demonstrated the impact of 2-DG on the cellular Ca^{2+} homeostasis and the motility of vesicular structures within cells. Furthermore, the structural integrity of ER and the microtubule network, as a crucial mediator of directed, long-distance intracellular transport, were investigated under severe energy stress. In an attempt to complement high-resolution fluorescence imaging methods, a novel genetically-encoded sensor based on new FP-technologies was introduced opening up new possibilities. By applying innovative methodical approaches we demonstrated a high stress-resistance of the secretory pathway in the cancer cell model. These new insights into ER-to-Golgi transport efficiency under energy and Ca^{2+} stress also emphasize the importance of the secretory pathway as a potential target in future cancer therapy.

Zusammenfassung

Sekretorische Proteine bilden einen großen und wichtigen Teil des humanen Proteoms. Bei diesen handelt es sich entweder um membran-assoziierte oder lösliche Proteine, deren erstes Ziel das Endoplasmatische Retikulum (ER) darstellt, als Eingang in den klassischen Sekretorischen Weg. Cargo Proteine beginnen ihre Reise durch diesen Weg vom ER zum Golgi über vesikuläre Strukturen, der erste Schritt in diesem Prozess. Moderne, hochauflösende Imaging-Methoden in Kombination mit innovativen genetisch-codierten, fluorescent protein (FP)-basierten Tools erlauben die Synchronisation und Visualisierung solcher Transportprozesse in Echtzeit. Viele Tumor-Zellen sind stark von der Proteinsekretion abhängig, um krebs-spezifische Eigenschaften wie hohe Wachstums- und Proliferationsraten sowie Metastasierung zu ermöglichen. Trotz dieses Wissens über die Rolle des Sekretorischen Weges in Krebszellen ist wenig über dessen Energieversorgung und Stress-Resistenz bekannt. In dieser Doktorarbeit wurden state-of-the-art Techniken verwendet, um einen genaueren Blick auf die komplexen Beziehungen zwischen metabolischer Aktivität und frühen sekretorischen Prozessen in Krebszellen zu ermöglichen sowie die Sensitivität von ER-Golgi Transport gegenüber Ca^{2+}- und Energiestress zu testen. Die Experimente zeigten eine bisher ungeahnte Stabilität des sekretorischen Transports unter signifikantem Energiestress durch Nährstoff-Entzug, einem Zustand, den Krebszellen im täglichen Leben begegnen können. Überraschenderweise zeigte das Krebszell-Modell auch unter kurzzeitigem Ca^{2+}-Stress hohe Effizienz des ER-Golgi Transports. Behandlung mit dem Antimetaboliten 2-Deoxy-D-Glukose (2-DG) hingegen verhinderte den sekretorischen Transport von luminalem und Transmembran-Cargo nahezu komplett, was die Wichtigkeit von Glycolyse-basierter Energieversorgung für die Aufrechterhaltung effizienten Proteintransports in Zellen mit Warburg-Effekt hervorhebt. Außerdem konnte der Einfluss von 2-DG auf die zelluläre Ca^{2+}-Homöostase sowie die Beweglichkeit vesikulärer Strukturen im Zellinneren demonstriert werden. Die strukturelle Integrität von ER und Mikrotubuli-Netzwerk, einem wesentlichen Mediator von gerichtetem intrazellulärem Transport, wurde ebenso unter hohem Energie-Stress untersucht. Um hochauflösende Fluoreszenzmikroskopie-Verfahren zu komplementieren, wurde ein neuartiger, genetisch-codierter Sensor auf Basis neuer FP-Technologien designt, der neue Möglichkeiten eröffnet. Durch den Einsatz innovativer methodischer Ansätze konnte eine hohe Stress-Resistenz des Sekretorischen Weges im Krebszell-Modell gezeigt werden. Diese neuen Erkenntnisse zur

Effizienz des ER-Golgi Transports unter Energie- und Ca^{2+}-Stress unterstreichen die Bedeutung des Sekretorischen Weges als mögliches Target in der Krebstherapie der Zukunft.

1 Introduction

It has been known for a long time that the classical secretory pathway represents a central element in cellular life enabling interactions with surrounding cells and the environment as well as long-distance communications (2,3). This holds true for single-cell organisms and also individual cells in multicellular organisms. Essential cell-to-cell communications by sending and receiving chemical signals and modifications of the extracellular space largely depend on functioning protein secretion. This includes transport of proteins, also referred to as “cargo” in that context, to the plasma membrane or in soluble form to the extracellular fluid.

Countless studies are addressing mechanistic aspects of protein secretion. Especially its crucial first step, the transport of cargo from the endoplasmic reticulum (ER) to the Golgi apparatus, has been well investigated (see 1.1.1). However, fundamental questions remain to be answered. A number of them have to do with how much energy is needed to maintain proper protein secretion and, in direct connection to that, how does exerting stress (energy stress in particular) on a cell impact its capacity to uphold a working secretory pathway. This aspect becomes even more important if we think about the role of this pathway in the development of certain diseases including cancer (3–5).

For these reasons, this study focuses on the impact of stress on the cancer cell secretory pathway, in particular its initial step, the ER-to-Golgi transport, and elaborates on methodical aspects instrumental to the research on this topic while providing novel approaches to shape its future.

1.1 The secretory pathway

The secretory pathway is based on complex interrelated and tightly regulated sorting and trafficking processes (3,6). A huge portion of proteins produced by a cell enters the ER as a cargo, i.e. a protein that is destined to run through anterograde trafficking, or as a regulatory component of this pathway, emphasizing the importance of protein secretion on the cellular level. Estimations reach up to one-third of the human proteome that enters the ER (4,7–10), resulting in the secretion of several thousand individual molecules every second (11). These

numbers underline the importance of this pathway in the context of cellular life and energy expenditure in protein production, folding, sorting and trafficking. Moreover, it is known that cells not only exhaust the capacities that they possess but even take steps to extend them in extreme situations. Certain cell types can expand organelles of the secretory pathway, like the ER and Golgi, as well as multiply the number of spots where transport vesicles emerge (12).

1.1.1 The classical secretory pathway – an overview

What is commonly understood to build up the protein secretion pathway, is more precisely defined as the “classical secretory pathway”. Over the last few decades, researchers have uncovered a great amount of detailed information about how the secretory transport of proteins works and have identified key players involved in this system (3). All of these findings add up to a rather simplified model of a very complex process: proteins enter the ER co-translationally and then move to the Golgi apparatus and from there to the plasma membrane or extracellular space – all based on vesicles, respectively vesicular tubular clusters, representing the transport carriers that mediate this journey (3,13–21).

The ER represents the initial organelle of the secretory pathway and an essential gatekeeper in these processes. It overtakes multiple functions in eukaryotic cells, only a part of which is connected to secretory trafficking (22). The ER is organized into distinct areas like e.g. mitochondria-associated membranes (MAM), plasma-membrane-associated membranes (PAM) or, especially interesting for protein secretion, regions of vesicle building for secretory transport, the so-called ER exit sites or ERES (15,22). Proteins of the secretory pathway, either of regulatory nature or actual cargo proteins for secretion, are formed at the rough ER (3), the part of the ER constantly covered with ribosomes (23).

The general mechanisms have been studied for a long time (24) - the recognition of signal peptides and recruitment of the ribosome machinery to the Sec61 pore, where the peptide chain is channeled through the ER membrane into the lumen, is well investigated (25). In the ER lumen all required folding processes supported by a large number of chaperone proteins take place (10). Moreover, this is the place, where the vast majority of posttranslational modifications are conducted (26). It is well known today that there are signal sequences that lead to an immediate retrograde transport of a protein required to reside in the ER (27), in

case it gets transported to the Golgi apparatus, which happens frequently based on the principle of bulk-flow transport (28).

There are certain principles describing which proteins are transported from the ER to the Golgi and which ones are not. There are five general mechanisms that describe how proteins are handled: cargo capture, bulk flow, retention, retrieval and ER-associated degradation (ERAD; (29)). ERAD is first and foremost a mechanism to eliminate proteins that fail to fold properly or reside in an unassembled state in the ER (30). The so-called unfolded protein response (UPR), which is activated upon an accumulation of unfolded proteins in the ER lumen, together with ERAD represents key quality control mechanisms in the ER (31,32). Protein retention and retrieval enable the cell to keep key proteins for dynamic folding and unfolding reactions or other ER-associated tasks in place or retrieve them (29,33). The retrieval of such proteins via retrograde transport has been studied in great detail to understand how the cell can maintain an ER environment enriched in chaperones and enzymes mediating folding processes (33). The most interesting mechanisms for this study, however, are bulk flow and cargo capture as well as their underlying principles, since the experiments described in this thesis focus on anterograde transport to the Golgi apparatus and beyond.

As demonstrated by applying a soluble viral capsid protein as a tracer molecule in eukaryotic cells, bulk flow, i.e. the anterograde transport of luminal proteins in the ER without active recruitment into transport vesicles, can also occur at very high rates and can represent a significant factor in protein secretion (34). It has been shown that this type of transport from ER to Golgi occurs quite fast in mammalian cells with cargo reaching the medial Golgi cisternae within roughly 15 minutes (35–37) and can even be significantly faster in yeast (38). However, not much is known about the bulk flow transport of transmembrane cargo.

Active sorting or cargo capture, in contrast to bulk flow, is relying on the recognition of certain amino acid motifs by according receptors, allowing the active recruitment of the respective cargo into transport vesicles (29,39). These motifs are found on the cytosolic side of transmembrane cargo proteins, where they get recognized by components of the vesicle coat complex (39–41). Soluble cargos on the other hand require additional membrane receptors, which recognize and recruit these proteins to the transport carriers after getting into direct contact with them. Because of the diversity of cargo and the consequent need for adaptation, there are at least 24 adaptors/receptors known to mediate cargo capture in

mammalian cells (29). Interestingly, the bulk flow principle ensures that even upon depletion of signals for active sorting, secretory transport might be slowed down but can be maintained by the cell as has been demonstrated in yeast (42).

1.1.2 ER-to-Golgi transport – a closer look at the initial step of secretory trafficking

Regulators of the secretory pathway and especially its crucial first step, the ER-to-Golgi trafficking, have been studied in great detail over the last decades (6). While there are significant differences between various species regarding the role of cytoskeleton elements in anterograde transport (19), the main steps in ER-to-Golgi transport are largely conserved (43). Typically, cargo proteins are recruited to distinct positions of the ER, the ER exit sites or ERES, where vesicular transport carriers are built and released (13–15), although it is known that not all cargos accumulate in these sites (44).

The vesicular carriers mediating the initial step in anterograde secretory transport are called coat protein complex II (COPII) vesicles and are built through a well-investigated multistep mechanism (13–15). The assembly factors Sec12 and Sec16 are found in increased numbers in ERES due to their functions in initiation and organization of these sites (14,29). Sec12 is instrumental for COPII-formation since it initiates binding of the small GTPase Sar1 to the ER membrane by mediating GDP to GTP exchange (13,14). After that, a so-called pre-budding complex consisting of Sar1-GTP as well as Sec23 and Sec24 is built (13). The Sec24 subunit of the Sec23-Sec24 complex is known to mediate cargo capture of various transmembrane cargos and adaptors by engaging and subsequent direct binding of export signals (13,14,40,41). The second large complex, Sec13-Sec31 (organized in heterotetramers), then binds pre-budding complexes and polymerizes (13–15). This leads to a gradually increased membrane curvature and finally release of a vesicle encompassed by a fully assembled COPII-coat by fission from the ER membrane (13,14). The disassembly of the COPII is later initiated by Sar1 GTP hydrolysis mediated by the GAP (GTPase-activating protein) function of Sec23 (13,45). Homotypic fusion events lead to the formation of larger vesicular tubular clusters (VTCs; (46,47)), which present the primary site for a concentration of protein cargo (44) and become part of an enigmatic intermediate structure with dynamic characteristics, the ER-Golgi intermediate compartment (ERGIC; (16–18,21)).

Recent studies suggest that COPII coat disassembly is conducted in connection to fusion to the ERGIC (48). Vesicle tethering and fusion represent highly complex processes involving numerous enzymes and supporting structural proteins (as reviewed in (39)). Tethering, i.e. the process of getting into contact with a target membrane for initiation of vesicle fusion, is often mediated by tethers of the TRAPP protein complex family in eukaryotic cells (49,50) or p115 (50,51). The most important regulatory enzymes in the process are members of the Rab family GTPases (39). Moreover, so-called N-ethylmaleimide-sensitive factor attachment protein receptors (SNARE) proteins are central mediators of membrane fusion (52). SNAREs on vesicle and target membrane (v-SNAREs and t-SNAREs) not only physically bring together the membranes but also ensure specificity (39,53). The major ER-Golgi SNARE complex consisting of syntaxin 5, membrin, Sec22 and Bet1 is assumed to mediate fusion at ERGIC and cis-Golgi (16,52). Together, SNARE complexes, Rab GTPases and tethers ensure the correct membrane fusion of transport carriers with the target membrane (39).

It has long been known that ER-to-Golgi transport does not only happen through vesicle diffusion but is also mediated by directed transport of these vesicles along cytoskeleton-elements. ER-to-Golgi transport has been shown to rely on the microtubule network in this regard (17–19,21). After the cargo reaches the Golgi stack further glycosylation and posttranslational modifications are conducted, which are known to play important roles in human health and disease (54). As mentioned before, proteins that need to be retrieved to the ER carry distinct signal peptides, most commonly the KDEL motif which is recognized by Erd2 in the Golgi, and such proteins are sent back on their way to the ER (27). This retrograde transport relies on COPI-vesicles – the counterpart of the COPII-vesicles mainly mediating anterograde movement – which are similarly built in a multistep process. Besides the main task of ensuring retrograde trafficking, other functions of the COPI-system are discussed frequently (28).

1.1.3 Alternative ways of secretory transport

This thesis is concentrating on the main secretory trafficking mechanism that a typical somatic cell exhibits – the classical secretory pathway as described in 1.1.1. However, in parallel to the well-known and most common protein secretion pathway of entering the ER as the first modification hub and then being transported to the Golgi via vesicular structures before reaching the cell plasma membrane or extracellular space (3), there are alternative

ways of secretory transport in existence. For the sake of completeness, also these pathways are described briefly in the following paragraphs.

While in plants unconventional protein secretion can amount to half of the secretome, the classical protein secretion is the prevalent pathway in other eukaryotic systems (55,56). Still, also in humans a significant number of proteins can be secreted via non-classical pathways independent from the ER and Golgi (56,57). These proteins involve major factors of intercellular communication in multicellular organisms including a variety of cytokines like interleukin 1 alpha and beta (IL1α and β; (58,59)) or fibroblast growth factor 1 and 2 (FGF1 and FGF2; (57,60)). Moreover, this heterogeneous group of non-classically secreted proteins involve annexins, heat shock proteins (HSP) and certain enzymes like sphingosine kinase 1 (61–63). Interestingly, unconventional secretion has also been suggested to contribute to cancer cell secretomes (64).

In general, four mechanisms of non-classical protein secretion can be distinguished: Membrane blebbing, the endolysosomal pathway, the exosome-mediated secretion, and translocation through the plasma membrane. Most of these proteins are released rather spontaneously from the secreting cells (reviewed in (56)). Despite all knowledge that we already gathered about unconventional protein secretion and the underlying mechanisms, its role often remains cryptic.

1.2 The importance of protein secretion in cancer

As elaborated, eukaryotic cells invest a large number of their resources (10) to maintain a functioning secretory pathway to be able to properly communicate with and adapt to their environment. Therefore, it does not come as a surprise that defects in this vital system of membrane and protein trafficking, often via mitochondrial dysfunction, can lead to severe disease (3,5,10,65–68). The vital role of protein secretion in cancer, for example, is undisputed. In a recent review cancer cells have even been termed “addicted to secrete” (4) – with good reason. It has not only been proven that protein secretion is a decisive factor in cancer cell malignancy (4,69–74), but in many cases, the exact protein factors responsible for this are characterized. These players are often shuttled through the secretory pathway and are responsible for numerous cancer-cell specific hallmarks like high growth and

proliferation rates or protect them from deregulation of cellular energetics, the immune system or imminent nutrient shortage by initiating angiogenesis (4,70,72,74).

1.2.1 Examples of specific secretory protein targets in cancer therapy

To name a well-known example for proteins maintaining cancer progression and metastasis, a very interesting protein family, matrix metalloproteinases or MMPs, are thought to play key roles in these processes (75). In particular, MMP-9, which is known to be overexpressed in colorectal cancer (76) and the zinc-dependent MMP-2 (77) have caught the attention of researchers as potential targets in cancer therapy. Although not undisputed in the scientific community due to their complex functions (78), studies searching for components targeting MMPs are ongoing (79,80). Formerly notoriously vilified primarily as enzymes degrading the extracellular matrix, the role of MMPs might be more nuanced after all (78,81). Another famous example for an essential factor that might represent a suitable target is vascular endothelial growth factor (VEGF), which promotes angiogenesis and thereby ensures upregulated bioenergetic activity in cancer cells (70,82).

Furthermore, we know that prooncogenic processes are supported by many more proteins passing through the secretory pathway like growth factors or certain receptor tyrosine kinases that rely on proper glycosylation (83). Based on the knowledge that these specific proteins can be found among the secretion output of a cancer cell, modern approaches frequently apply secretomics applications, meaning the analysis of all secreted proteins of a sample e.g. a cell population by using methods like proteomic analyses and mass spectrometry to learn more about this aspect (72). These factors render the secretory pathway a promising target in future approaches for fighting malignant tumors (4,70).

1.2.2 The energy supply of the secretory pathway as a potential target in cancer therapy?

However, while discussing single secreted proteins as potential therapeutic targets we still do not fully understand the general functional aspects of the secretory machinery itself. One of them, in particular, is of large interest to us: the general energy demand and especially the potential sensitivity to energy stress in cancer cells. It has indeed been shown that a large

number of steps in protein secretion beginning from protein quality control and folding over vesicle formation and fusion to vesicle transport itself require energy in the form of ATP or GTP (10).

Before the actual transport of cargo proteins via vesicular structures can occur, proper folding must be guaranteed in the ER, otherwise quality control mechanisms step in to degrade unfolded proteins (31,32). The ER energy supply has largely been a mystery (84), however, the discovery of ATP/ADP exchanger AXER has shed some light on it recently (85). A lot of energy-requiring steps are found in ER-to-Golgi transport, including COPII coat formation, microtubule-associated transport of vesicles and their tethering and fusion to target membranes (10). Some older publications have already illustrated the general dependency of secretory transport on ATP by demonstrating a strong decrease in the secretion of certain cargo proteins (86–89).

Direct correlations between secretory transport and metabolic activity have been discussed regularly in recent years (90,91), but not a lot of experiments have been conducted on this fascinating topic. To this day, the energy demand and energy stress resistance of the secretory pathway remains enigmatic despite representing a potentially promising target in cancer therapy.

1.3 Cancer cell metabolism and energy stress

To understand how the cancer cell metabolism and potentially the secretory pathway of a cancer cell can be influenced by certain energy stresses, it is crucial to comprehend their typical metabolic phenotype. Commonly, many cancer cells exhibit a characteristic metabolic setting, which has been known for a long time as the so-called Warburg effect (92). This phenotype is the result of massive metabolic rewiring by the cell to maintain high proliferation and growth rates and ensure long-time survival (93). The main feature of this effect lies in strongly increased glucose uptake and glycolysis with subsequent production of lactate while relying less on oxidative phosphorylation despite potentially intact mitochondrial bioenergetics and abundance of oxygen – also commonly known as aerobic glycolysis (92–94).

Over the past decades, the cancer cell metabolism has been studied extensively. Novel approaches allowing the investigation of the metabolic setting of single living cells have further strengthened our understanding of this particular metabolic phenotype (84,95). With these methods, it has been demonstrated that HeLa cells, a well-investigated model cell line for malignant solid tumors, likely produce most of their ATP via glycolytic processes and display a strong dependency on glucose supply (84). Interestingly, HeLa cells have also been applied in the past to investigate the modulation of secreted MMPs that play a huge role in tumor invasion, as explained before (96).

Based on the profound knowledge that we have about how tumor cells produce ATP, glycolysis and glucose supply present themselves as the ideal targets to apply energy stress and investigate its impact on protein secretion. As a result of their immense growth and proliferation rates, tumor cells can indeed run into natural glucose and nutrient shortage by default. The rapidly proliferating cells naturally aim to counteract this by inducing angiogenesis (97), which brings us back to the secretory pathway.

1.4 Other crucial cellular parameters influencing ER-to-Golgi transport

As described, secretory trafficking is a tightly controlled process relying on sufficient energy supply at several stages (10). However, in addition to the demand for ATP and GTP, the trafficking machinery also requires certain other structural and chemical preconditions to function properly.

1.4.1 Interrelations of Ca^{2+} dynamics and trafficking processes

One of the most influential factors in protein trafficking is assumed to be subcellular Ca^{2+} content and dynamics. Though it has been known for a longer time that cytosolic Ca^{2+} mediates fusion of vesicles e.g. carrying neurotransmitters to the plasma membrane, the role of Ca^{2+} as a regulator of intracellular membrane fusion has only recently been suggested (98,99). Data collected from experiments selectively chelating Ca^{2+} in intracellular pools suggests a complex role of Ca^{2+} as a regulatory agent throughout a mosaic of different steps in protein trafficking (100).

Modern methodical approaches like the development of genetically encoded tools for monitoring secretory protein transport as well as single-FP or Förster Resonance Energy Transfer (FRET)-based biosensors to measure Ca^{2+} in living cells have significantly contributed to recent advances in our understanding of the role of Ca^{2+} as a central regulator in exocytosis and ER-to-Golgi transport (45,98,99,101). Studies applying antibody-based or live-cell time-lapse imaging techniques have already uncovered some of the important players in Ca^{2+} regulated ER exit and the early secretory pathway. While some proteins like calmodulin have been identified as Ca^{2+} sensing regulators of protein secretion for quite a while now (102), the role of other essential Ca^{2+}-dependent mediators in early protein secretion like ALG-2 or peflin has only been described in detail in recent years (45,101,103,104).

Another fascinating aspect of Ca^{2+} potentially regulating intracellular trafficking events is its predicted regulating effect on motor proteins and the cytoskeleton in eukaryotic cells (105–108). It has also been demonstrated that an inositol 1,4,5-triphosphate (IP_3)-mediated Ca^{2+} release from the ER lumen and consequently a strong transient increase in the cytosolic Ca^{2+} pool leads to an immediate freeze in the movement of GPI-positive vesicles (109), hinting at a prevention of long-distance, directional transport of vesicular carriers along cytoskeleton elements. This effect might be highly meaningful for ER-to-Golgi transport as well, since this crucial, initial step in secretory transport is known to also rely on microtubule-dependent transport (19).

While a lot of questions regarding Ca^{2+} mediated regulation of ER-to-Golgi and secretory protein transport overall remain unanswered, the general importance of physiological subcellular Ca^{2+} concentrations and unrestricted Ca^{2+} dynamics is undisputed. Given that the maintenance of healthy levels in subcellular Ca^{2+} pools also heavily relies on subcellular ATP (110,111), the interrelations of Ca^{2+} and ATP household are likely to present a major focus in future secretory pathway research.

1.4.2 Structural basis for fast and essential secretory trafficking from the ER

The ER is a multifunctional organelle (22) and represents the first entry point into the secretory pathway (3). Proper morphology of the ER network and an adequate number of

ERES as the location of COPII-vesicle formation is important to guarantee proper transport (50). The ER is a highly dynamic organelle (103,112) and disturbances in the membrane trafficking system can lead to severe disease (3). This high amount of variety is also reflected in the differences in the number and composition of ERES, which can vary significantly between different cell types (50).

Another interesting aspect of ER-to-Golgi transport is its dependence on the structural integrity of the cytoskeleton. It has been shown that COPII-positive vesicular carriers move in a microtubule-dependent manner (18,21,47), suggesting a dynein/dynactin-mediated translocation (47). Therefore, besides validating the ER network structure in examined cells, it might be very meaningful to also monitor the stability of the microtubule-network in studies and the motility of vesicular carriers when examining early secretory transport.

1.5 Investigating protein secretion using high-resolution fluorescence live-cell imaging

Early visualization attempts of the basic principles of how proteins are transported by secretory trafficking in a cell have already been conducted over 50 years ago using electron microscopy (113,114). Over the last few decades, researchers have started to uncover the mechanisms of the cellular secretory transport machinery via successful ex vivo approaches (115,116). The secretory pathway was formerly examined mainly by making use of biochemical or molecular biological techniques in combination with electron microscopy (117). However, the high dynamics in membrane and protein trafficking are characterized by fast-paced processes often happening simultaneously within short periods, which are difficult to capture with these methods. For this reason, the massive impact of live-cell optical approaches on the field was rightly predicted early on (117).

Unsurprisingly, the discovery of green fluorescent protein (GFP) as a versatile tool for monitoring and visualizing expression of genes and localization of proteins (118) further boosted the impact of high-resolution microscopy approaches on this research field (119).

For a long time now, fluorescence microscopy approaches have been commonly used to investigate the early secretory pathway and its components (119). Over the years optical methods have improved drastically and the demand for visualization of the actual dynamics

in such a highly dynamic process like protein trafficking increased. To complement the solid approaches based on cell fixation, more and more experiments were also conducted via time-lapse live-cell imaging.

Naturally, the direct FP-labeling approach does not exclusively comprise secretory pathway experiments with fluorescent cargo proteins, but e.g. also examinations involving the visual tracking of ERES: antibody-based visualization of the COPII element Sec31 (120), for example, has been shown to also work nicely via direct expression of an FP-labeled Sec31 variant (121). This is only one example, where the fusion of a protein of interest in the secretory pathway (regulation) has replaced or complemented antibody-based labeling.

1.5.1 Synchronizing ER-to-Golgi transport to uncover its dynamics and allow quantitative examinations

To allow proper examination and quantification of secretory processes in mammalian cell models, transport of the protein cargo of choice has to be synchronized (90,122). This synchronization process is characterized by the simultaneous release of a cohort of a (fluorescent) probe from the ER, which enables a precise determination of the starting point of secretory transport thereby providing crucial information about temporal dynamics. Over the last decades, several different approaches have been developed, improvements of these concepts and the development of novel techniques are ongoing (90,122).

One of the first milestones in secretory transport synchronization was the discovery of the thermosensitive mutant tsO45 of the vesicular stomatitis virus G protein (VSVG; (123)). The temperature-sensitive, monomeric VSVGtsO45 accumulates in the ER at a restrictive temperature (higher than 39.5 °C). Upon a switch to the permissive temperature of 32 °C trimerization and proper folding can occur leading to immediate trafficking to the plasma membrane through the Golgi apparatus. This principle can be exploited for (live-cell) fluorescence imaging by simply labeling the mutant VSVGtsO45, or more precisely its transmembrane region ($VSVG_{tm}$), with GFP (**Figure 1**), which has been performed successfully in the past to investigate ER-to-Golgi transport and involved components and regulators (18,47). The approach is still found today in the context of modern imaging methods (124).

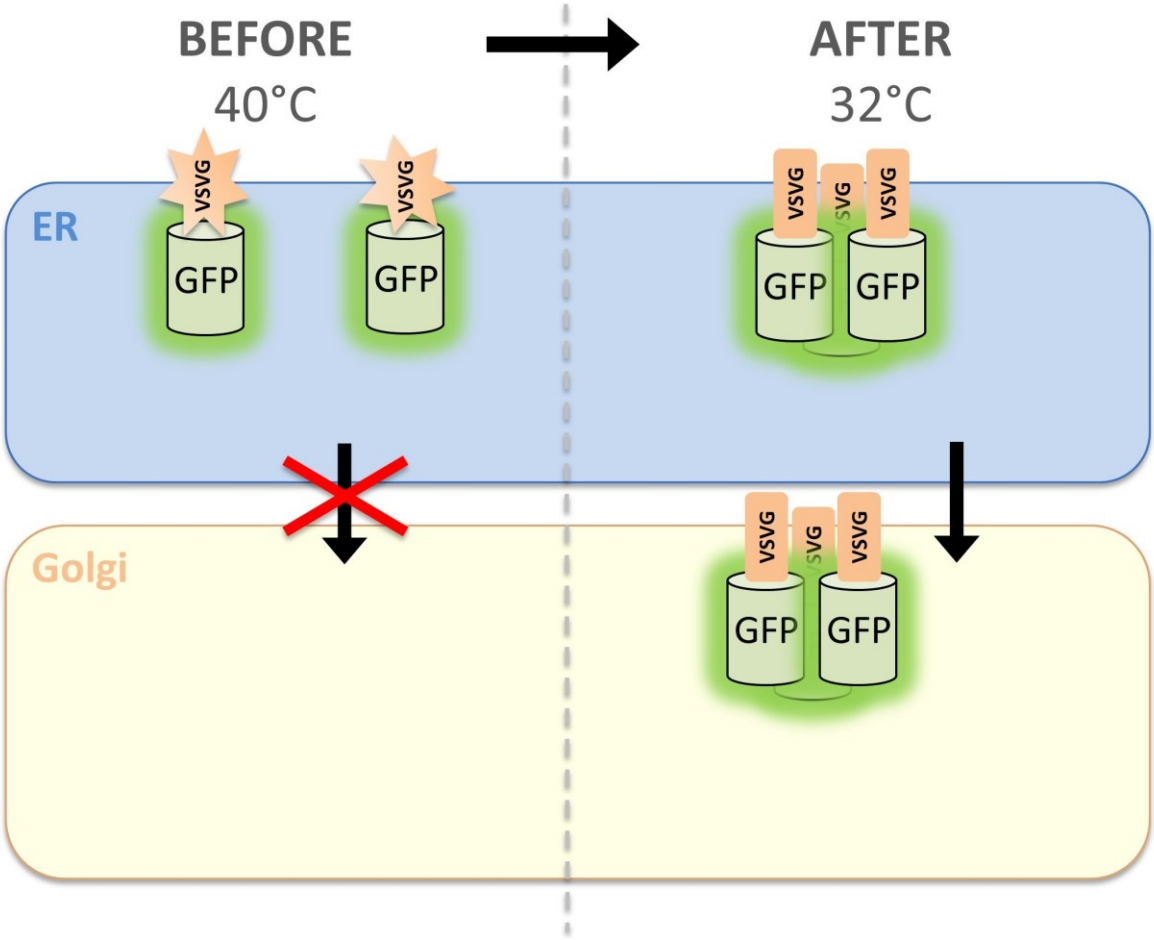

Figure 1: The principle of VSVG$_{tm}$-GFP transport constructs. Reversible misfolding of the VSVG transmembrane domain (VSVG) fused to GFP leads to retention of the construct in the ER at 40 °C. A temperature switch to 32 °C leads to proper folding and homotrimerization of the probe subsequently allowing transport initiation from the ER towards the Golgi.

A more modern approach to synchronize ER-to-Golgi transport is the use of ligand-sensitive probes to study protein trafficking. Famous examples for this would be the application of so-called conditional aggregation domains (or CAD; (125)) or the RUSH-system ("Retention using selective hooks"; (126)). Both principles are again based on an aggregation of the engineered construct in the ER, however, transport is not initiated by a temperature switch but by the addition of chemical ligands (122).

The RUSH-system is based on the interaction between streptavidin and the streptavidin-binding peptide (SBP, (126)). Streptavidin is fused to an ER-residing membrane protein and keeps the SBP-fused cargo protein in the ER (i.e. donor compartment), until biotin is added, which binds streptavidin with higher affinity and thereby induces the release of the cargo (126). A big advantage of CAD-based constructs is that, in comparison to the RUSH-system,

they do not require two parts, but aggregate into lattice-like oligomers by themselves (122). These constructs, which were initially invented for selective gene therapy approaches (127), can be disaggregated by a small chemical ligand (e.g. D/D Solubilizer), initiating transport. In combination with cutting-edge imaging technologies, GFP-tagged CAD constructs present a powerful tool to visualize secretory trafficking (**Figure 2**).

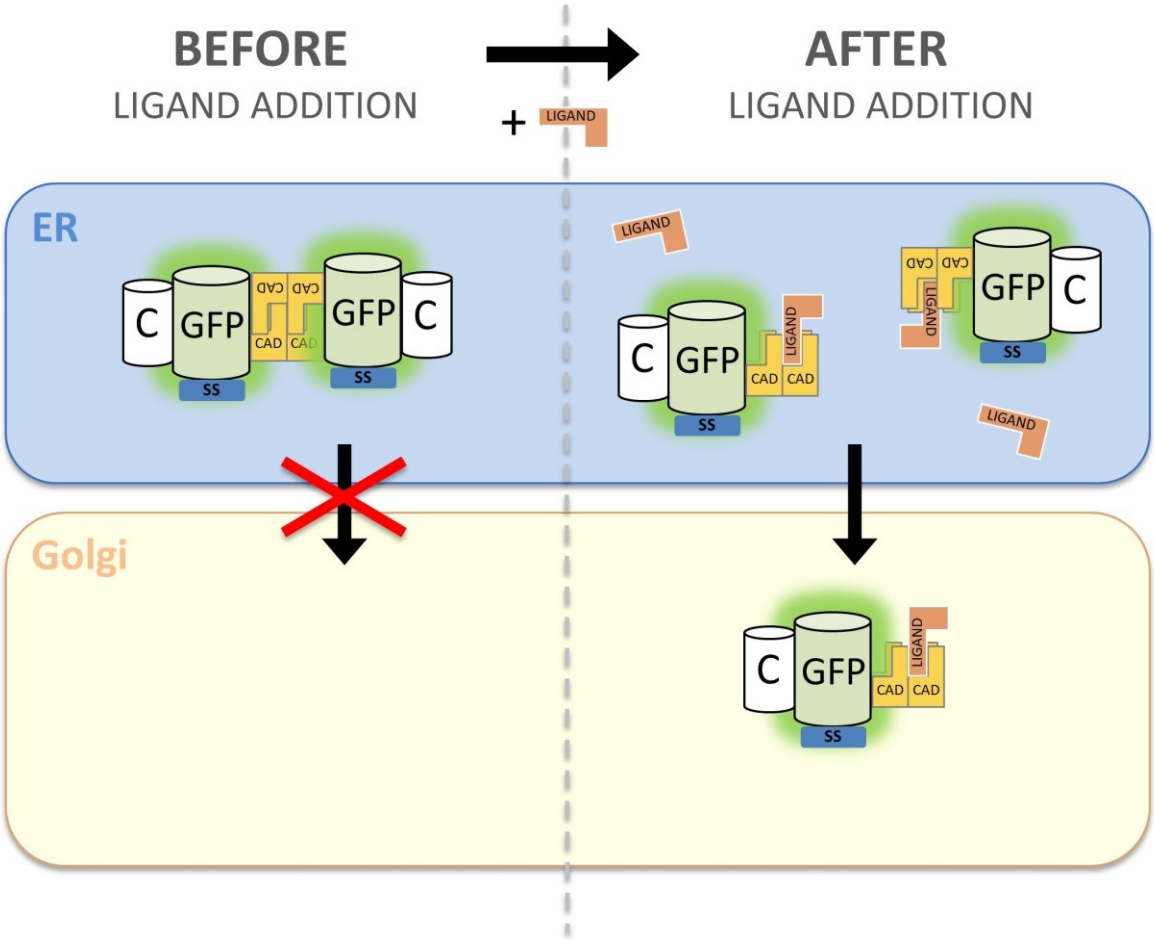

Figure 2: The principle of CAD-based transport constructs. Constructs consisting of a cargo protein (C; in this case a soluble protein), GFP, a secretion signal sequence (SS) and 4x conditional aggregation domains (CAD) aggregate in the ER, thereby preventing secretory transport. The addition of a small chemical ligand (LIGAND) leads to immediate disaggregation and initiation of ER-to-Golgi transport of the construct.

Recent efforts aim at eliminating ligand-addition for transport initiation by introducing the concept of photosensitive oligomerization into ER-to-Golgi transport constructs (90,122). For this, the plant ultraviolet-B resistance 8 (UVR8) domain is introduced into the probe, which leads to the formation of aggregates in the ER. Seven-second UVB light pulses serve as the trigger leading to de-aggregation and release of the cargo into the secretory pathway (128).

1.5.2 Novel FP technologies providing tools for innovative ER-to-Golgi transport sensor design

Unfortunately, in the modern scientific world time and money are often rare. Due to their quick and easy application, often without the need for expensive technology like high-resolution microscopy equipment, assay-based systems to investigate cellular pathways have taken over in many laboratories. With the application of certain novel FP technologies, it might not be necessary to make any tradeoffs in the scientific work and even adequately complement high-resolution imaging methods. Some of these technologies, two of which are explained briefly, could also help facilitate ER-to-Golgi transport investigations.

The first one is the split FP technology (129). Starting from the well-known principle of bimolecular fluorescence complementation (BiFC), where two non-fluorescent parts build a fluorescent protein when coming into proximity of each other, the split FP technology has come a long way. The most recent approaches have broken up sfGFP, respectively sfCherry, asymmetrically, to create a small epitope tag consisting only of the eleventh beta-strand of the FPs. This “FP11” part can be used as a minimally perturbing tag on a protein of interest, binding the rest of the FP to allow visualization of these interactions via fluorescence microscopy (129). Approaches of this kind have already been successfully implemented to design innovative genetically encoded sensors for cellular processes like mitochondrial import (130).

Another very interesting discovery in recent years was the dimerization dependent fluorescent proteins (ddFP; (131,132)). This promising principle is based on a potentially-fluorescent FP part, and a second non-fluorescent FP part, which upon proximity and subsequent reversible heterodimerization induces the fluorescence properties of the first part. Since monomer partners of differently colored FPs can interchangeably interact with the inducing monomer, there have already been attempts to use this principle for the design of ratiometric sensors for Ca^{2+} and caspase activity (132).

So far, no one has attempted to weave in these techniques into innovative probes to create an assay for ER-to-Golgi transport quantification. However, there might be a lot of potential in these approaches for future sensor design.

2 Hypothesis and Aims

Research on cellular secretory activities and specifically ER-to-Golgi transport processes has largely focused on gaining mechanistic insights and on identifying molecular players that accomplish protein sorting and transport. However, not much is known about the energy demand and supply of the secretory pathway. Also the resilience of protein secretion to energy stresses and other types of stresses have only been marginally investigated. However, due to the high importance and efficiency of protein secretion in different tumors (4), it seems particularly relevant to better understand the energy dependency and stress resilience of the secretory pathway of cancer cells.

Most cancer cells of very malignant tumors show a typical metabolic setting, well known as the Warburg effect, with high rates of aerobic glycolysis and low rates of mitochondrial oxidative phosphorylation (92–94). Interestingly, very little is known about a potential link between cancer cell-specific metabolism and high rates of protein biosynthesis and protein secretion of tumors. Answers to this major research question in cancer biology might have the potency to pave the way for developing novel interventions to treat cancer patients by targeting the energy supply of the cancer cell secretory pathway. Here, we exploit FP-based tools and genetically encoded fluorescent biosensors to correlate ER-to-Golgi transport with metabolic activities of cancer cells using state-of-the-art high-resolution fluorescence microscopy approaches.

The main hypothesis of this dissertation is that cancer cells do have an optimal energy supply of the secretory pathway to maintain high rates of protein secretion even under stress conditions. Thus, targeting the secretory activity by blocking its energy supply and suppressing its resilience to stresses might represent a specific and effective anticancer strategy.

Based on this hypothesis, the following main aims were defined:

- Establish quantitative time-lapse imaging of synchronized ER-to-Golgi transport efficiency on the level of individual cells using high-resolution fluorescence imaging of different FP-labeled cargo tools.

- Test different stress conditions for their impact on ER-to-Golgi transport in HeLa cells, a golden standard *in vitro* cancer cell model

- Correlate the ER-to-Golgi transport efficiency with cell metabolic activities, morphological alterations, and Ca^{2+} signals using fluorescent sensors in live cell imaging experiments

- Design and generation of dimerization dependent fluorescent protein (ddFP)-based tools to study ER-to-Golgi transport in cell populations without the need for high optical resolution

3 Material and Methods

The description of material and methods used in the course of these studies is based on the detailed explanations in Rauter et al., 2020 (1).

3.1 Chemicals and Buffers

The majority of compounds used for the preparation of buffers were purchased at Carl Roth (Graz, Austria). These compounds include calcium chloride ($CaCl_2$), magnesium chloride ($MgCl_2$), potassium chloride (KCl), sodium chloride (NaCl), L-glutamine, $NaHCO_3$, NaH_2PO_4, 4-(2-hydroxyethyl)-1-piperazineethanesulfonic acid (HEPES), adenosine-5'-triphosphate disodium salt ($ATPNa_2$), 2,5-di-t-butyl-1,4-benzohydroquinone (BHQ), dimethylsulfoxide (DMSO), yeast extract, trypton/pepton from casein, agar-agar (Kobe I), ethylene glycol-bis(β-aminoethyl ether)-N,N,N′,N′-tetraacetic acid (EGTA) and D(+)-glucose monohydrate. Other required chemicals include 2-deoxy-D-glucose (2-DG; Alfa Aesar, Kandel, Germany), KH_2PO_4 (Merck, Darmstadt, Germany) and Agarose (VWR International, Vienna, Austria). Gibco MEM vitamin solution and Gibco MEM amino acid solution as well as the antibiotics penicillin-streptomycin and amphothericin B were purchased from Thermo Fisher Scientific (Vienna, Austria). The solubilizing agent for synchronized transport experiments, D/D Solubilizer, was obtained from Takara (St. Germain-en-Laye, France) and will be referred to as „solubilizer" from this point on for the sake of simplicity.

Storage buffer (SB) and measurement buffers (MB) were prepared to contain isotonic salt concentrations and set to a physiological pH of 7.4 using NaOH. All buffer compositions can be found in **Table 1**.

3.2 Cell Culture

Different cell lines were used to establish the experimental frameworks. The cell lines HeLa, NRK (normal rat kidney epithelial cells) and HEK293a come from ATCC (Guernsey, UK). INS-1 cells were obtained from C. B. Newgard, Department of Pharmacology and Cancer Biology, Duke University School of Medicine, USA.

HeLa, NRK and HEK293a were grown in Dulbecco's Modified Eagle Medium (DMEM; Sigma-Aldrich, Vienna, Austria) with 10% foetal bovine serum, 100 U/ml penicillin, 100 µg/ml streptomycin and 2.5 µg/ml Fungizone (Thermo Fisher Scientific, Vienna, Austria). Gibco RPMI medium 1640 (Thermo Fisher Scientific) with 10% foetal bovine serum was used as the standard medium for INS-1 cells. All cell types were kept at 37 °C and 5% CO_2 in a humidified incubator to guarantee optimal growth conditions.

Table 1: Storage buffer (SB) and measurement buffer (MB) compositions.

Component	Concentration		
	SB	MB	MB; "0Ca"
NaCl	138 mM	138 mM	138 mM
KCl	5 mM	5 mM	5 mM
$CaCl_2$	2 mM	2 mM	
$MgCl_2$	1 mM	1 mM	1 mM
HEPES	10 mM	10 mM	10 mM
$NaHCO_3$	2.6 mM		
Na_2HPO_4	0.34 mM		
KH_2PO_4	0.44 mM		
D(+)-Glucose Monohydrate *	10 mM		
Gibco™ MEM Vitamin solution (100x)	1x		
Gibco™ MEM Amino Acid solution (50x)	1x		
Penicillin-Streptomycin (10,000U/ml)	1 %		
L-Glutamine	2.5 mM		
Amphotericin B	0.5 %		
EGTA			0.1 mM
ddH_2O			
NaOH	to pH 7.4	to pH 7.4	to pH 7.4

* in MB+2-DG (+2-DG) 10 mM D(+)-Glucose Monohydrate is substituted by 10 mM 2-deoxy-D-glucose, while glucose starvation buffer (-Glu) contains neither glucose nor 2-DG.

3.3 Preparation and transfection of plasmids

All transfections were carried out using highly purified plasmid preparations derived from of overnight cultures (37°C, shaking) inoculated with respective *E. coli* culture stocks (by PureYield Midiprep/Maxiprep system, Promega, Mannheim, Germany). For constructs produced in the course of this study, chemically competent 10-beta *E. coli*, purchased from New England Biolabs (Ipswich, MA, USA), were transformed according to the company manual before creating *E. coli* stocks.

The transfection of plasmids was carried out using Polyjet In Vitro Transfection Reagent (SignaGen, Rockville, MD, USA) or TransFast Transfection Reagent (Promega, Mannheim, Germany). The transfection itself was performed according to the protocols provided by the manufacturers. Cells were seeded on 30 mm 1.5 H high-precision glass cover slides (MarienfeldSuperior, for SIM) in 6-well plates, transiently transfected and left for expression of the constructs coded on plasmids for 24-36 hours before the experiments.

3.4 Cloning of ER-to-Golgi transport constructs with different FPs

Transport construct plasmids GFP-F_M4-GH, GFP-F_M4-VSVG$_{tm}$ (101), VSVG$_{tsO45}$-GFP (18,47) and the non-published mRuby2-F_M4-GH were kindly provided by Andrew Peden's lab. For cloning the constructs with different fluorescent proteins mRuby2-F_M4-hGH was taken as a starting plasmid. The sequence of mseCFP was taken from the GEPII1.0 potassium sensor developed in our lab (133), the one of mCherry was taken from the mCherry-Golgi-7 plasmid; both acquired via PCR. Primers were designed to additionally complement the sequences with the respective restriction sites (5'- AGATCTAGAATGGTGAGCAAGGGCGAGG-3' as a forward primer for both and 5'- AGACTCGAGCTTGTACAGCTCGTCCATGC-3' as a reverse primer for mCherry and 5'- AGACTCGAGGGCGGCGGTCACGAACTC-3' as a reverse primer for mseCFP). The PCR products were then cut and inserted into the mRuby2-F_M4-hGH plasmid instead of the mRuby2 sequence using the XbaI- and XhoI-cutting sites, yielding mCherry-F_M4-GH and mseCFP-F_M4-GH. Restriction enzymes were purchased from New England Biolabs (Ipswich, MA, USA).

3.5 Design and cloning of novel innovative ER-to-Golgi transport constructs based on the ddFP technology

The design of a novel genetically-encoded ER-to-Golgi transport sensor based on conditional aggregation domains, self-cleavage (134) and the dimerization dependent fluorescent protein (ddFP) technology (131,132) was based on our expertise in logical biosensor design (109,130,133,135) as well as recent experience with P2A-based self-cleavage in genetically encoded sensors (unpublished). The construct TRAPT1.0 was designed by me (**Figure 3**), synthesis was conducted at Gene Universal Inc. (Newark, USA).

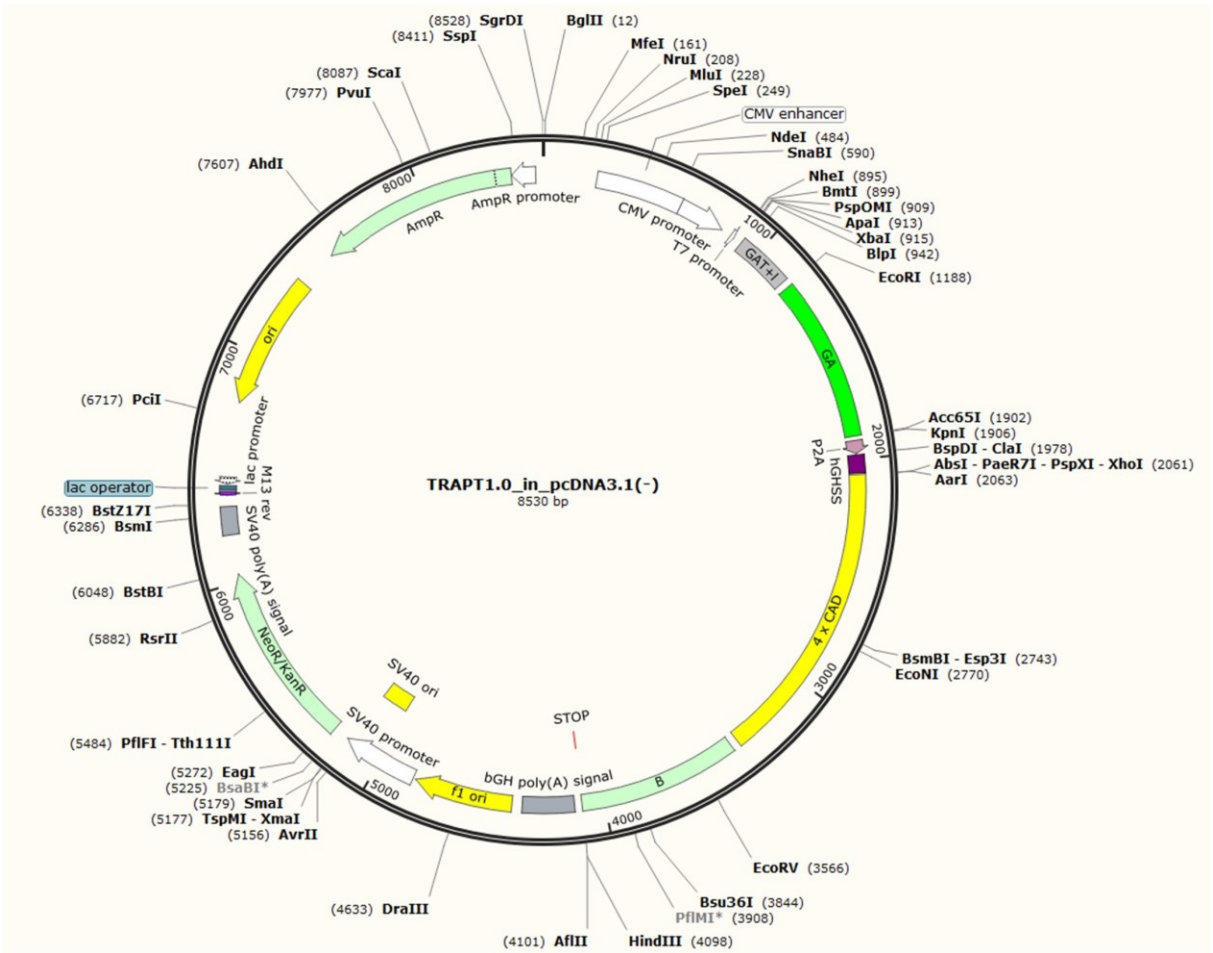

Figure 3: Vector map of TRAPT1.0 in pcDNA3.1(-). The features of the insert TRAPT1.0 coding for the ER-to-Golgi transport sensor are shown as: GAT+I (Golgi anchor plus short linker sequence), GA (green fluorescent A part of ddFP heterodimer), P2A (self-cleavage site), hGHSS (hGH signal sequence/secretion signal), 4xCAD (four repeats of the conditional aggregation domain), B (non-fluorescent, fluorescence-mediating B part of ddFP heterodimer).

Variations of the construct were cloned by ourselves. For the generation of TRAPT_SScontrol, sfGFPnuc was inserted into the 4xCAD-B locus using XbaI and HindIII. All restriction enzymes and according solutions were acquired from New England Biolabs (Ipswich, MA, USA). To yield TRAPT_GAcontrol, CPV was cut from a GEPII construct produced in our lab (133) and inserted into the GA locus using EcoRI and KpnI restriction enzymes. TRAPT_SIZEcontrol was cloned in a two-step process: first, the N-terminal part of TRAPT1.0 (GAT+linker-GA) was cut out via XbaI and KpnI and inserted into pcDNA3.1(-) (Invitrogen, Vienna, Austria) and then CPV from GEPII was inserted using EcoRI and KpnI.

3.6 High-resolution fluorescence imaging

Experiments were performed using a wide-field microscopy system optimized for measuring small changes in excitation of genetically encoded FRET- and single FP-based biosensors as well as on a high-resolution array confocal system according to experimental requirements. The open source image analysis software ImageJ (https://fiji.sc/) and the program MetaMorph from Molecular Devices were used to analyze all images captured, quantify required parameters and for preparation of figures.

3.6.1 Wide-field microscopy

ATP, GTP and Ca^{2+} measurements were performed with an inverted wide-field microscopy setup. An IX73 Olympus stage (IX73 System; Vienna, Austria) was used alongside an Omicron LEDHub for excitation (Omicron-Laserage, Dudenhof, Germany) that featured 340 nm, 385 nm (for FURA-2AM), 455 nm (for CFP/YFP-FRET) and 470 nm (for GFP range) LED light sources. For all experiments performed on this system, a 40x magnification oil immersion objective (UPLXAPO40XO, NA 1.4; Olympus, Vienna, Austria) and a Retiga R1 CCD camera (TELEDYNE QIMAGING, Surrey, Canada) with a binning of 4 were used. Furthermore, the system featured a Photometrics DV2 optical beam splitter (Photometrics, Tucson, AZ, USA) to enable simultaneous CFP/YFP-FRET measurements. The wide field system has a Semrock 427/10 Brightline HC and a Semrock LED-CFP/YFP/mCherry-3x filter system (IDEX Health & Science LLC, Rochester, NY, USA) for CFP/YFP-FRET measurements. Furthermore a GFP-3035D filter system (IDEX Health & Science LLC, Rochester, NY, USA) for measurements in the GFP-range can be applied. The whole system

was controlled using the VisiView software (VisiView v4.2.0.1, Visitron Systems, Puchheim, Germany).

3.6.2 Array confocal laser scanning microscopy (ACLSM)

All experiments to determine structural changes in organelle morphology as well as approaches to determine ER-to-Golgi transport efficiency and vesicle motility were performed on the array confocal laser scanning microscope (ACLSM) Zeiss Axiovert 200 M (inverted system; Zeiss Microsystems, Jena, Germany). This system featuring a Nipkow spinning disk is better suited for live-cell imaging compared to conventional confocal systems. An argon ion laser system (series 543, CVI Melles, Griot, CA, USA) with 445 nm, 488 nm, 515 nm and 561 nm excitation lasers was used and imaging information was collected using a CoolSnap HQ2 CCD camera (Photometrics, Tucson, Arizona, USA). All images at the confocal system were taken with a 100x objective (NA 1.45, oil; Zeiss Microsystems, Jena, Germany).

3.7 Measuring ions and metabolites using genetically encoded fluorescent biosensors and small chemical fluorescent sensors

The abundance of metabolites and certain ions crucial for cellular signaling and metabolic processes was determined by applying genetically encoded fluorescent sensors as well as the chemical sensor FURA-2AM for cytosolic Ca^{2+} imaging. All time-lapse imaging experiments with sensors were conducted on a wide-field system (3.6.1) using gravity-based perfusion (PC30 perfusion chamber and perfusion system; both NGFI GmbH, Graz, Austria) for optimal buffer exchange and a Chemistry Diaphragm vacuum pump ME1c for keeping a constant flow (Vacuubrand, Wertheim, Germany). Before the experiments the cells were taken out of the incubator, washed and kept on storage buffer (3.1) for a minimum of 45 minutes to equilibrate. For all cells and all sensors, a baseline at respective excitations (see 3.6.1) was recorded for at least five minutes before applying treatment buffers to acquire a stable reference value.

Adenosine-5'-triphosphate (ATP), the central metabolite for readily available chemical energy storage in cells, was measured in cytosol and mitochondria using the CFP/YFP FRET-sensors AT1.03 with a nuclear export sequence as well as mtAT1.03 (136). Calcium

concentrations were determined with FURA-2AM in the cytosol and with the CFP/YFP-FRET sensor D1ER (137) in the endoplasmic reticulum. Guanosine-5'-triphosphate (GTP) was measured using GEVAL530 (138). For ATP, GTP and Ca^{2+} measurements the changes upon switch to glucose-starvation buffer or 2-DG containing buffer were determined (3.1). For Ca^{2+} additional measurements using measurement buffer without calcium chloride and instead with EGTA (3.1, **Table 1**), respectively buffer containing the (sarco)endoplasmic reticulum Ca^{2+} ATPase (SERCA) inhibitor and ATP as an inositol 1,4,5-triphosphate (IP_3) generating agonist, were performed. Exact timings of treatments can be found in the respective figures in the Results part.

3.8 Live-cell imaging of ER-to-Golgi transport

The imaging experiments to determine ER-to-Golgi transport efficiency were all performed on an ACLSM system (3.6.2). In preliminary experiments GFP-F_M4-GH, GFP-F_M4-$VSVG_{tm}$, GFP-F_M4-GPI (101), $VSVG_{tsO45}$-GFP (18,47) as well as the self-cloned variants mCherry-F_M4-GH and mseCFP-F_M4-GH (3.4) were expressed in different cell lines and excited at 445 nm (CFP), 488 nm (GFP) and 561 nm (RFP), respectively. Constructs are described in detail in Sargeant et al. (101).

Due to the highest consistency and best applicability in the experimental setup all quantification experiments in HeLa cells were performed with the established constructs GFP-F_M4-GH and GFP-F_M4-$VSVG_{tm}$. Both transport constructs are ligand-sensitive. This implies that they build aggregates in the ER thereby preventing secretory transport of the construct to allow for synchronization of secretion processes. Upon addition of a chemical ligand, hereinafter called "solubilizer" (250 nM D/D Solubilizer, Takara, St. German-en-Laye, France), the protein constructs disaggregate and enter the secretory pathway. As a reference for Golgi apparatus position, cells were co-transfected with the Golgi-marker mCherry-Golgi-7 to enable quantification of live-cell time-lapse imaging data. The mCherry-Golgi-7 was a gift from Michael Davidson (Addgene plasmid #55052, http://n2t.net/addgene:55052, RRID: Addgene_55052). The Golgi marker also allowed an optimal focus on the Golgi apparatus from the starting image. In order to check for energy stress sensitivity of ER-to-Golgi transport, HeLa cells were treated 3 x 10 minutes with measurement buffer containing 10 mM glucose (control; "+Glu"), 0 mM glucose (glucose starvation, "-Glu") or 10 mM 2-DG ("+2-DG") instead of glucose before initiating transport.

Images of different positions were taken before (“0 min”) and 3, 7, 15 and 30 minutes after transport initiation by ligand addition. Time points are based on empirical data. A custom-made ImageJ-macro was applied for analysis and quantification of the imaging data. After capturing regions of interest (ROI) manually, the semi-automated approach enabled maximum objectivity in analyzing time-lapse images. Images of the Golgi-marker (red channel) were thresholded using the Otsu method plus two eroding steps after background subtraction (rolling ball) to define the region where the Golgi apparatus is located. Everything inside the ROI and outside the Golgi region was defined as non-Golgi region in the binary image produced from these algorithms. This “Golgi-mask” was then used to automatically calculate the integrated densities of Golgi and non-Golgi region in the corresponding GFP images showing the transport constructs and a ratio between these two (GFP signal in Golgi divided by GFP signal in non-Golgi region). After normalizing to the first time point for each individual cell this resulted in a variable displaying ER-to-Golgi transport efficiency, which was named “Transport Index” or “TI”. Increase of GFP-signal in the Golgi and simultaneous decrease in the ER over time hereby leads to an increase in TI, which can be interpreted as ER-to-Golgi transport over time.

3.9 Live-cell imaging and quantification of vesicle movements

Experiments to determine speed and directionality of movement of vesicular structures in HeLa cells were performed using an ACLSM system (3.6.2). HeLa cells stably expressing pH-Lemon-GPI (109) were used to visualize glycosylphosphatidylinositol (GPI)-positive vesicular structures due to the optimal fluorescence properties of mTurquoise for this purpose (139). The excitation wavelength of the construct was set to 445 nm, and imaging occurred with high frequency (5 images per second) for two minutes. A self-designed ImageJ algorithm was applied to analyze time-lapse images and quantify transport. The macro featured a rolling ball background subtraction and enabled bleaching correction using an exponential fit. Using the Otsu threshold method in ImageJ all GPI-positive structures between 5 and 30 pixels could be defined as vesicular structures within ROIs. The plugin TrackMate allowed subsequent quantification of vesicle movements over time. Using another custom macro the variables of interest were extracted from result sheets and transferred into Excel-files. The two most important calculated parameters were MeanSpeed, describing the arithmetic mean of mean speed calculated over all single vesicle tracks in each cell, and the so-called MeanDisplacement. Displacement describes the distance between the first point in

a track of a vesicular structure to the last point i.e. the directionality of transport in the XY-plane. MeanDisplacement can therefore also be interpreted as a readout for long-distance vesicle transport, which is generally accomplished by energy- and cytoskeleton-dependent steps, in comparison to non-directional diffusion.

3.10 Analysis of ER and microtubule network

The endoplasmic reticulum and microtubule (MT) network were investigated regarding changes upon introducing energy stress in the cancer cell model HeLa. To check the sensitivity of MT to glucose starvation or 2-DG treatment conditions (3.1) HeLa cells transiently transfected with a plasmid coding for GFP-α-tubulin were used. Measurement buffers containing 10 mM glucose (control), 0 mM Glucose ("-Glu", glucose starvation condition) or 10 mM 2-DG ("+2-DG") were applied. To prevent a collapse of the highly temperature-sensitive MT network and thereby loss of important information, the cells were directly transferred into one of the pre-warmed buffers from the incubator, and imaging was started immediately. Potential changes in the nocodazole-sensitive microtubule network over time were observed using a high-resolution confocal microscopy system (3.6.2). Due to the photosensitivity, the construct exposure time and laser intensity were optimized to a minimum and images were only made at time points 0 min, 30 minutes and 60 minutes. After one hour nocodazole (Noc) was added to a concentration of 10 µM as a positive control to check if MT can still depolymerize properly, and two more images were made (10 min and 20 min after Noc-addition). For analysis of time-lapse images, a custom algorithm in ImageJ was applied. At first background subtraction and additional median and Fast Fourier Transform (FFT) bandpass filter was used. After that the images were thresholded (using the Otsu algorithm) and opened, a particle analysis was conducted. This allowed distinguishing microtubule structures from the cytosolic signal. It has to be taken into account that due to the dynamic nature of the MT network characterized by constant polymerization and depolymerization there will always be a slight cytosolic background signal. The resulting mask was then used to determine signal intensities in MT and cytosol regions and calculate the according ratio for easy data visualization.

For analyzing the ER morphology CP450-CPV was expressed in HeLa cells. The construct is built up by an N-terminally truncated version (27 aa) of cytochrome P450 linked to the yellow fluorescent protein circularly permuted venus (CPV) via the linker KQKVMNH. Cells were

then imaged after 3 x 10 min treatment with the same buffers as for transport and microtubule experiments – glucose starvation buffer, 10 mM 2-DG buffer (+2-DG) or control buffer (10 mM glucose; 3.1). After taking multiple images at different positions of the glass slide for every sample the ER network structures in all cells were checked for differences in morphology.

3.11 Calculation of form factor changes in fluorescent structures

The method to measure ER-to-Golgi transport efficiency described in 3.8 is based on fluorescence intensities and can therefore not distinguish between cells that show no secretory transport over time due to lacking disaggregation of the transport construct or cells that have impaired construct secretion for other reasons. Though the disaggregation of the construct despite severe energy stress could nicely be seen by eye in every cell an additional calculation was performed to quantify this in an objective manner. This also allows ruling out dysfunction of the solubilizing agent under energy stress conditions as a reason for lacking ER-to-Golgi transport.

For this, the same images as for the calculations of ER-to-Golgi transport efficiency were taken and re-analyzed aiming to quantify successful disaggregation of the transport construct within the first few minutes. The image from the red channel (Golgi-marker) was taken as a reference to subtract the Golgi region from corresponding GFP-images. This step prevents that the Golgi form factor has any influence in calculations regarding the form factor (FF) of transport construct aggregates. After defining the regions of interest, all fluorescent structures in the GFP image were captured using a local threshold (Otsu algorithm) and the form factor was calculated for all of them. As the last step, the median form factor per cell was taken as a reference at every time point. The form factor is a variable that describes a perfect circle at value 1 – if shapes are less circular (e.g. more elongated like ER structures) the value is higher than 1. Thus, successful disaggregation of the rather round transport construct aggregate signal to a more net-like ER structure signal over time can the described by a continuous increase of FF over time.

3.12 Statistical analysis

The applied statistical tests to determine the significance of differences in experimental data as well as the exact n values are given in the respective figure legend for each experiment and n was at least 3 in all statistical tests to guarantee optimal comparability as well as reliability. Experiments were performed on different days, using cells of different passage numbers (except expression screenings). For statistical testing and graphic depiction of results GraphPad Prism (version 5.01; GraphPad Software, San Diego, CA, USA) was used. The D'Agostino & Pearson omnibus normality test was used to determine if the data follows a normal distribution. Unpaired t-test and Mann-Whitney U test were applied to compare two groups of normally distributed, respectively non-normally distributed, data. For some experiments, the 2-way ANOVA (two groups) or Kruskal-Wallis test and Dunn's post hoc test (more than two groups, non-normally distributed data) was conducted. Frequency distributions were compared using the Chi-square test. By default, the significance levels were defined as $p < 0.05$, $p < 0.01$ and $p < 0.001$ depicted by one, two or three asterisk/symbols (*, #), respectively, unless otherwise defined in the figure legend.

4 Results

This chapter includes results representing all steps of my thesis work, from identification of the right constructs and techniques, establishing protocols to data collection and quantification as well as the development of other novel approaches. Part of the results presented in this section can also be found in my first-author publication (1).

4.1 Establishing synchronizable secretory transport tools for high resolution fluorescence imaging

As the first step, a toolbox allowing the investigation of secretory transport, specifically the initial step of protein secretion, ER-to-Golgi transport, had to be established. In order to find the optimal construct to test for stress-resistance of the secretory pathway in cancer cells later on in the project, numerous genetically encoded, fluorescent transport constructs were tested in the cancer-cell model HeLa, a well-investigated model for a malignant solid tumor exhibiting a typical metabolic setting for cancer (84). The most reliable constructs were also tested for their functionality in the commonly used cell lines HEK293a, INS-1 and NRK.

4.1.1 Testing different transport constructs in HeLa cells

I tested several constructs with different underlying principles for transfection efficiency, expression levels and applicability for potential experimental setups and further approaches in our HeLa cell model. The general idea behind these constructs is a controlled secretory transport initiation. The respective constructs carry a cargo protein, either a soluble protein like human growth hormone (hGH or short GH) or (part of) a transmembrane protein like vesicular stomatitis virus G protein (VSVG) functioning as a transmembrane anchor. They aggregate in the ER based on an additional conditional aggregation domain (CAD or F_M4 meaning four consecutive repeats of the domain to increase reliability and reduce leakage) preventing protein trafficking from the ER to the Golgi and beyond. Only in response to a specific stimulus, which de-aggregates the CADs, the fluorescent cargo constructs ca be released from the ER. In the case of the ligand-sensitive constructs (GFP-F_M4-GH, GFP-F_M4-

GPI and GFP-F_M4-$VSVG_{tm}$) this stimulus is the addition of a small chemical ligand, referred to as D/D Solubilizer, or short “solubilizer” (**Figure 4**, first three panels). Alternatively, a temperature sensitive construct VSVGtsO45, fused with GFP ($VSVG_{tsO45}$-GFP), was used. In this case a temperature switch from 40 °C to 32 °C leads to disaggregation and initiation of ER-Golgi transport (**Figure 4**, bottom panel).

Both types of construct performed nicely in our HeLa cells model (**Figure 4**). Pre-tests were conducted at a cell confluency of around 80%. The most consistent results at high expression levels while keeping proper Golgi morphology could be achieved with GFP-F_M4-GH and GFP-F_M4-$VSVG_{tm}$ (**Figure 4**, first and second panel). The construct featuring a GPI anchor did not work as consistently and led to an untypical Golgi morphology in some HeLa cells (**Figure 4**, third panel). Despite working fine in terms of expression levels and consistency in ER-Golgi transport initiation upon introducing a fast temperature switch, $VSVG_{tsO45}$-GFP (**Figure 4**, bottom panel) was immediately ruled out for further experiments. Fast temperature switches were rather impractical for more complex experimental setups requiring different pre-treatment steps and subsequent live-cell fluorescence microscopy as compared to the more straight-forward ligand-sensitive approach.

The intention of quantifying transport while following the shift in fluorescence intensity from ER to Golgi in real time in living cells relied heavily on an easy, reproducible start signal. For this reason ligand-sensitive constructs were chosen due to their high reliability and reproducible transport initiation protocols: GFP-F_M4-GH as the main construct representing soluble, bulk flow cargo (**Figure 4**, top panel) as well as GFP-F_M4-$VSVG_{tm}$ (**Figure 4**, second panel) representing transmembrane cargo relying on active sorting for ER-Golgi transport. The cargo proteins human growth hormone and the vesicular stomatitis virus G protein also represent the more commonly found cargos discussed in literature and therefore allow optimal comparability to published studies and between the two constructs within this study due to the fact that they rely on the same transport initiation principle. To exclude any solvent-effects of the solubilizer-solution on transport initiation, effects of ethanol were ruled out in a separate experiment using GFP-F_M4-GH (n = 3). Proper initiation in GFP-F_M4-$VSVG_{tm}$ and GFP-F_M4-GH in HeLa cells was confirmed in independent experiments on different days (n = 5).

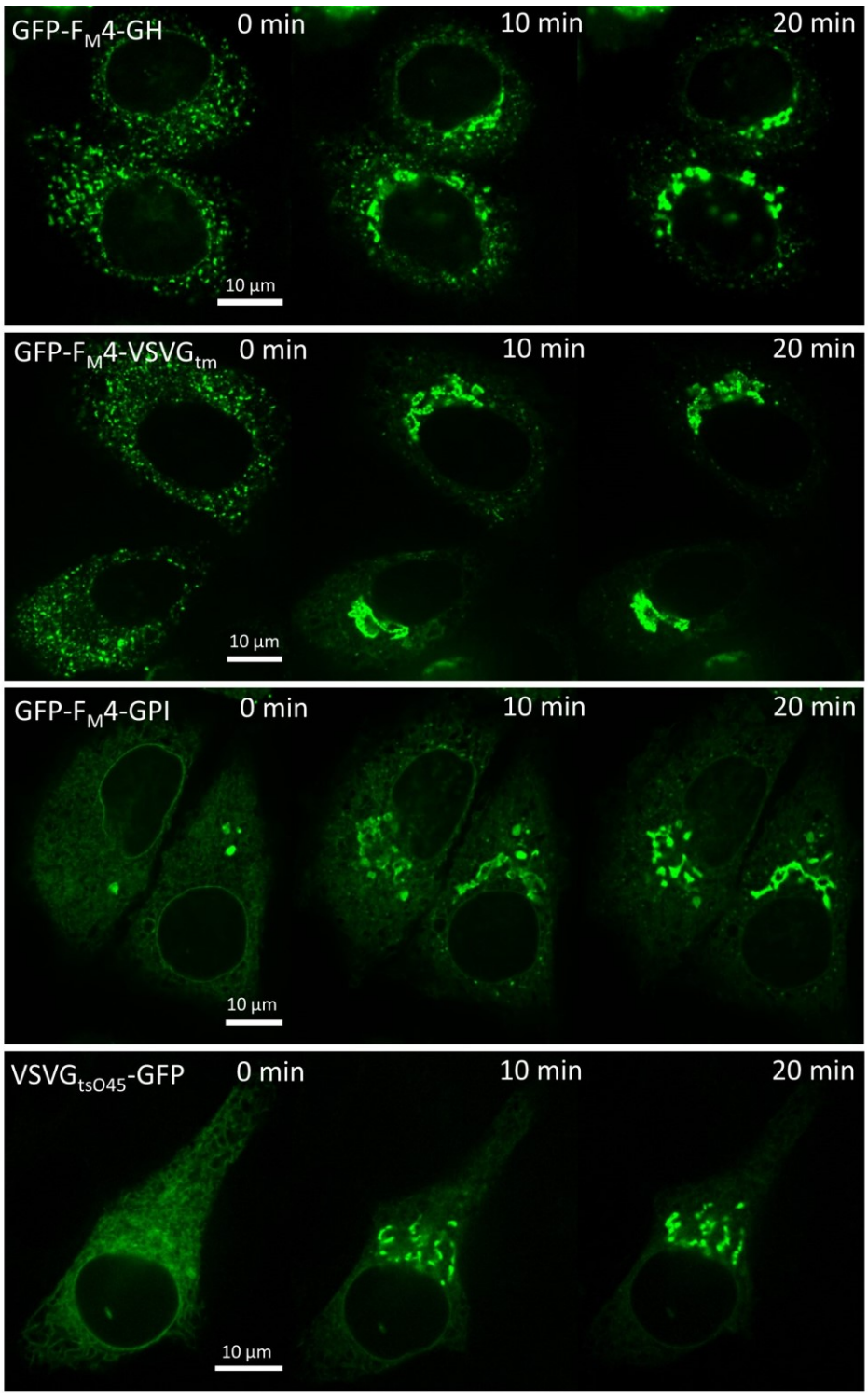

Figure 4: ER-to-Golgi transport of different synchronizable fluorescent cargos in HeLa cells. Representative images show the occurring translocation of GFP-tagged cargo to the Golgi apparatus at 10 and 20 minutes after setting the respective transport initiation stimulus. GFP-F$_M$4-GH, GFP-F$_M$4-VSVG$_{tm}$ and GFP-F$_M$4-GPI (first three panels): addition of D/D Solubilizer at time point 0 min. VSVG$_{tsO45}$-GFP (last panel): temperature switch from 39.5 °C to 32 °C at time point 0 min. Scale bar represents 10 µm.

4.1.2 Cloning and testing transport constructs with different fluorescent proteins

To test if in addition to GFP other FP variants can be used to follow ER-to-Golgi transport on the single cell level, several variations of a bulk flow cargo construct were generated. An obvious advantage of functional constructs carrying differently colored FPs would be the potential simultaneous measurement of distinct cargoes in future approaches.

The constructs containing different FP variants were tested for transfection rates and expression in HeLa cells and revealed less consistent results than GFP-F_M4-GH. The expression of mseCFP-F_M4-GH did show superior rates as compared to the GFP- and mCherry-constructs, but initiated transport upon ligand-addition was slower and incomplete in the majority of analyzed cells (40 out of 43 cells) after 30 minutes (**Figure 5a and b**). In case of mCherry-F_M4-GH the transport initiation upon solubilizer-addition worked in almost 80 % of analyzed HeLa cells (n = 50 cells; **Figure 5c**), however, two thirds of these cells also showed slow ER-to-Golgi transport kinetics resulting in incomplete cargo trafficking into the Golgi after 30 minutes. Expression rates were also lower than for GFP-constructs. Concluding these preliminary experiments of the novel cloned constructs only mCherry-F_M4-GH is applicable in certain experimental setups, while GFP-F_M4-GH was identified as the best solution for our experimental setup to further investigate stress-resistance of ER-to-Golgi transport in cancer cells.

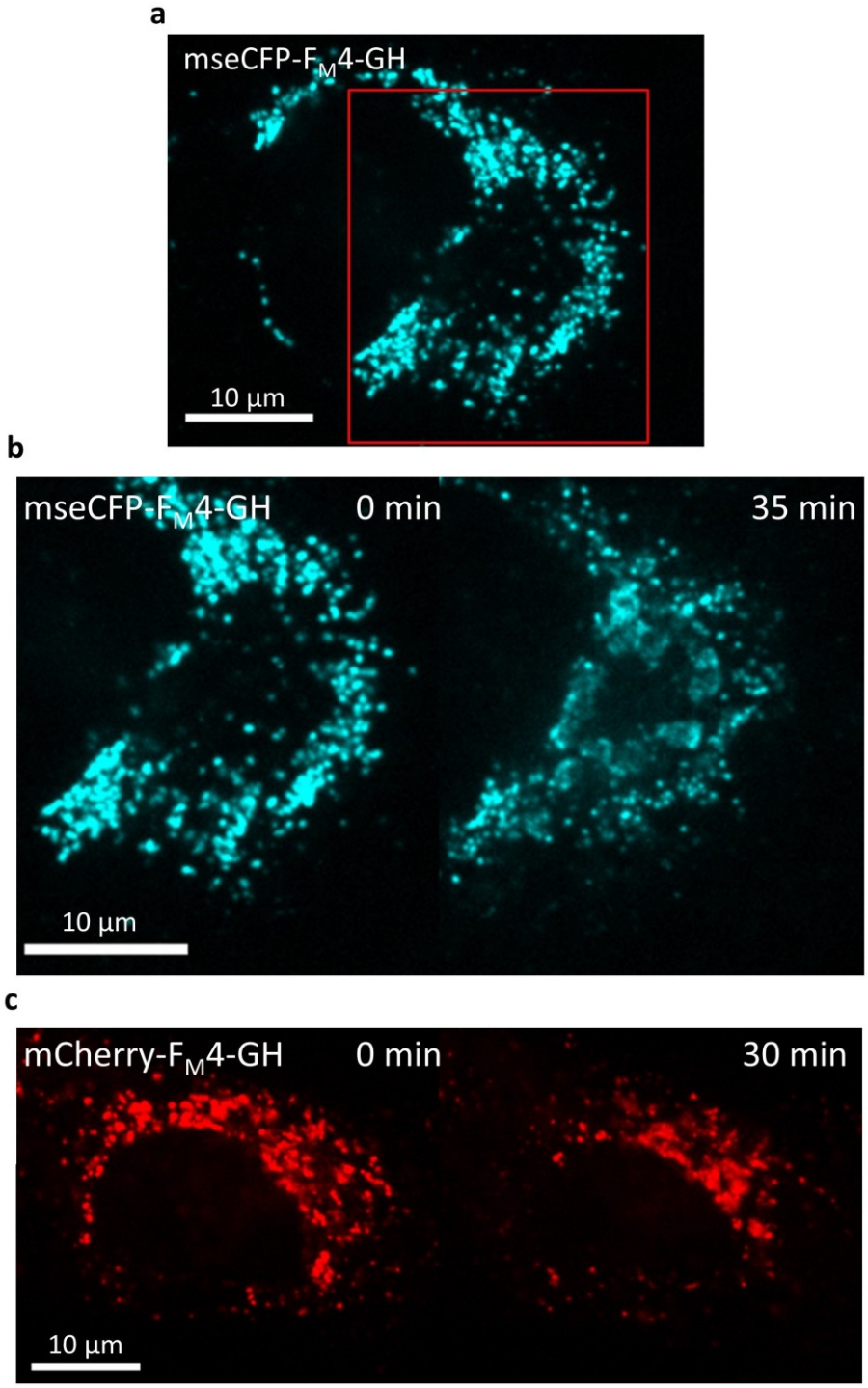

Figure 5: ER-to-Golgi transport of soluble cargo constructs labeled with mseCFP and mCherry in HeLa cells. Transport in all examined cells (mseCFP-F$_M$4-GH, n = 43 cells; mCherry-F$_M$4-GH, n = 50 cells) was initiated with D/D Solubilizer at time point 0 min and ER-to-Golgi transport was monitored at indicated time points after solubilizer addition. **(a)** Representative image of an mseCFP-F$_M$4-GH expressing cell before transport initiation. Marked with a red square is the zoomed image in (b). **(b)** Zoomed time-lapse of ER-to-Golgi transport of mseCFP-F$_M$4-GH. **(c)** Representative time-lapse of a cell expressing mCherry-F$_M$4-GH before (0 min) as well as at indicated time points after solubilizer addition. Scale bar represents 10 µm.

4.2 HeLa cells as a cancer cell model with high secretory activity

The HeLa cell represents a well-investigated *in vitro* cancer cell model and it is widely known that cancer cells are relying on their secretion capacity a lot to uphold numerous cancer-specific features (4,69–74). To estimate if HeLa cells also possess high secretory activity the transport constructs were tested and synchronized ER-to-Golgi transport was compared with that in other cell lines as well.

In a first approach, two cell lines with well-known metabolic properties (84) were tested, INS-1 and HEK293a. Both expressed the transport construct GFP-F_M4-$VSVG_{tm}$ adequately, making imaging via array confocal laser scanning microscopy possible (**Figure 6**). Also, solubilizer-addition initiated visible ER-to-Golgi transport in both cell lines (**Figure 6**). However, the distinct cell morphology and positioning of organelles in HEK293a as well as the small cell size of both cell lines made estimations of transport efficiency and comparisons difficult. Furthermore, proper comparisons using the soluble cargo construct GFP-F_M4-GH in the given cell lines were not possible for the same reasons.

For this reason we applied an additional cell line, which has been widely used in ER-to-Golgi transport investigations and secretory pathway studies in general: normal rat kidney cells (NRK). NRK cells exhibit quite high rates of protein trafficking and are therefore a good indicator for comparison to HeLa cell secretory activity. In all tested NRK cells the bulk flow construct (GFP-F_M4-GH) and the transmembrane cargo (GFP-F_M4-$VSVG_{tm}$) was mainly found in Golgi structures within 15 minutes of solubilizer addition. Similarly fast rates can be observed in HeLa cells in equivalent experimental setups. As expected, the HeLa cells displayed high protein secretion efficiency manifested by fast trafficking of both soluble construct (**Figure 7a**) and transmembrane construct (**Figure 7b**).

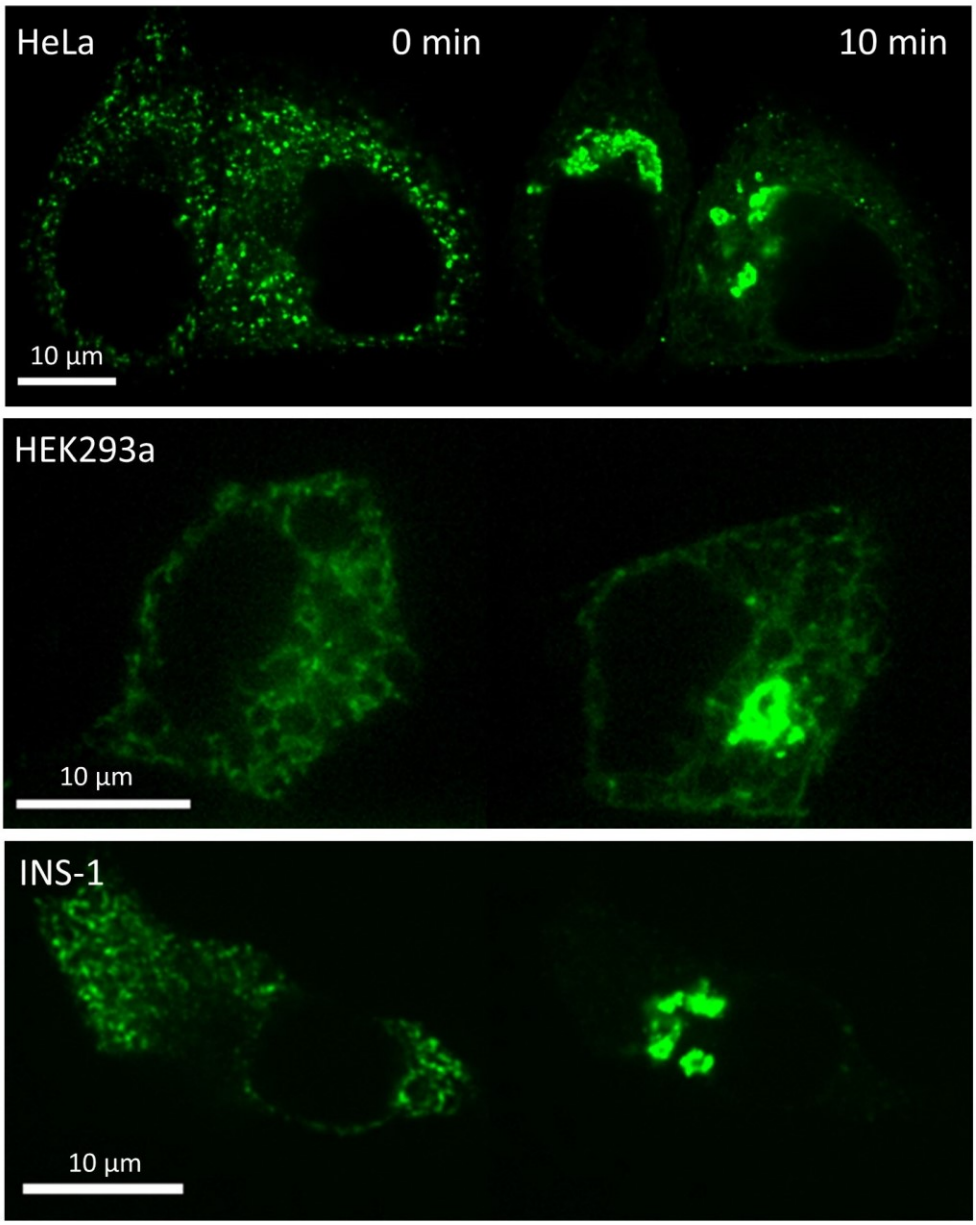

Figure 6: Representative time-lapse images showing ER-to-Golgi transport of transmembrane cargo in different cell lines. Shown is a comparison of time-lapse images between the established HeLa (top panel) and the respective cell lines of interest: HEK293a (middle panel, n = 16 cells) and INS-1 cells (bottom panel, n = 14 cells). Transport from the ER to the Golgi was initiated with D/D Solubilizer at time point 0 min. Scale bar represents 10 µm.

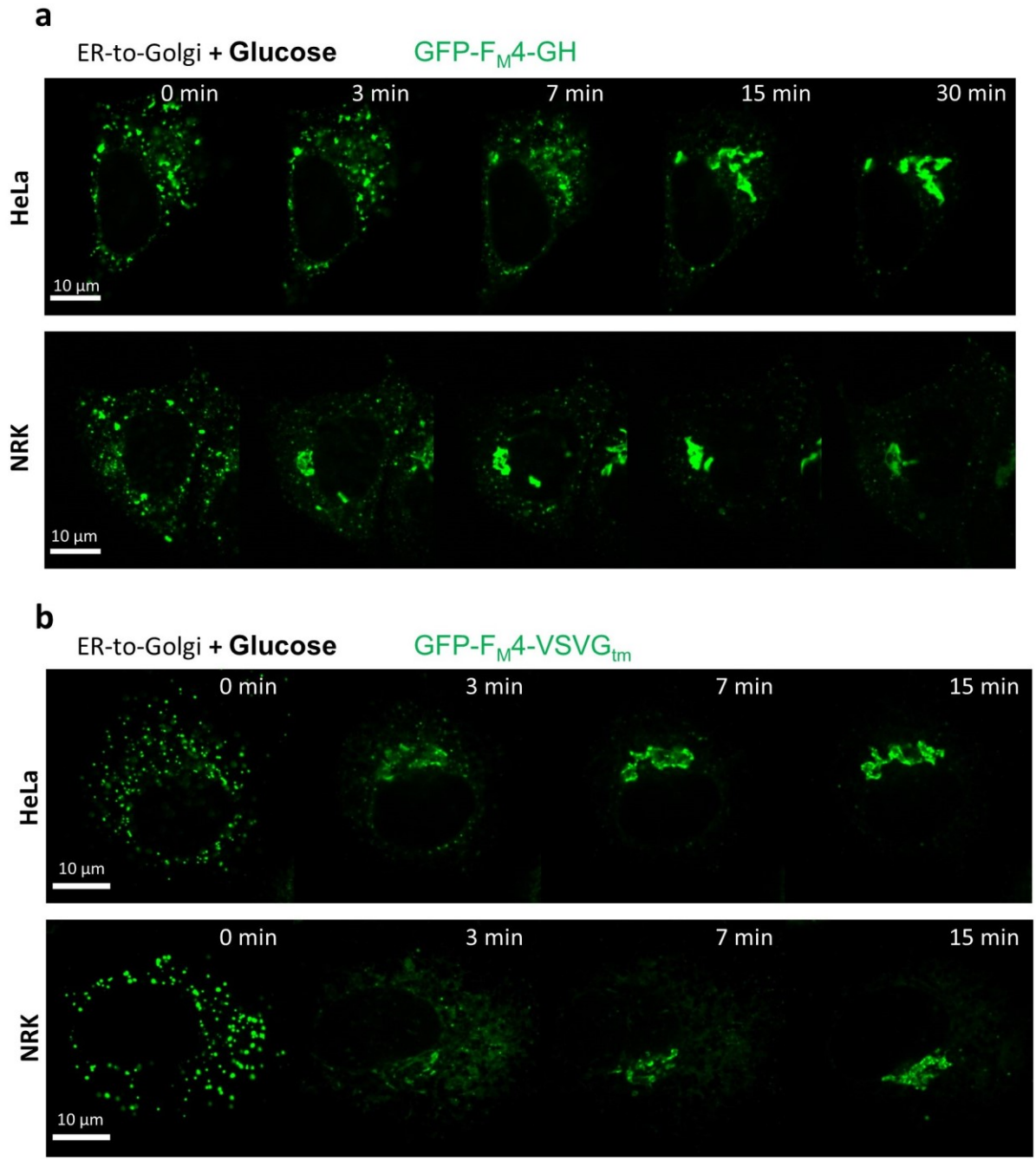

Figure 7: Comparison of ER-to-Golgi transport efficiency of soluble and transmembrane cargo construct in HeLa versus NRK cells. Both cell lines express soluble cargo **(a)** or transmembrane cargo constructs **(b)**, respectively. Transport was initiated by addition of 250 nM solubilizer to HeLa cells (upper panels) and NRK cells (lower panels) at time point 0 min, respectively. The cells were pre-treated with 10 mM glucose containing buffer for 30 minutes and imaged at 37 °C. A clear and fast localization of the green fluorescent cargo over time at indicated time points from the ER to the Golgi can be observed in HeLa cells (n = 66 cells for soluble, n = 58 cells for transmembrane cargo) as well as NRK cells (n = 18 cells for soluble, n = 18 cells for transmembrane cargo). Scale bar indicates 10 µm. (1) [Figure panels reproduced from Rauter et al., Cells 2020.]

4.3 Developing a quantification model for imaging data of ER-to-Golgi transport

Up until now, many studies investigating ER-to-Golgi transport and protein trafficking dynamics and describing regulatory factors in these vital processes have relied on cell fixation and subsequent immunostaining via FP-coupled antibodies for visualization. As indicated in the introductory part of this thesis, these methods have serious disadvantages in the attempt to visualize and comprehend these highly dynamic events. This is why we decided to apply live-cell imaging to this research question to capture the single-cell dynamics of synchronized ER-to-Golgi transport. Furthermore, the usage of semi-automated image analysis via custom-made algorithms in ImageJ provides highly objective readouts in this experimental setup.

4.3.1 Standardized ER-to-Golgi transport measurement protocol for co-transfected cells using ligand-sensitive protein trafficking constructs

To ensure maximum comparability and reproducibility of results a standard measurement protocol for determining ER-to-Golgi transport efficiency was set up. The overall protocol consisted of three phases: the preparation phase, the treatment phase and the measurement phase (**Figure 8**).

In the preparation phase the HeLa cells are co-transfected with two different constructs. The first one is the respective transport construct carrying GFP and allowing ligand-based synchronization and initiation of secretory trafficking. As determined based on the results of the preliminary experiments (see 4.1) this can be either GFP-F_M4-GH, representing soluble, luminal cargo, or GFP-F_M4-VSVG_{tm}, as a transmembrane cargo requiring active sorting. As for the second transfected plasmid, a marker for the target organelle in ER-to-Golgi transport, the Golgi apparatus, was applied. The marker had to carry a different FP to allow easy multichannel imaging of single living cells. The construct mCherry-Golgi-7 was chosen for this (**Figure 8**). HeLa cells were left for expression of the co-transfected constructs until the treatment phase.

The treatment phase occurred directly before the measurement on the microscope (**Figure 8**). The underlying treatment involves introducing energy stress in cells – the process of determining the parameters for treating the cells are described in 4.4. HeLa cells were all treated while attached to glass slides placed in the well of a 6-well plate (**Figure 8**).

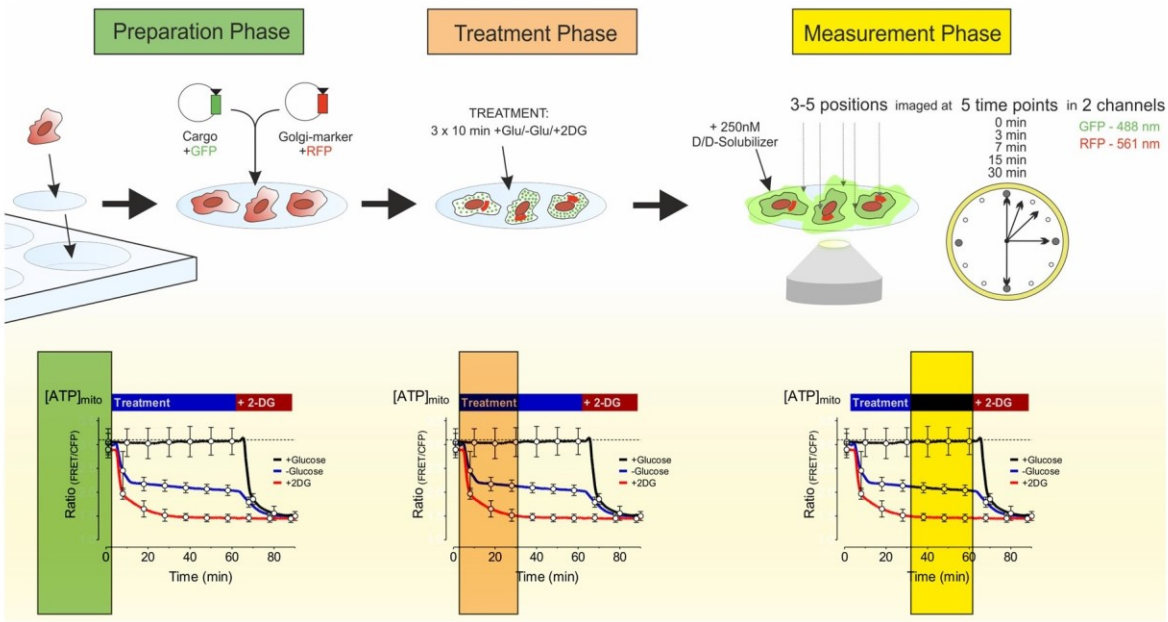

Figure 8: Schematic representation of ER-to-Golgi transport measurements. Schematic overview depicting the workflow (upper lane) and the respective ATP dynamics (for details see chapter 4.4) HeLa cells are undergoing (lower lane) during the three phases of the experiment. The preparation phase (green) includes two steps: 1. Cell plating on glass coverslips and cultivation in 6-well plates and 2. Co-transfection of HeLa cells with a green fluorescent transport construct and the red Golgi marker via lipid-based transfection. During the treatment phase (orange) the cells are treated for a total of 30 minutes (3 x 10 min) with different treatment buffers directly prior to transport initiation. In the measurement phase (yellow) the 3-5 positions are imaged, their position is saved and 250 nM solubilizer are added. The same positions are imaged 3, 7, 15 and 30 minutes after transport initiation i.e. addition of the solubilizer at 488 nm excitation to follow the GFP-tagged cargo and at 561 nm to have a reference of the target organelle in ER-to-Golgi transport for every time point and every position. (1) [Figure panel reproduced from Rauter et al., Cells 2020.]

In the third and last step, the measurement phase, 3-5 different positions distributed on the slide with cells that express both constructs and feature a healthy cell and Golgi apparatus morphology were selected. These positions were then imaged in the red and green fluorescence channel sequentially, directly before (0 min) and 3 min, 7 min, 15 min and 30 min after addition of the solubilizing agent to induce ER-to-Golgi transport (**Figure 8**). The time points are based on empirical data and previous studies and could be confirmed to best illustrate the dynamics of the process within this setup as well.

4.3.2 Semi-automated image analysis of ER-to-Golgi transport

Objective quantification of ER-to-Golgi transport is always a difficult task due to the high dynamics, unknown cell population heterogeneity and potential complications in the region of interest (ROI) selection. The task of optimally representing single-cell dynamics in protein trafficking was tackled by applying live-cell imaging as compared to antibody-based methods. Co-transfection with a red fluorescent Golgi-marker was applied to avoid a more subjective manual drawing of the ROI for the target organelle. The marker also served as a reference focal point, since the Golgi structure does not change significantly throughout the measurement, while the image in the green channel illustrates the dynamic process of protein trafficking. Hence, for the quantification process, the GFP image is used to estimate the amount of construct (i.e. green fluorescence) in certain areas, while the RFP image marks the position of the Golgi (**Figure 9a**).

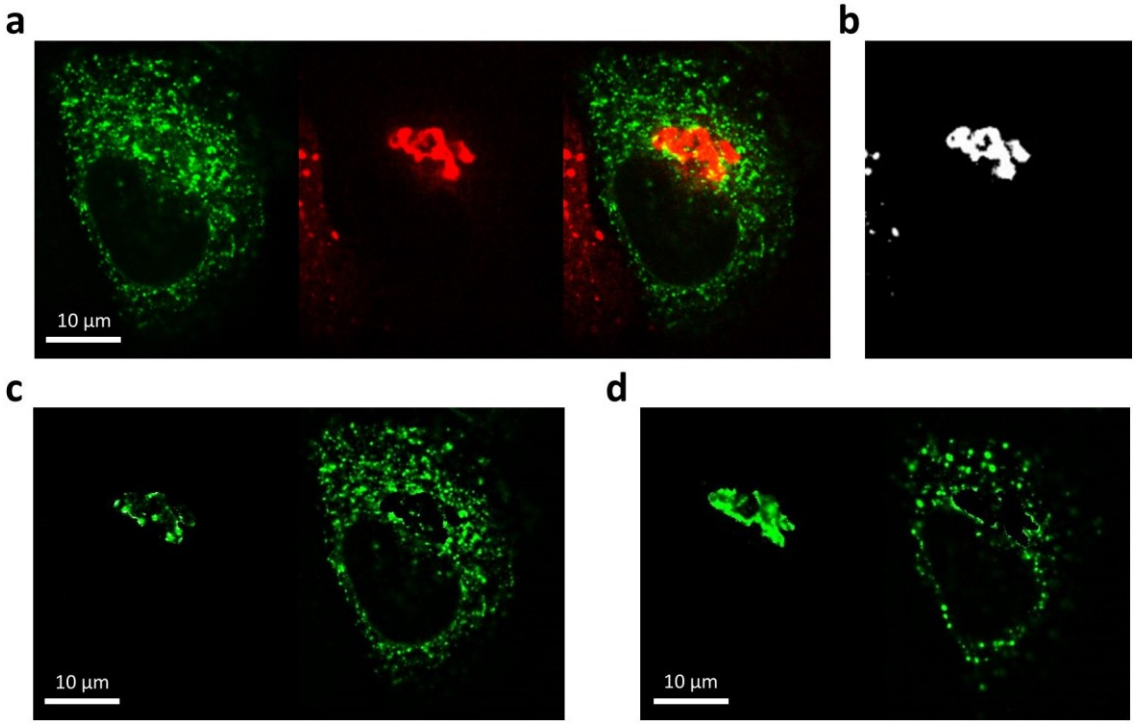

Figure 9: Illustration of the principle of secretory transport quantification in live cells. (a) Example image of a HeLa cell co-transfected with GFP-F_M4-GH (green, left) and mCherry-Golgi-7 (red, middle) as well as the merged image (right). **(b)** Binary mask derived from threshold of the region marked by mCherry-Golgi-7 signal to estimate Golgi position (as described in M&M). **(c and d)** Images showing GFP-F_M4-GH signal in Golgi- (left) and non-Golgi areas (right) as defined by the binary masks (see (b)) before (c) and 30 minutes after transport initiation (d). Scale bar represents 10 µm.

The quantification algorithm for this application consisted of creating a binary mask out of the image gathered from the red fluorescence channel (**Figure 9b**) and apply this mask to enable a differentiation between Golgi and non-Golgi area in the green channel, yielding an image for each of the two showing the green fluorescence (i.e. amount of transport construct) in the respective area (**Figure 9c and d**). As this was done for all time points in each cell individually (**Figure 9c and d, Figure 10a**), a ratio of transport construct in the Golgi area versus construct outside the Golgi area could be calculated. The ratio was normalized to the time point before transport is initiated (0 min) for each cell and was named “Transport Index” or “TI”. This type of ratio has been used in a similar form before and qualifies as an accepted expression of ER-to-Golgi transport in the research field (45). By applying these principles on time-lapse imaging data from living cells (**Figure 10a**) an increase of ratio over time represents working ER-to-Golgi transport for each cell (**Figure 10b**).

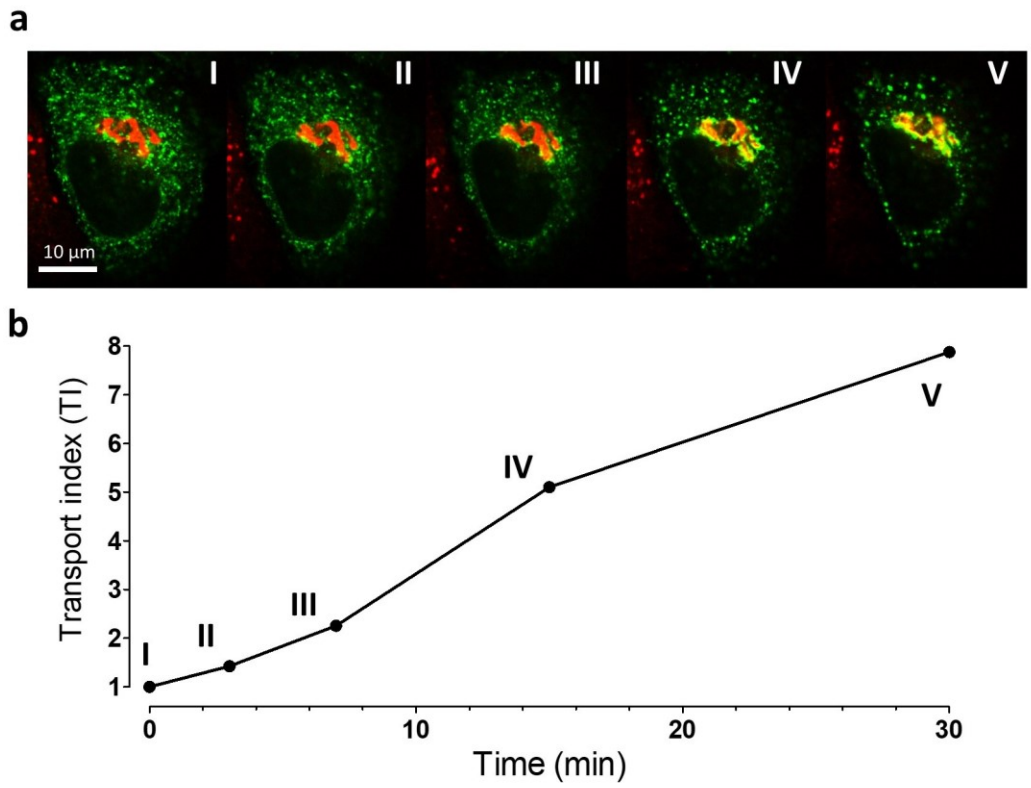

Figure 10: Time course representation of quantified example for ER-to-Golgi transport in a HeLa cell. (a) Time-lapse images of a HeLa cell expressing GFP-F_M4-GH and mCherry-Golgi-7. Images I, II, III, IV and V represent time points 0, 3, 7, 15 and 30 min after initiation of transport via D/D Solubilizer. Scale bar represents 10 µm. **(b)** Diagram representing the Transport Index (TI), a value calculated as the normalized ratio of the integrated intensity of the Golgi-region in the green channel divided by the integrated intensity of the non-Golgi region in the green channel for images I to V as shown in (a).

4.4 Establishing energy stress conditions to investigate the sensitivity of ER-to-Golgi secretory transport

As explained in detail in the introductory part, cancer cells tend to rely on (anaerobic) glycolysis as their main energy production pathway because of their distinct metabolic setting (92–94). Furthermore, cancerous cells in a tumor are likely to encounter low-glucose conditions during their lifetime due to excessive growth and proliferation while the blood vessel formation cannot keep up in this tissue. These factors make glycolysis-based stress induction an ideal option to test for stress-resistance of ER-to-Golgi transport in the HeLa cancer cell model. It has been demonstrated that not only the cytosolic ATP pool plays a major role for the energy supply of the secretory pathway, but also mitochondrial bioenergetics are crucial (10). To estimate the impact of this energy stress on (sub)cellular ATP levels, the genetically encoded FRET-based ATP sensors AT1.03 (featuring a nuclear export sequence to measure cytosolic ATP) and the mitochondrial ATP sensor mtAT1.03 were applied (**Figure 11a and b**).

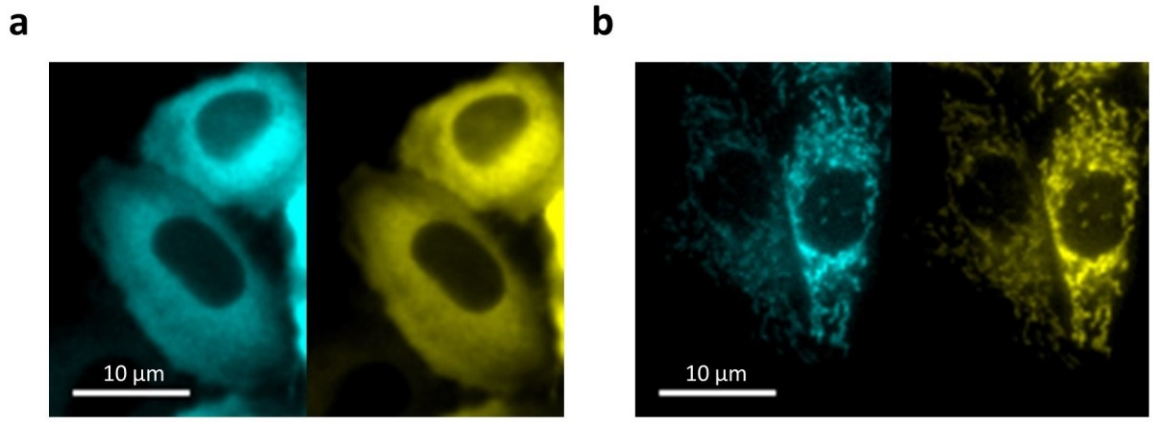

Figure 11: HeLa cells expressing genetically encoded FRET-based ATP sensors. Representative wide field fluorescence microscope images of HeLa cells expressing the cytosolic ATP sensor AT1.03 **(a)** or the mitochondria-targeted ATP sensor mtAT1.03 **(b)**, respectively. Panels display CFP-images (left) and FRET-images (right) for both constructs. Scale bar represents 10 µm.

To simulate energy stress conditions that mimic a situation of nutrient shortage a cancer cell might encounter during its life in a tumor, a glucose starvation condition was set up (-Glu). Treatment with the anti-metabolite 2-deoxy-D-glucose (+2-DG), instead of glucose in the measurement buffer, was used as a positive control to completely deplete cellular ATP levels. The drastic ATP-depleting effect has been shown in very short protocols before (84).

4.4.1 Cytosolic ATP levels are characteristically lowered upon energy stress

We first looked at cytosolic ATP levels ($[ATP]_{cyto}$), which represent a very large ATP pool in the cell and are likely crucial for secretory trafficking due to the energy requirements in vesicle building and cargo sorting (10). To our knowledge, subcellular ATP measurements using high-resolution fluorescence microscopy on single living cells under energy stress have mostly been performed over short periods (84), and not over extended periods as executed during this study (**Figure 12a-c**).

First, HeLa cells were rinsed with measurement buffer (experimental salt buffer) in the absence of glucose, as well as amino acids or other substances the cells might utilize for catabolic processes, for 60 minutes. The result was a very heterogeneous decrease in $[ATP]_{cyto}$ throughout the measured single cells upon glucose removal (**Figure 12a**). While in some cells ATP levels declined slowly and steadily seemingly running into a plateau, sharper drops could be observed in others with an overall significant decrease in mean ATP content (**Figure 12a and d**). Interestingly, in some cases, oscillations in FRET ratio signals occurred under glucose starvation conditions (**Figure 12a**). This might indicate potential regulatory measures of the cell to counteract persistent nutrient deprivation leading to transient increases in $[ATP]_{cyto}$. The addition of 2-DG after 60 minutes then rapidly reduced ATP levels to a minimum in all examined cells (**Figure 12a**). To ensure that external factors (e.g. shear stress due to constant perfusion) exert any effect on $[ATP]_{cyto}$, the same protocol was performed in the presence of glucose (**Figure 12b and d**). In these control measurements $[ATP]_{cyto}$ remained stable over 60 minutes and dropped rapidly upon the subsequent perfusion with 2-DG (**Figure 12b**) to reach the same minimum levels as observed in glucose-starved cells before (**Figure 12a**). Finally, the consistency of 2-DG mediated impact on glycolysis and the associated $[ATP]_{cyto}$ depletion were tested by applying experimental buffer containing the antimetabolite to the HeLa cells already from the start of the experiment. As expected, cytosolic ATP levels declined immediately in every single cell and stayed at this minimum over the whole time (**Figure 12c and d**).

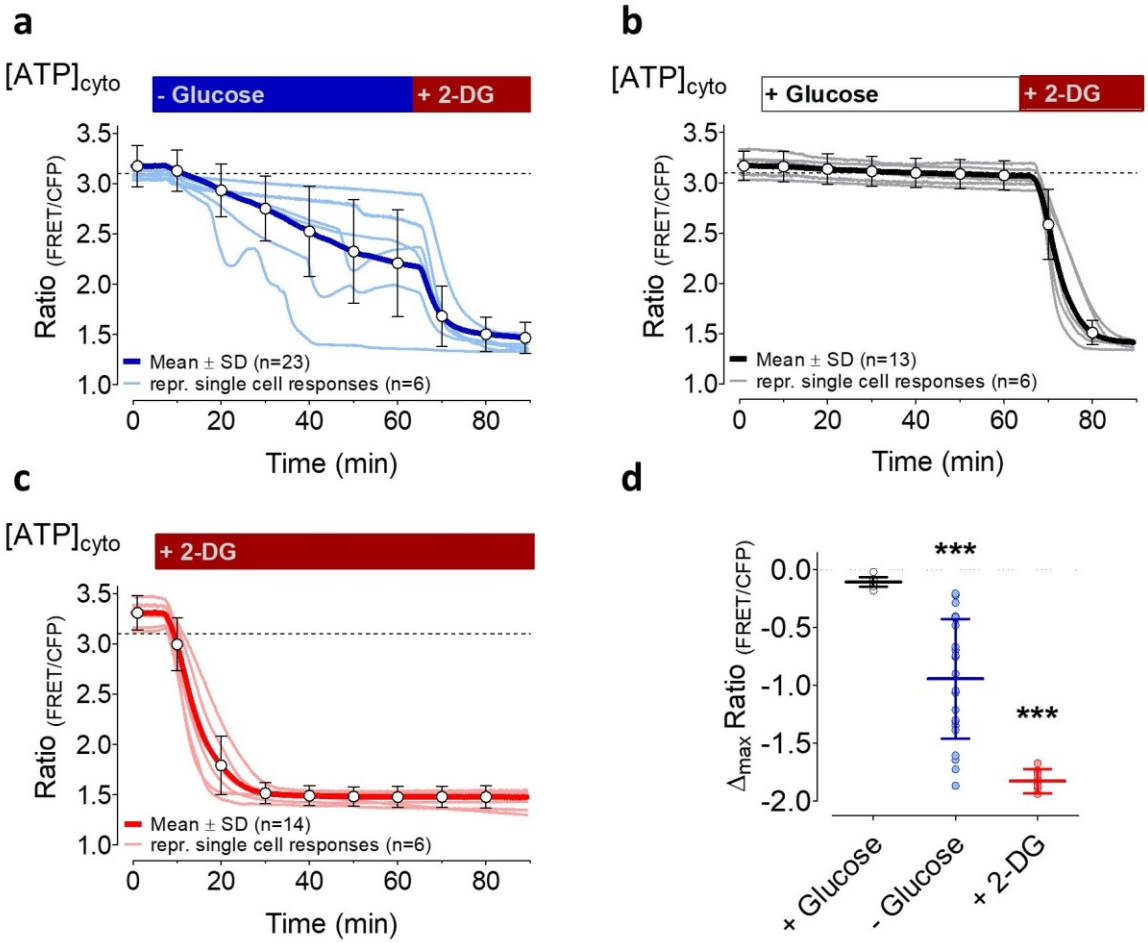

Figure 12: Cytosolic ATP dynamics over time in response to energy stress. (a) Representative curves (light blue) and the mean response (± SD, blue curve, n = 23 cells from three independent experiments) of FRET ratio changes of cytosolic AT1.03 in HeLa cells over time upon the removal of 10 mM glucose and the subsequent addition of 10 mM 2-deoxy-D-glucose (2-DG), as indicated; **(b)** Representative FRET ratio changes (grey) and mean curve (± SD, black curve, n = 13 cells from three independent experiments) of cytosolic AT1.03 in HeLa cells in the presence of 10 mM glucose and upon the addition of 10 mM 2-DG; **(c)** FRET ratio changes (light red) and mean curve (± SD, red curve, n = 14 cells from three independent experiments) of cytosolic AT1.03 in HeLa cells that were treated with 10 mM 2-DG; **(d)** Aligned dot plot with mean of maximal FRET ratio changes of AT1.03 between basal values and at time point 60 min. *** significant versus control (+ glucose); unpaired t-test, $p < 0.001$. (1) [Figure panels reproduced from Rauter et al., Cells 2020.]

These results indicate that while 2-DG maximally reduces $[ATP]_{cyto}$ persistently, glucose starvation leads to a more heterogeneous decline in cytosolic ATP levels. Despite this heterogeneity, however, a severe decrease in $[ATP]_{cyto}$ was observed in each tested cell underlining the essential role of glucose for the HeLa cell energy household.

4.4.2 The mitochondrial ATP pool is depleted to distinct plateau levels upon different energy stresses

Mitochondria are the powerhouse of the cell and the mitochondrial ATP pool can be defined as a central hub in cellular energy dynamics (140). As indicated, the measurements of mitochondrial ATP concentrations ($[ATP]_{mito}$) in single living HeLa cells were conducted via a genetically encoded FRET sensor targeted to the mitochondrial matrix (mtAT1.03 (136); **Figure 13a-c**).

To be able to correlate subcellular ATP levels in cytosol and mitochondria under the given energy stress conditions, the protocols were kept the same as described above. Strikingly, persistent glucose deprivation of HeLa cells over 60 minutes did not lead to such a heterogeneous depletion in $[ATP]_{mito}$ as seen for $[ATP]_{cyto}$. Nevertheless, a severe decrease in ATP levels could also be observed in mitochondria (**Figure 13a and d**). After a small transient peak, following the switch to glucose starvation buffer, $[ATP]_{mito}$ dropped quickly in all cells. Interestingly, mitochondrial ATP levels remained consistently lowered during the experiment (**Figure 13a**). The final addition of 2-DG after 60 minutes then further depleted $[ATP]_{mito}$ to a minimum, suggesting a different severity of energy stress in 2-DG treatment as compared to glucose starvation. In the constant presence of glucose, HeLa cells retained stable mitochondrial ATP levels over 60 minutes, while subsequent 2-DG treatment completely depleted ATP in the organelle to a minimum (**Figure 13b and d**). Finally, the consistency of 2-DG mediated ATP depletion was also tested for mitochondria. Immediate 2-DG treatment resulted in a rapid drop in $[ATP]_{mito}$ to a minimum in all cells and remained at this level over the observation period (**Figure 13c)**, as seen for $[ATP]_{cyto}$ (**Figure 12c and d**).

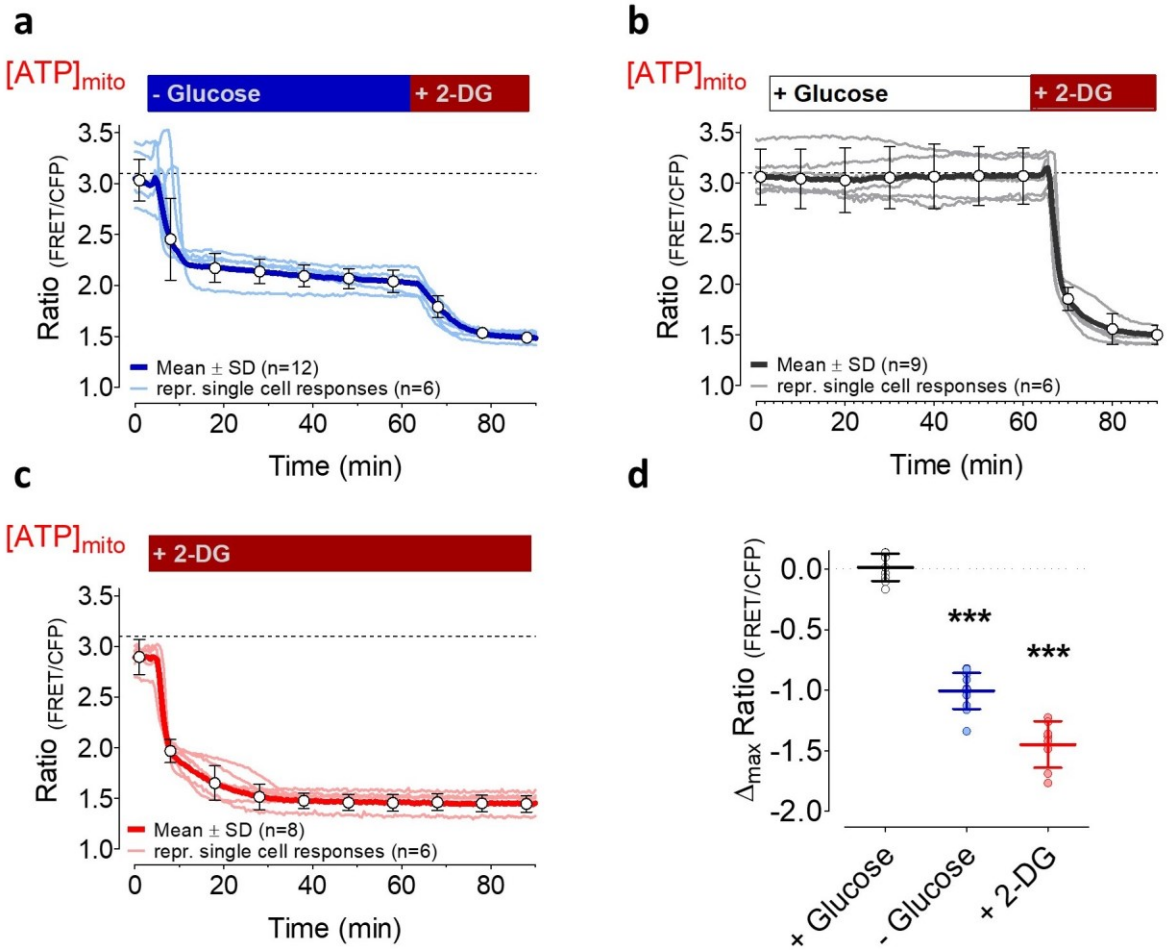

Figure 13: Mitochondrial ATP dynamics over time in response to energy stress. (a) Representative FRET ratio changes (light blue) and mean ratio changes (± SD, blue curve, n = 12 cells from three independent experiments) of mitochondria-targeted ATP-sensor mtAT1.03 upon glucose removal; **(b)** FRET ratio changes (grey) and mean response (± SD, black curve, n = 6 cells from three independent experiments) of mtAT1.03 over time in the presence of 10 mM glucose and the addition of 10 mM 2-DG; **(c)** Representative curves (light red) and mean ratio changes (± SD, red curve, n = 8 cells from three independent experiments) of mtAT1.03 upon replacement of glucose by 10 mM 2-DG, as indicated; **(d)** Aligned dot plot showing mean values of maximal FRET ratio changes of mtAT1.03 between basal values and values at time point 60 min. *** significant versus control (+ glucose), $p < 0.001$, unpaired t-test. (1) [Figure panels reproduced from Rauter et al., Cells 2020.]

These experiments demonstrate that ATP levels in cytosol and mitochondria can be influenced differentially. This is very much dependent on the kind of energy stress deployed. Glucose starvation represents a more moderate but still significant energy stress concerning its impact on ATP levels whilst treatment with the antimetabolite 2-DG is a much more severe and persistent stress for the HeLa cell (**Figure 13c and d**). These insights also indicate that the applied conditions of glucose starvation and 2-DG treatment are nicely

applicable to estimate the energy stress-resistance and dependency of ER-to-Golgi transport in HeLa cells in further experiments.

4.5 The impact of energy stress on ER-to-Golgi transport of HeLa cells

As the next step, the ER-to-Golgi transport quantification approach using high-resolution fluorescence imaging of single cells was combined with the established medium (-Glu) and harsh (+2-DG) energy stress conditions to assess the stress-resistance of HeLa cells. For this, our main cargo construct GFP-F_M4-GH, representing common bulk flow cargo, was expressed in HeLa cells and the transport was initiated after a 30 min (3 x 10 min) pre-treatment period (**Figure 8**). In subsequent analyses, the approach was also conducted with GFP-F_M4-VSVG_{tm} to confirm if the results were the same for cargo proteins requiring active sorting into COPII-vesicles. In all experiments, cells were co-transfected with the Golgi marker mCherry-Golgi-7 to allow quantification and proper focus as described above. Besides the classical depiction of changes in transport index over time, i.e. ER-to-Golgi secretory transport efficiency, a grouping approach was performed to gain additional information. This was possible because of the live cell measurements that allow following single cells over time and better projection of potential heterogeneities.

4.5.1 ER-to-Golgi transport efficiency in HeLa cells is robust and cargo-dependent

At first, ER-to-Golgi transport of soluble and transmembrane constructs was quantified using the newly established method (see 4.3) under control conditions i.e. in measurement buffer containing glucose. This allowed testing the consistency in this secretion step in HeLa cells upon initiation of the process via the addition of the solubilizer.

As observed in the other experiments, both constructs appeared as green fluorescent puncta before the addition of the solubilizing agent. Furthermore, the signal was quite homogenously distributed throughout the ER of each cell (**Figure 14**). There was hardly any leakage of the signal into the Golgi before transport initiation for any of the constructs. A clear disaggregation of transport construct followed by an efficient transport to the Golgi apparatus within minutes was observed in the tested cells – this was the case for both, the luminal

(GFP-F_M4-GH; **Figure 14a**) and the transmembrane construct (GFP-F_M4-$VSVG_{tm}$; **Figure 14b**). The visually conclusive results were then confirmed for both cargo types by the semi-automated image analysis approach in ImageJ (see 4.3.2 and **Figure 9**).

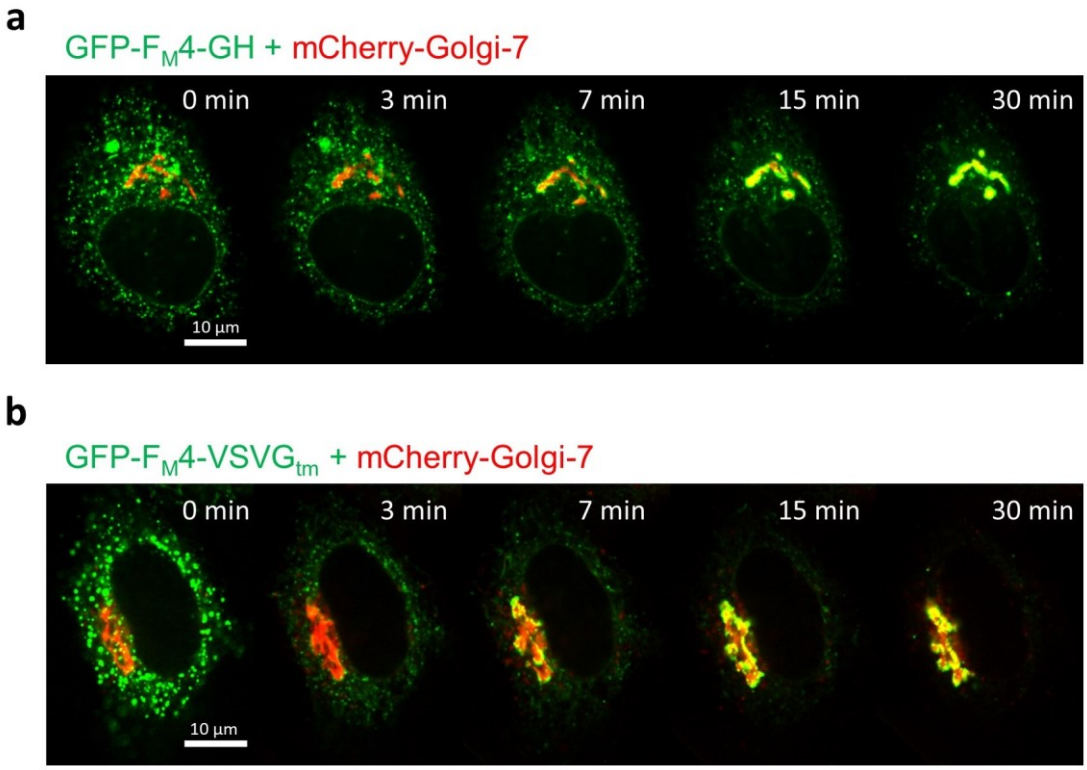

Figure 14: Visualizing the robust ER-to-Golgi transport of different cargos in living HeLa cells within minutes. Representative time-lapse image series showing the efficient ER-to-Golgi transport of soluble cargo (GFP-F_M4-GH, green, **(a)**) and transmembrane cargo (GFP-F_M4-$VSVG_{tm}$, green, **(b)**) over time in HeLa cells after D/D Solubilizer addition (at time point 0 min). Cells were co-transfected with mCherry-Golgi-7 (red channel). Scale bar represents 10 µm. (1) [Figure panel (a) reproduced from Rauter et al., Cells 2020.]

Interestingly, the dynamics for soluble and transmembrane cargo turned out to be quite different from each other. A comparison of quantification data for ER-to-Golgi transport of GFP-F_M4-GH versus GFP-FM4-$VSVG_{tm}$ revealed that the latter exhibits much faster kinetics (**Figure 15**). This might be due to the nature of this transmembrane cargo, which – in contrast to bulk flow cargo – is actively sorted (141) potentially increasing efficiency in its trafficking processes. These results indicate that HeLa cells display fast and efficient secretory protein trafficking from ER to Golgi, likely also in a cargo-dependent manner. Interestingly, actively sorted transmembrane cargo shows faster trafficking than bulk-flow cargo.

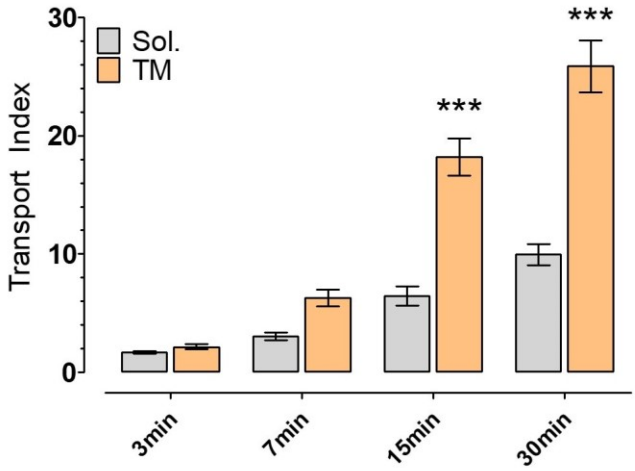

Figure 15: Differences in ER-to-Golgi transport efficiency between different cargo constructs in HeLa cells. Comparison of the calculated mean transport indices of cell populations for illustration of the ER-to-Golgi transport efficiency of soluble cargo (Sol.; GFP-F_M4-GH; n = 66 cells from 4 independent experiments) or transmembrane cargo (TM; GFP-F_M4-$VSVG_{tm}$; n = 58 cells from 4 independent experiments), respectively. Bars represent mean values ± SEM. *** significant versus Sol. at the same time point $p < 0.001$; Two-way ANOVA and Bonferroni post hoc test.

4.5.2 Strong ATP depletion by glucose starvation does not decrease ER-to-Golgi transport but 2-DG treatment completely abolishes it

In the next step, we looked at the ER-to-Golgi transport in HeLa cells that were pre-treated to induce energy stress. As established before, glucose starvation representing a more moderate energy stress condition mimicking natural conditions that cancer cells might encounter in a tumor as well as 2-DG treatment as a variation of harsh stress induction were applied. The treatments started 30 minutes before transport initiation for both, glucose removal and 2-DG treatment (**Figure 8**).

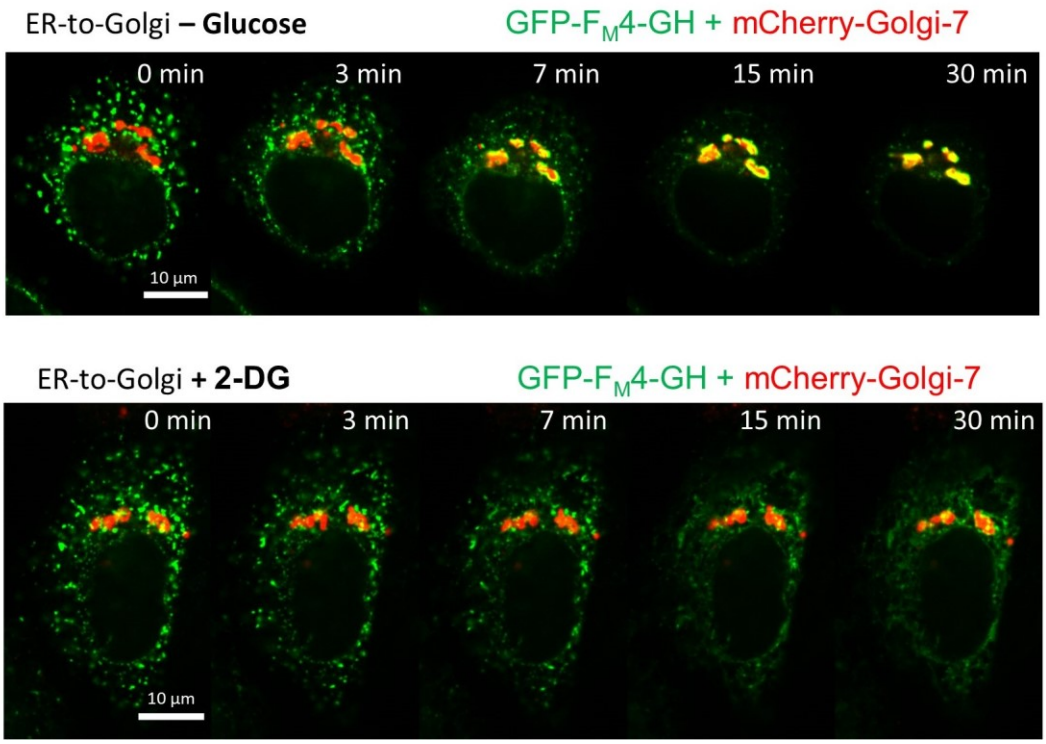

Figure 16: Different effects of mild and severe energy stress on ER-to-Golgi protein trafficking. Representative time-course images of HeLa cells expressing GFP-F$_M$4-GH and mCherry-Golgi-7 showing the effect of short-term glucose starvation (top) and 2-DG treatment (bottom) on ER-to-Golgi transport. Images showing an overlay of green and red fluorescence channel were taken before (0 min) and 3, 7, 15 or 30 min after transport initiation by solubilizer addition. Scale bar represents 10 µm. (1) [Figure panels reproduced from Rauter et al., Cells 2020.]

Surprisingly, despite the severe reduction in cytosolic and mitochondrial ATP under glucose starvation (**Figure 12 and Figure 13**) the quantification of ER-to-Golgi transport data shows no decrease in transport efficiency at any time point for the soluble cargo (GFP-F$_M$4-GH, **Figure 16**, upper panel). On the contrary, there is even a trend hinting at a slightly enhanced transport under these conditions as compared to control cells in transport quantification data (**Figure 17**). After 30 minutes of 2-DG treatment, however, the transport in the vast majority of tested HeLa cells was abolished completely (and visibly, **Figure 16**, lower panel), yielding constantly low transport indices over the whole transport process (**Figure 17**).

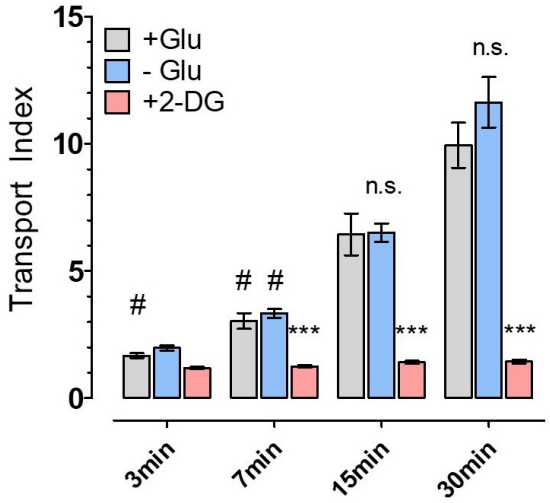

Figure 17: ER-to-Golgi transport of luminal cargo is not decreased by glucose deprivation but abolished by 2-DG treatment. Mean transport index comparison of HeLa cells of different pretreatment conditions (+ Glu (grey), n = 66 cells, − Glu (blue), n = 78 cells, + 2-DG (red), n = 61 cells; measured in ≥ three independent experiments) at the indicated time points after transport initiation. Bars represent mean ± SEM. n.s. not significant versus control (+ Glu) at the same time point, *** significant versus control (+ Glu) at the same time point $p < 0.001$, # significant versus all other time points of the same condition $p < 0.05$, Kruskal–Wallis test and Dunn's post hoc test. (1) [Figure panel reproduced from Rauter et al., Cells 2020.]

To investigate if the transport of transmembrane cargo follows the same trends as the bulk-flow cargo, the experiments were repeated with GFP-F_M4-VSVG$_{tm}$, co-transfected again with mCherry-Golgi-7 as the Golgi marker. Interestingly, despite the different trafficking mechanisms for these cargo constructs, the analysis confirmed that the energy stress-resistance of ER-to-Golgi transport in HeLa cells challenged by glucose deprivation is also very high for actively sorted transmembrane cargo. Under glucose starvation conditions HeLa cells showed slightly enhanced transport efficiency for GFP-F_M4-VSVG$_{tm}$ (**Figure 18**) compared to controls. 2-DG treatment led to similarly striking prevention of ER-to-Golgi transport (**Figure 18**) as seen for the soluble cargo (**Figure 17**); over 90 % of cells did not show any visible transport of the construct to the Golgi in the presence of 2-DG.

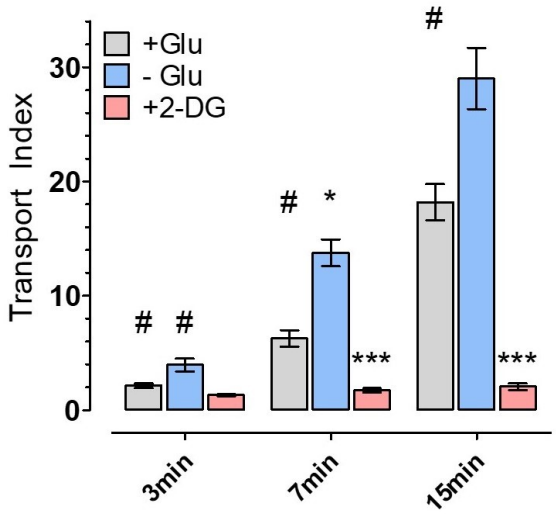

Figure 18: Impact of energy stress on ER-to-Golgi transport of transmembrane cargo is higher compared to soluble cargo. Transport index comparison of HeLa cells of different pretreatment conditions (+ Glu (grey), n = 58 cells, − Glu (blue), n = 39 cells, + 2-DG (red), n = 51 cells; measured in ≥ three independent experiments) at the indicated time points after transport initiation. Bars represent mean ± SEM. * significant versus control (+ Glu) at the same time point $p < 0.05$, *** $p < 0.001$; # significant versus all other time points of the same condition $p < 0.05$, Kruskal–Wallis test and Dunn's post hoc test. (1) [Figure panel reproduced from Rauter et al., Cells 2020.]

Based on this data, it can be concluded that although glucose starvation for 30 minutes significantly diminishes subcellular ATP pools (**Figure 12 and Figure 13**), there is no decrease in ER-to-Golgi transport efficiency for soluble or transmembrane cargo. This might have implications in cancer cell life since a functioning secretory pathway allows the secretion of matrix metalloproteinases, growth factors and many other crucial factors. Interestingly, 2-DG treatment abolished secretory transport of both cargo types, potentially hinting at a multiplicity of inhibitory effects on the secretory and sorting machinery by the antimetabolite.

4.5.3 A novel classification approach allows the superior depiction of cell-to-cell heterogeneity and confirms transport facilitation under glucose starvation

Since the secretory transport data was collected in time-lapse experiments following single living HeLa cells over time, there is additional information about temporal dynamics in ER-to-

Golgi transport for each cell. During the quantification process, it became clear that there is certain heterogeneity in ER-to-Golgi transport efficiencies of HeLa cells for both cargo protein types. To better depict this and also illustrate the temporal dynamics in transport indices, a clustering – or classification – approach was introduced based on the data collected in 4.5.1 and 4.5.2. The cells were clustered based on the semi-automatically calculated transport indices of control samples and visualized by arbitrarily classifying them into certain groups of different ER-to-Golgi transport efficiency. These groups were defined to contain cells with “no visible transport”, “moderate”, “high” or “very high” transport efficiency. Such a classification can be performed on soluble and on transmembrane cargo results (**Figure 19**) and was confirmed by checking the respective images in the four clusters (**Figure 20**).

Within this arbitrary classification system, the different stress conditions can be compared to the controls for a certain construct in the HeLa cell model (**Figure 21a-c**). The results for the main cargo construct – the luminal, bulk-flow cargo GFP-F_M4-GH – revealed that despite marginally increased mean transport efficiency (**Figure 17**) there is roughly a 10% increase in the group of cells showing very high ER-to-Golgi transport efficiency (**Figure 21a**, left panel, **and b**) as compared to control conditions (**Figure 21c**). On the other hand, this means there was a lower percentage of cells to be classified as showing moderate or low transport (**Figure 21a**) underlining the potential facilitation of ER-to-Golgi transport of bulk-flow cargo upon glucose starvation. 2-DG treatment almost completely prevented ER-to-Golgi transport of the soluble construct, as reflected in the mean transport index (**Figure 17**), resulting in a hard shift of percentages in favor of the group showing no visible transport. Over 80 % of cells did not show any visible ER-to-Golgi transport, while the rest only displayed moderate trafficking capacity (**Figure 21b and c**).

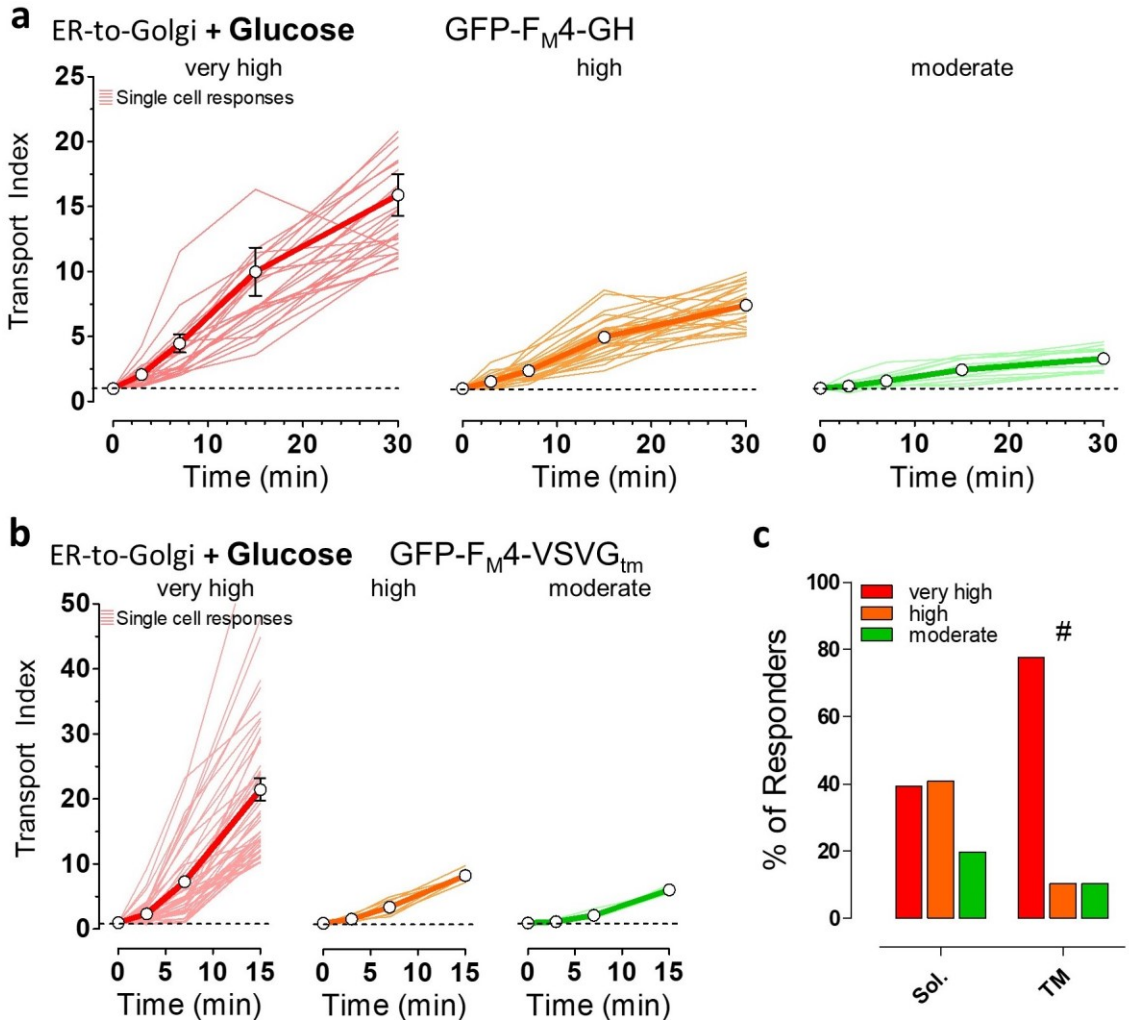

Figure 19: Classification of synchronized ER-to-Golgi transport using soluble and transmembrane FP-labeled cargos. (a) ER-to-Golgi transport of the soluble transport construct, GFP-F$_M$4-GH in single HeLa cells (thin lines, n = 66 cells from 4 independent experiments) and respective mean ± SEM curves over time upon the addition of 250 nM solubilizer in the presence of 10 mM glucose. Transport efficiency was classified as very high (red curves, transport index >10 at 30 min), high (orange curves, transport index >5, <10 at 30 min), and moderate (green curves, transport index >2, <5 at 30 min); **(b)** ER-to-Golgi transport of the transmembrane cargo construct (GFP-F$_M$4-VSVG$_{tm}$) under same conditions as described for panel (a). Classification of transmembrane cargo transport efficiency is based on the transport index after 15 min, i.e., very high transport (red curves, transport index > 10), high transport (orange curves, transport index >7, <10), and moderate transport (green curves, transport index >4, <7); **(c)** Bars showing the percentage of the different ER-to-Golgi transport efficiencies (very high, high, and moderate) of the soluble (Sol., left bars) and transmembrane (TM, right bars) cargo. Data are extracted from panels (a) and (b), respectively. # significant versus Sol. $p < 0.05$, Chi-square test. (1) [Figure panels reproduced from Rauter et al., Cells 2020.]

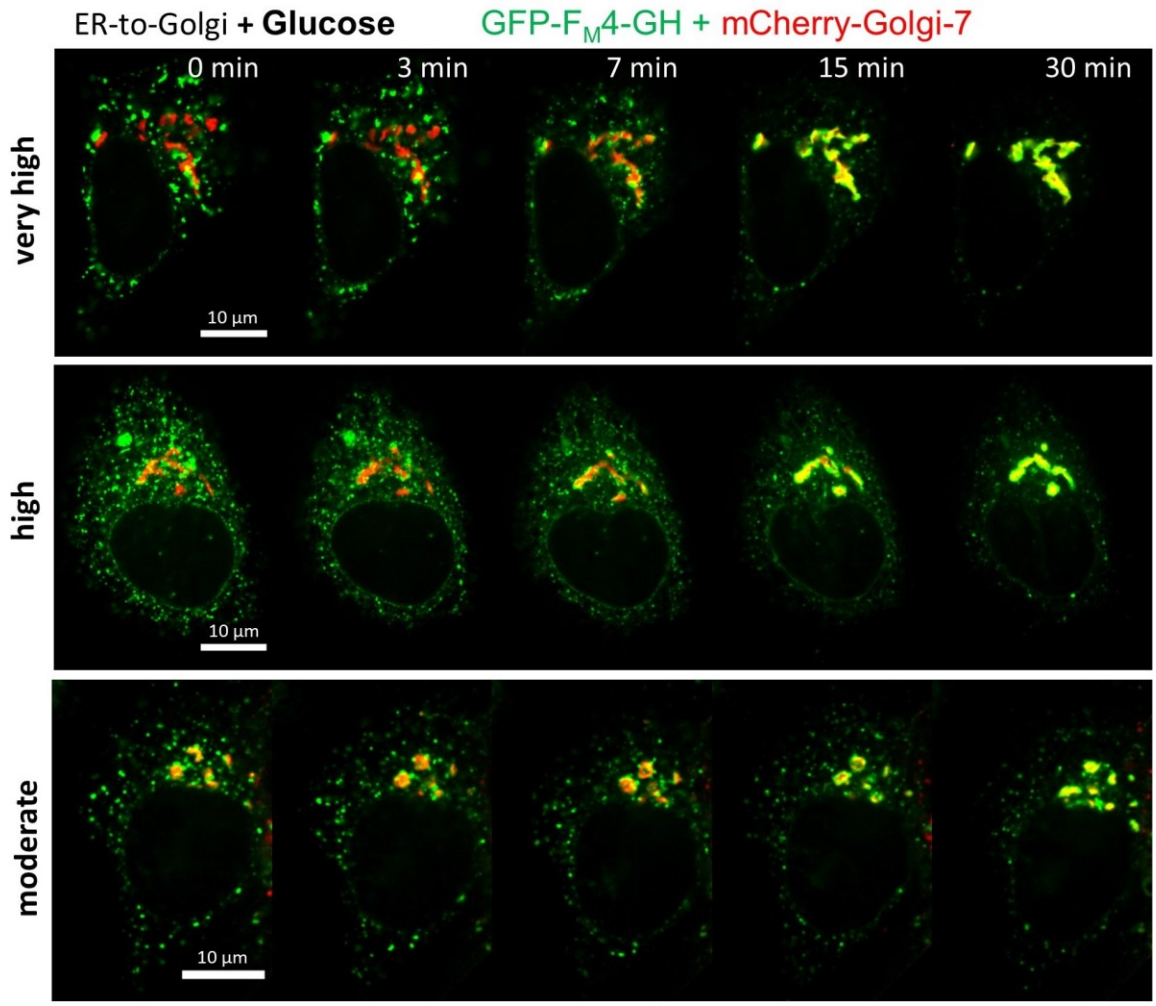

Figure 20: Time-lapse images of ER-to-Golgi transport in cells showing different trafficking efficiency based on the arbitrary classification system. Representative images showing HeLa cells expressing GFP-F_M4-GH, soluble cargo construct (in green), and mCherry-Golgi-7, Golgi marker (in red), and merged signals (in yellow) at the indicated time points upon the addition of 250 nM solubilizer in the presence of 10 mM glucose ("control conditions"). ER-to-Golgi transport was classified as very high (upper panel), high (middle panel), and moderate (lower panel). A 100× magnification objective was used, scale bars indicate 10 µm in every image of the time course. (1) [Figure panels reproduced from Rauter et al., Cells 2020.]

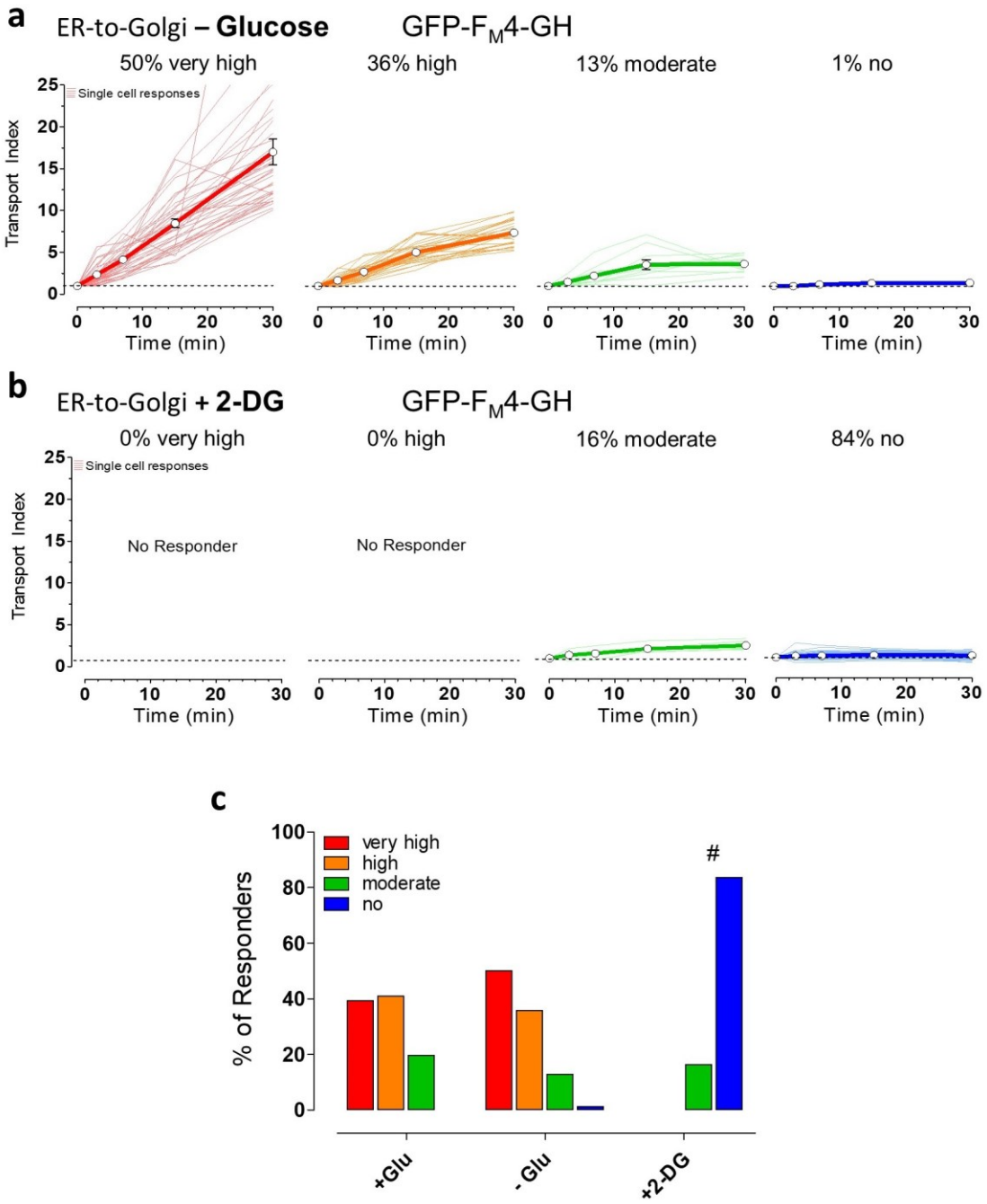

Figure 21: The classification system for ER-to-Golgi transport efficiency confirms cell population results and offers additional readouts. (a) ER-to-Golgi transport of GFP-F$_M$4-GH in glucose-deprived single HeLa cells (n = 78 cells from 3 independent experiments) showing very high (red, transport index at 30 min >10), high (orange, transport index >5, <10), moderate transport index (green, transport index >2, <5), and no transport (blue, transport index <2). Cells were treated with buffer without glucose for 30 min prior to transport initiation by the addition of 250 nM solubilizer at 37 °C; **(b)** Classification as described in panel (a) of ER-to-Golgi transport in HeLa cells that were treated with 10 mM 2-DG, during and before (30 min) the addition of 250 nM solubilizer (n = 61 cells from 4 independent experiments). **(c)** Bars show the percentages of different ER-to-Golgi transport

efficiencies in presence of 10 mM glucose (left bars, + Glu, control, n = 66 cells from 4 independent experiments), the absence of glucose (middle bars, − Glu, n = 78 cells from 3 independent experiments) and upon cell treatment with 10 mM 2-DG (right bars, + 2-DG, n = 61 cells from 4 independent experiments). # significant versus + Glu $p < 0.05$, Chi-square test. (1) [Figure panels reproduced from Rauter et al., Cells 2020.]

When looking at the classification for transmembrane cargo, the trend of an increased ER-to-Golgi transport efficiency under glucose starvation conditions and the massive depletion effect by 2-DG (**Figure 18**) could be confirmed as well (**Figure 22a-c**). Compared to the percentages of control cells clustered into the groups showing no, moderate, high or very high efficiency in anterograde ER-to-Golgi trafficking, there was a clear shift for both energy stress conditions (**Figure 22a and b**). Again, there were 10% more of the cells showing very high transport efficiency under glucose starvation (**Figure 22a and c**) than under control conditions (**Figure 22c**), accompanied by a decrease in the categories defined to contain less efficiently transporting cells. Interestingly, the trend of facilitating effects of glucose starvation on ER-to-Golgi transport was found to be more distinct in transmembrane cargo experiments – especially early after transport initiation (**Figure 23**), indicating not only implications of transport itself, but potentially also cargo sorting processes. On the other hand 2-DG mediated a similarly striking preventing effect on ER-to-Golgi transport for both cargos (**Figure 23**).

Overall, the classification system allowed a superior visualization of single-cell responses and offered an additional readout to the more established mean and variance measures of transport indices. Furthermore, the depiction method nicely illustrates the heterogeneity in dynamics of ER-to-Golgi transport between individual cells.

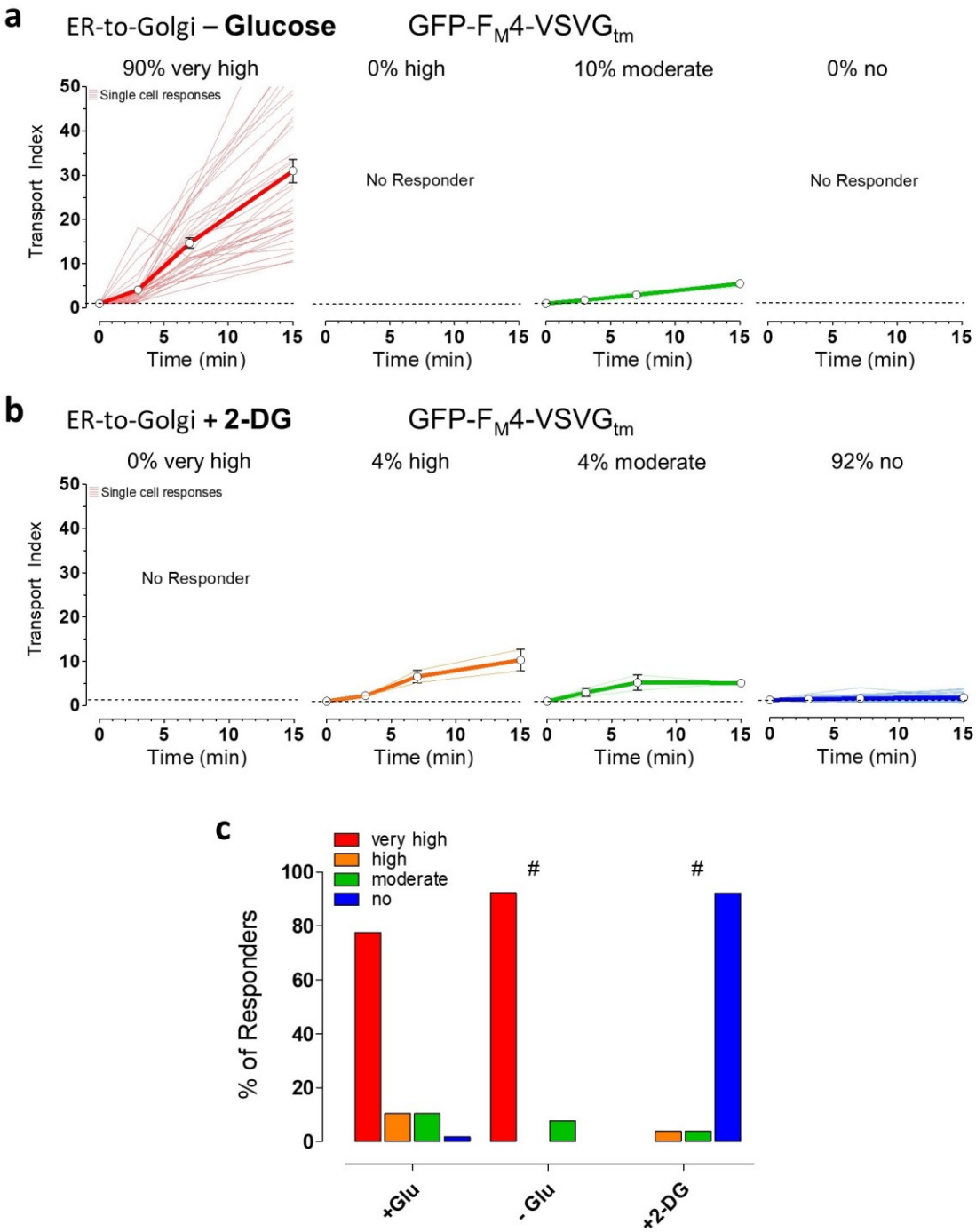

Figure 22: ER-to-Golgi transport of transmembrane cargo is slightly facilitated under glucose starvation, while almost completely prevented under 2-DG. (a) Classification of glucose-deprived HeLa cells (n = 39 cells from 3 independent experiments) based on the efficiency of ER-to-Golgi transport of GFP-F$_M$4-VSVG$_{tm}$. Cells were treated with buffer lacking glucose for 30 min prior to transport initiation. Transport was classified as very high (red, transport index at 15 min >10), high (orange, transport index >7, <10), moderate (green, transport index >4, <7), or no transport (blue, transport index <4); **(b)** Classification of 2-DG-treated HeLa cells (n = 51 cells from 4 independent experiments) based on ER-to-Golgi transport efficiency. Transport was initiated and measured after pretreating cells with buffer containing 10 mM 2-DG for 30 min before the addition of solubilizer; **(c)**

Comparison of the percentages of tested HeLa cells in the four classes for each pretreatment condition. Cells were treated for 30 min before transport initiation with buffer containing 10 mM glucose (+ Glu, control, n = 58 cells from 4 independent experiments), no glucose (− Glu, n = 39 cells from 3 independent experiments), or 10 mM 2-DG (+ 2-DG, n = 51 cells from 4 independent experiments). # significant versus + Glu $p < 0.05$, Chi-square test. (1) [Figure panels reproduced from Rauter et al., Cells 2020.]

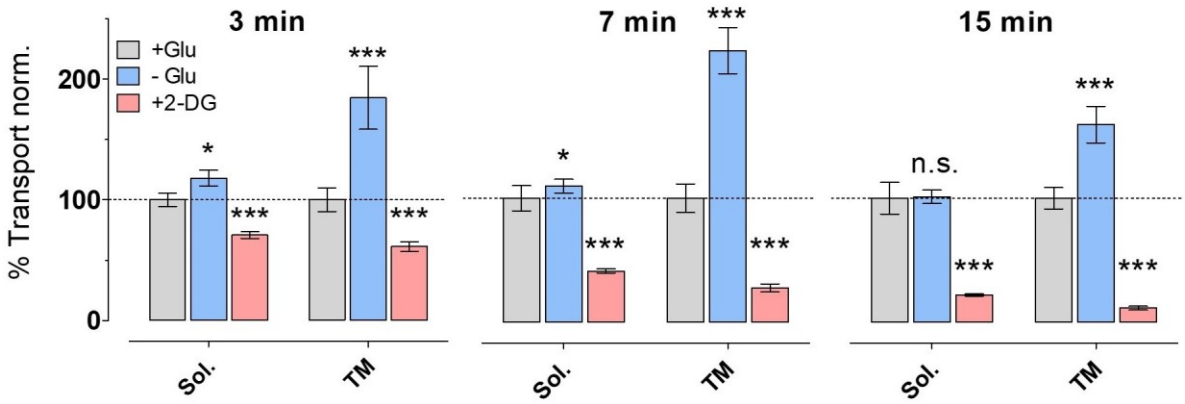

Figure 23: Comparison of energy stress effects on ER-to-Golgi transport of soluble vs. transmembrane cargo via mean transport index at early time points. Transport of soluble (Sol., GFP-F_M4-GH) and transmembrane construct (TM, GFP-F_M4-$VSVG_{tm}$) normalized to control conditions at indicated time points. Data from Figure 21 and 22. Bars represent mean values ± SEM. * significant versus control (+ Glu) at the same condition $p < 0.05$, *** $p < 0.001$, Mann–Whitney U test. (1) [Figure panel reproduced from Rauter et al., Cells 2020.]

4.5.4 Disaggregation of ligand-sensitive protein transport constructs is not impaired under severe energy stress

The drastic decrease of ER-to-Golgi transport efficiency upon introduction of severe energy stress in the form of 2-DG addition can indeed have several biological reasons. It is therefore important to exclude that a mechanistic feature of the transport constructs applied in the experiments might be an influencing factor. The specific properties of these constructs, as described before, involve the aggregation in the ER, which can only be reversed by the addition of solubilizer thereby leading to disaggregation of the fluorescent puncta and subsequently allow their ER-to-Golgi transport initiation. To make sure that the energy stress induction by 2-DG did not impair proper disaggregation in the first place (which would result

in similarly low transport indices) the time-lapse images of 2-DG treated HeLa cells before and after solubilizer-addition were re-analyzed.

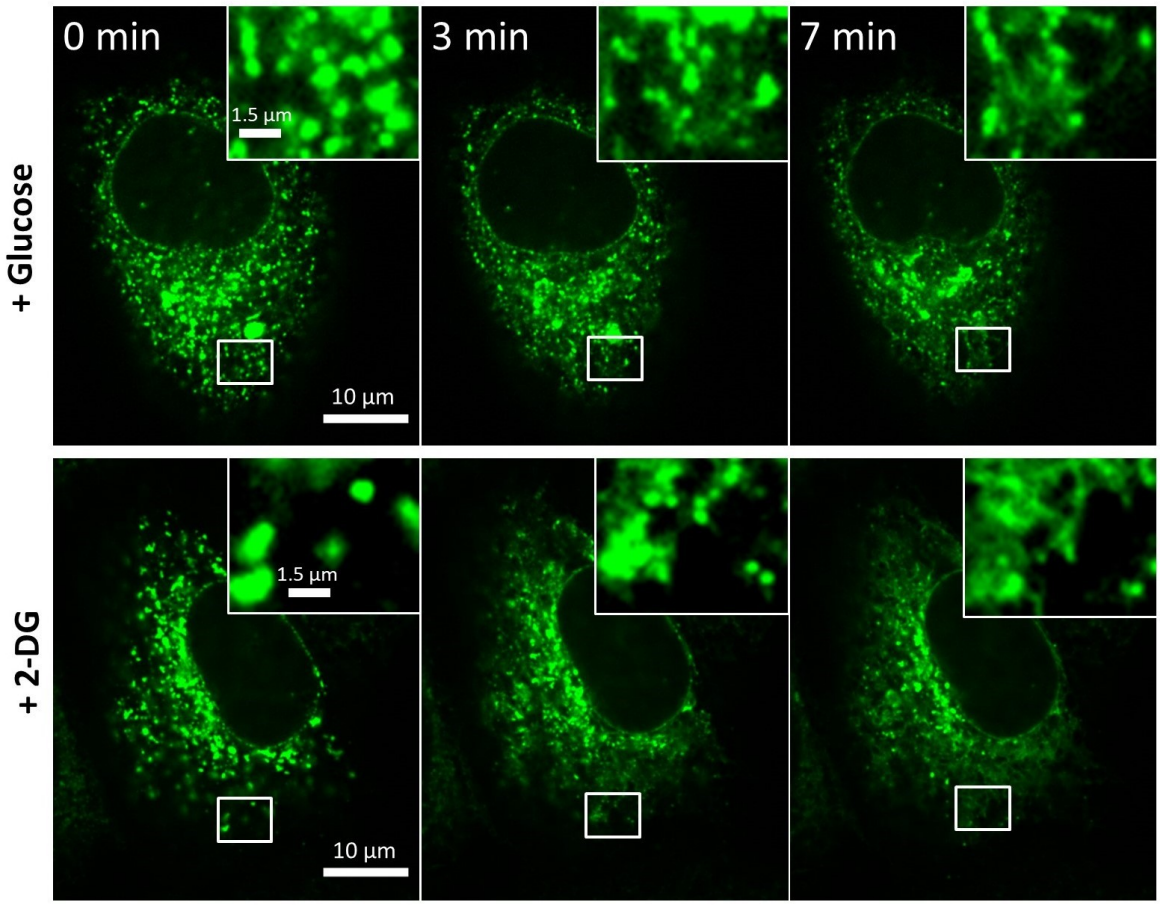

Figure 24: Disaggregation of CAD-based constructs is not impaired under severe energy stress. Representative images showing HeLa cells expressing the soluble cargo construct GFP-F_M4-GH treated with 10 mM glucose containing buffer (upper row, n = 66 cells from 4 independent experiments) or 10 mM 2-DG containing buffer (lower row, n = 61 cells from 4 independent experiments) prior to and at indicated time points after solubilizer-addition (250 nM). Zoom-in with optimized scaling of a representative region (white square) was added for each image. Images were taken with a 100x magnification objective; scale bars in large images represent 10 µm, scale bar in zoomed images 1.5 µm for every image in the respective time course. (1) [Figure panel reproduced from Rauter et al., Cells 2020.]

All tested cells displayed clear disaggregation within minutes upon solubilizer addition regardless of the treatment (**Figure 24**). To further quantify these results, a custom ImageJ algorithm was written to analyze the form factor of fluorescent constructs within the first time points (0 min, 3 min, 7 min). The form factor is a value representing the circularity of a structure. A value of 1 hereby describes a perfect circle and the higher the number gets the

less circular a form is. Based on this principle numbers closer to 1 were expected as a mean form factor of the more circular puncta structures on images taken before solubilizer addition, while a disaggregation would reveal the net-like, elongated structures of the ER (as seen in **Figure 24**; form factor >1). Time-lapse images of the first few minutes for control cells and 2-DG treated cell expressing GFP-F_M4-GH were analyzed and the hypothesis and the results from the visual image analysis were confirmed. Form factors of control and 2-DG treated cells start at similar values close to 1 describing a comparable starting situation of more circular fluorescent aggregates in the ER, while both groups show significantly increased form factors after 7 minutes confirming proper disaggregation (**Figure 25**). Interestingly, the form factor values at time point 7 min for 2-DG treated cells are significantly higher than for control cells. This is likely because 2-DG cells lack proper ER-to-Golgi transport and display ER-like net structures with increasing fluorescence intensity over time, while control cells already start to transport the construct into the Golgi immediately upon disaggregation.

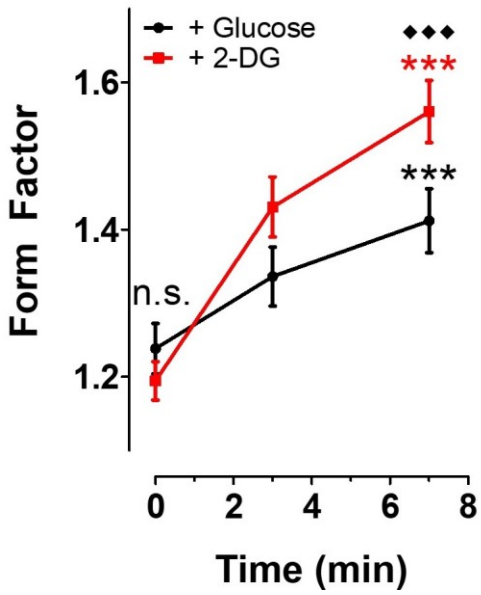

Figure 25: Form Factor changes confirm unrestricted disaggregation of CAD-constructs upon 2-DG treatment. Statistical evaluation of disaggregation of cargo construct upon solubilizer addition represented by increase in form factor. Data from HeLa cells pre-treated for 30 min with 10 mM glucose buffer (n = 66 cells from 4 independent experiments) and 10 mM 2-DG buffer (n = 61 cells from 4 independent experiments) were taken for the analysis. A custom-made macro enabled the calculation of the median form factor of all green structures in the non-Golgi region. Mean of all cells ± SEM is plotted in the graph. n.s. not significant versus +Glu 0min, *** significant versus +Glu 0min $p<0.001$, *** (red) significant versus +2-DG 0min $p<0.001$, ◆◆◆ significant versus +Glu 7min $p<0.001$; Mann-Whitney-U test. (1) [Figure panel reproduced from Rauter et al., Cells 2020.]

4.6 Investigating the impact of energy stress on crucial parameters in protein secretion

The secretory transport of proteins is a highly complex process relying on numerous, often energy-dependent steps and cellular structures. As elaborated, cell treatment with the antimetabolite 2-DG even for a short time completely emptied subcellular ATP pools (**Figure 12 and Figure 13**) and abolished ER-to-Golgi transport in the cancer cell model HeLa (**Figures 17-23**). However, it is difficult to say if there is a direct causal impact of lacking ATP on ER-to-Golgi transport leading to an almost complete stop in the secretory activity. Some of the crucial parameters in secretory transport may be influenced first by 2-DG treatment or the ATP depletion followed by it, and then in turn prevent ER-to-Golgi trafficking. These parameters involve the cellular microtubule network, ER-morphology and the cellular GTP content.

4.6.1 The microtubule network is persistent and remains dynamic under energy stress

It is assumed that a large number of anterograde and retrograde trafficking processes rely on energy-dependent transport via motor proteins along cytoskeleton elements like microtubules – it is known that this is also the case for ER-to-Golgi transport (17–19,21). This brings up the question if 2-DG treatment, which prevents ER-to-Golgi transport in our cancer cell model, destroys the microtubule (MT) network thereby mediating this effect. Thus, we tested if MTs collapse upon the same energy stress induction by 2-DG, as applied in 4.5, by investigating GFP-α-tubulin signal distribution within HeLa cells using high-resolution confocal fluorescence imaging.

In both groups, the control group and the 2-DG treated group, sample cells displayed clear MT network structures immediately upon the start of treatment and imaging (0 min). Furthermore, a high dynamic of the green fluorescent MTs was observed, manifested in continuous re-organization and re-shaping of the MT network over time (**Figure 26a**). This also indicated similar functioning cytoskeleton dynamics under control conditions and upon 2-DG treatment. After 60 minutes nocodazole, a chemical agent interfering with MT-polymerization processes, was added in a high concentration to provoke the collapse of the

MT-network and prove the natural property of MTs to quickly disintegrate. All samples showed fast and efficient disintegration of MTs within 10 minutes of nocodazole treatment and an almost complete collapse of green fluorescent tubule structures into free cytosolic signal after 20 minutes (**Figure 26a**).

To determine potential minor differences in MT stability for controls versus 2-DG treated cells, the images were analyzed using a custom-made ImageJ algorithm. A ratio of cytosolic versus microtubule fluorescence intensity was calculated. An increasing ratio represented more cytosolic respectively less MT signal, meaning a collapse of the MT network. The quantification data confirmed the visual impression of sample images, no difference in MT stability or amount was found between control and 2-DG samples (**Figure 26b**). This finding excludes lacking MT stability upon 2-DG treatment as a reason for 2-DG mediated ER-to-Golgi transport prevention.

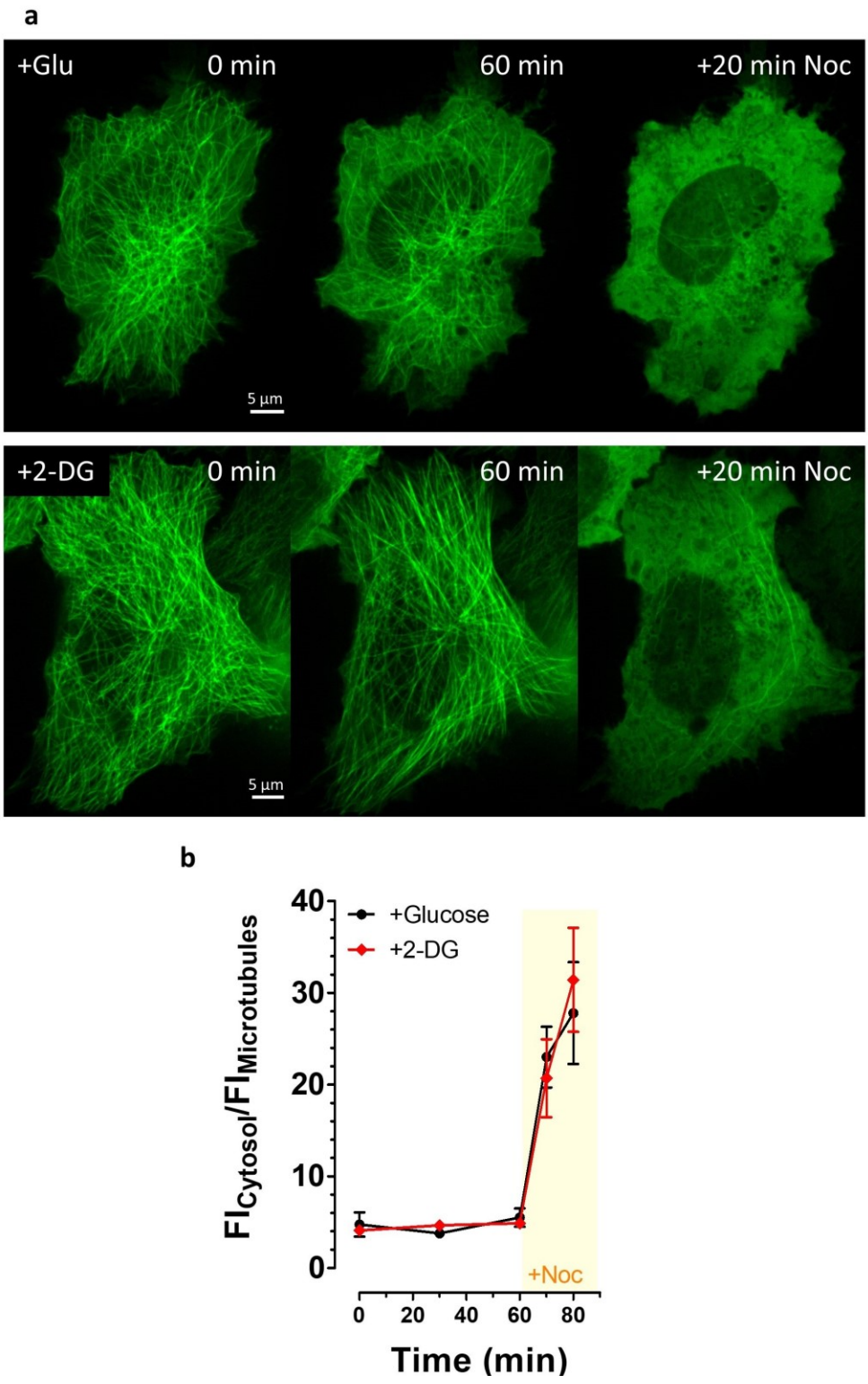

Figure 26: Severe energy depletion via 2-DG does not affect the microtubule network in HeLa cells. (a) Representative confocal images displaying HeLa cells expressing GFP-α-tubulin in buffer with 10 mM glucose (upper panel) or 10 mM 2-DG (lower panel). Images are shown for start (left), after 60 min (middle) and after subsequent 20 minutes of treatment with nocodazole ("+Noc", 10 µM,

right). A 100x magnification objective was used; scale bars represent 5 µm in both time courses. **(b)** Statistical analysis of microtubule disassembly expressed by the ratio of FI in cytosol divided by FI of microtubules. Ratios for controls (+Glu, black bullets, n = 12, from three independent experiments) and 2-DG treated cells (+2-DG, red squares, n = 15, from three independent experiments) are depicted over time, symbols represent mean ± SEM. The nocodazole treatment (10 µM) is indicated in yellow, beginning at 60 minutes, directly after the 60 min image was taken. (1) [Figure panel reproduced from Rauter et al., Cells 2020.]

4.6.2 ER-morphology is unchanged under energy stress

The ER is the first organelle in the secretory pathway and the initial trafficking and modification hub (3,26). Severe changes in the morphology of this crucial organelle might change the way cargo proteins are distributed. A comparison of the ER-morphology enabled by the expression of the fluorescent construct CP450-CPV in control cells (measurement buffer containing 10 µM glucose) and cells treated with measurement buffer lacking glucose (- Glucose) or containing 10 µM 2-DG (+2-DG) for 30 minutes was conducted. No changes were observed after this short-term energy stress period (**Figure 27**) marking the equivalent time point of transport initiation in ER-to-Golgi transport measurements.

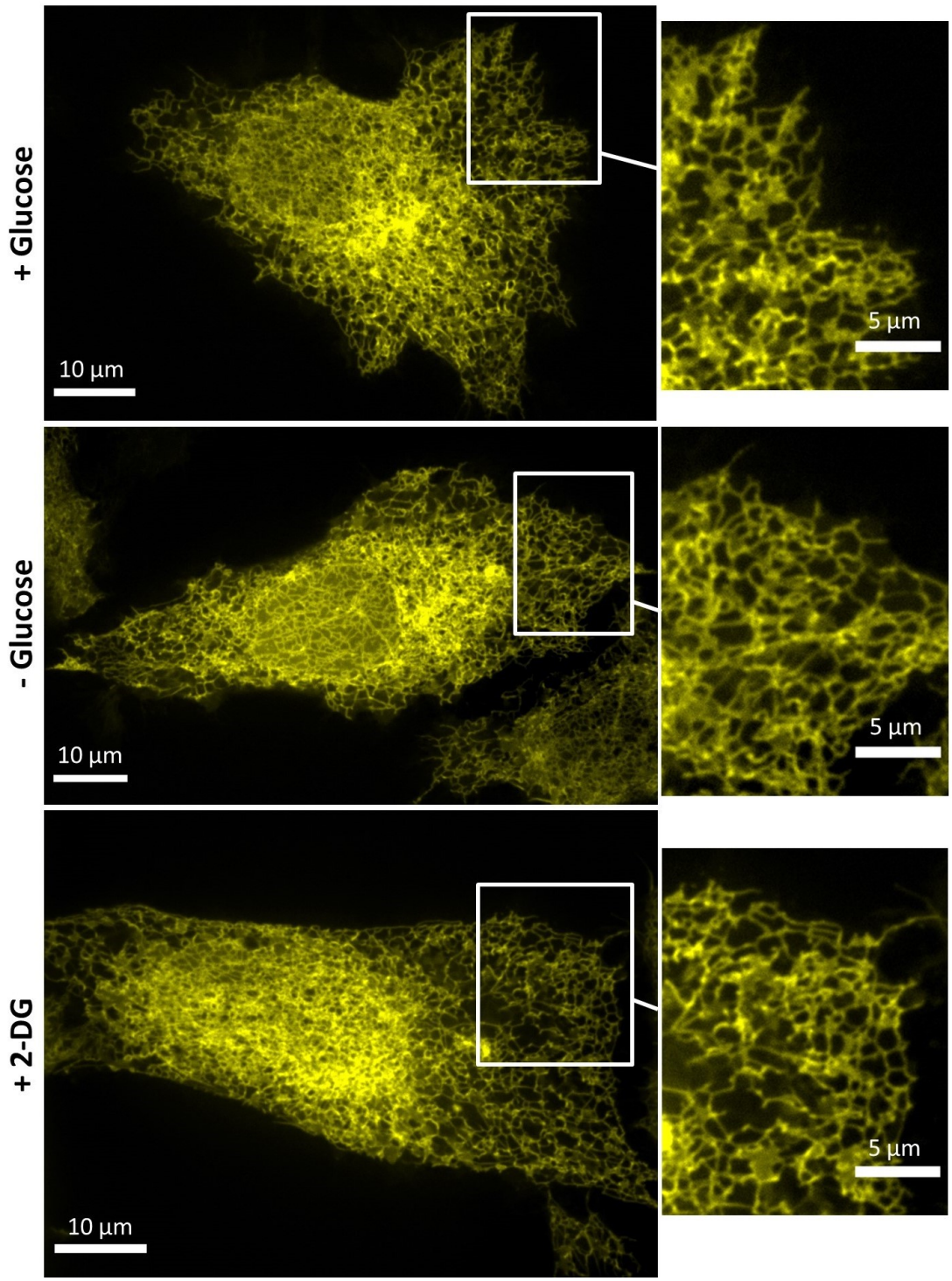

Figure 27: ER-morphology is not changed upon short-term energy stress in HeLa cells. Representative images in the left column show HeLa cells expressing CP450-CPV, a yellow fluorescent construct targeting to the ER membrane surface, under control conditions (+ Glucose), glucose deprivation (- Glucose), or 2-DG treatment (+ 2-DG) for 30 minutes prior to imaging. As indicated scale bars represent 10 µm and 5 µm in respective zooms. In the right column, a zoom into the outer regions of the fine ER-network structure is shown. (1) [Figure panel reproduced from Rauter et al., Cells 2020.]

4.6.3 Subcellular GTP concentrations are slightly increased upon 2-DG treatment

Guanosine-5'-triphosphate (GTP) is an important chemical energy carrier, which provides readily available energy for a variety of enzymatic reactions within a cell – especially in the context of protein trafficking (10). A lot of GTPases, which convert GTP during their respective enzymatic reaction, are involved in secretory processes. A crucial step in ER-to-Golgi transport is the initial formation of COPII transport vesicles (13,14) with Sar1, for example, being a well-investigated GTPase involved specifically in COPII-formation. The question of the influence of 2-DG on the cytosolic GTP concentration was therefore investigated by expressing the genetically encoded GTP-sensor GEVAL (GEVAL530 (138)) in HeLa cells.

HeLa cells were transfected with the respective construct and changes in cytosolic GTP levels ($[GTP]_{cyto}$) were measured via live-cell wide field microscopy in single cells. The cells were excited at 385 nm and 470 nm (**Figure 28a**) and a ratio was calculated, since due to its properties this single FP-based sensor reacts with an increase of emission at excitation < 450 nm and a decrease at excitation > 450 nm, when GTP increases (138). There were no differences in basal GTP values among the tested cells indicating a balanced starting situation (**Figure 28b**). Under control conditions ratio signals remained consistent over the observation time of 60 minutes (**Figure 28c**), indicating stable GTP levels. Upon glucose starvation, however, a consistent increase of the GEVAL fluorescence ratio signal over time was observed, indicating GTP elevations in response to the moderate energy stress (**Figure 28c**). Surprisingly, 2-DG treatment, which led to a complete depletion of ER-to-Golgi transport (see 4.5), did not lower GTP levels as expected, but promptly and strongly elevated cytosolic GTP (**Figure 28c and d**). These remarkable results suggest that 2-DG does not prevent ER-to-Golgi transport by depleting GTP levels similarly strong as ATP levels.

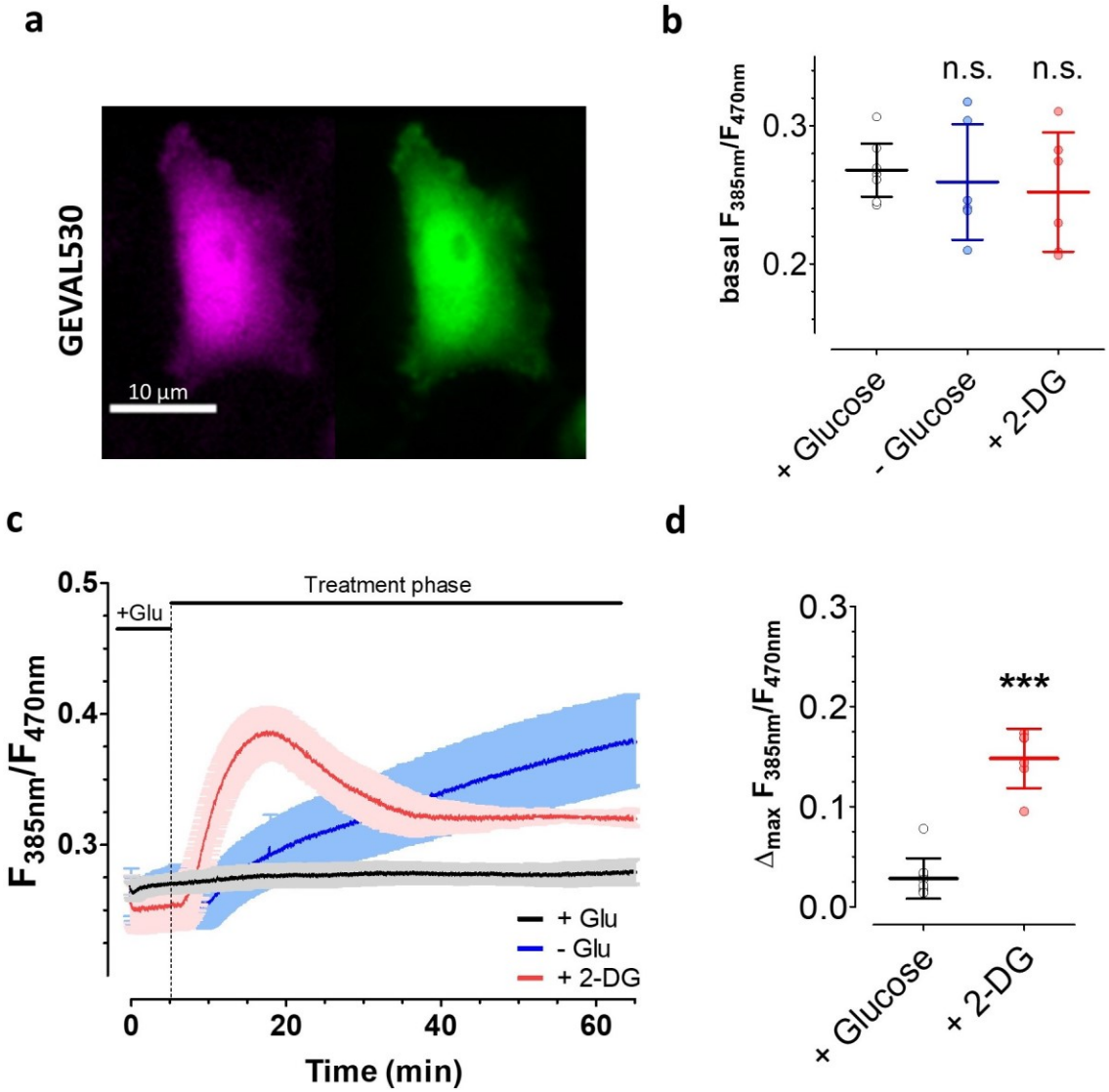

Figure 28: Global GTP concentrations are not decreased but slightly increased upon short-term energy stress in HeLa cells. (a) Representative Images showing a HeLa cell expressing the genetically encoded GTP-sensor GEVAL530 excited at 385 nm (left) and 470 nm (right) as taken for ratio calculations in (b-d). Scale bar represents 10 µm. **(b)** Aligned dot plot showing mean basal ratios for controls and energy stress conditions (+ Glu; n = 9 cells, - Glu: n = 6 cells, 2-DG: n = 6 cells; each from three independent experiments). n.s. not significant against control (+Glu); Kruskal-Wallis test and Dunn's post hoc test. **(c)** Dynamic GTP signals (mean value) over time upon perfusion switch from control buffer (+Glu) to respective color-coded treatment buffer ("Treatment phase") containing 10 mM glucose (+ Glu), no glucose (- Glu) or 10 mM 2-DG (+2-DG) from time point 5 min. Light colored halos represent ± SEM. **(d)** Dot plot illustrating maximum delta in GTP concentrations upon conducted protocol from (c). *** significant versus + Glu, $p < 0.001$; Mann-Whitney U test.

4.7 Induction of short-term energy stress alters subcellular Ca^{2+} concentrations and dynamics

Ca^{2+}-concentrations in cytosol and cellular organelles as well as their dynamics and mobilization properties are amongst the most considerable factors when investigating energy metabolism due to the inseparable connection between ATP and Ca^{2+} signals and signaling (110,111). Hence, we investigated if the introduction of energy stress leads to a modification of subcellular Ca^{2+} levels and dynamics in HeLa cells by applying the small chemical Ca^{2+} indicator FURA-2 and the genetically encoded ER-targeted fluorescent Ca^{2+} biosensor D1ER.

The main transporter suggested to uphold elevated Ca^{2+} concentrations in the ER against the cytosolic pool under natural conditions, the (sarco)endoplasmic reticulum calcium ATPase (SERCA), is known to be highly energy-dependent (142). For this reason, we expected the ER Ca^{2+} content ($[Ca^{2+}]_{ER}$) to be reduced due to the ATP depletion under energy stress. However, we found no significant differences between controls and energy stress conditions in the FRET ratio signal of D1ER (**Figure 29a**, left panel), an established genetically encoded Ca^{2+} sensor targeted to the lumen of the ER (137). This indicates that energy stress does not lead to a lower $[Ca^{2+}]_{ER}$ despite the strong energy-dependency of SERCA. The basal Ca^{2+} concentrations in the cytosol, on the other hand, were slightly increased under glucose starvation compared to control cell values (**Figure 29a**, right panel), as measured with the small chemical Ca^{2+} sensor FURA-2 in parallel experiments. Exchange of glucose with 2-DG, which rapidly depletes subcellular ATP pools (**Figure 12 and Figure 13**), led to an even stronger elevation of basal cytosolic Ca^{2+} concentrations ($[Ca^{2+}]_{cyto}$) compared to mere glucose starvation.

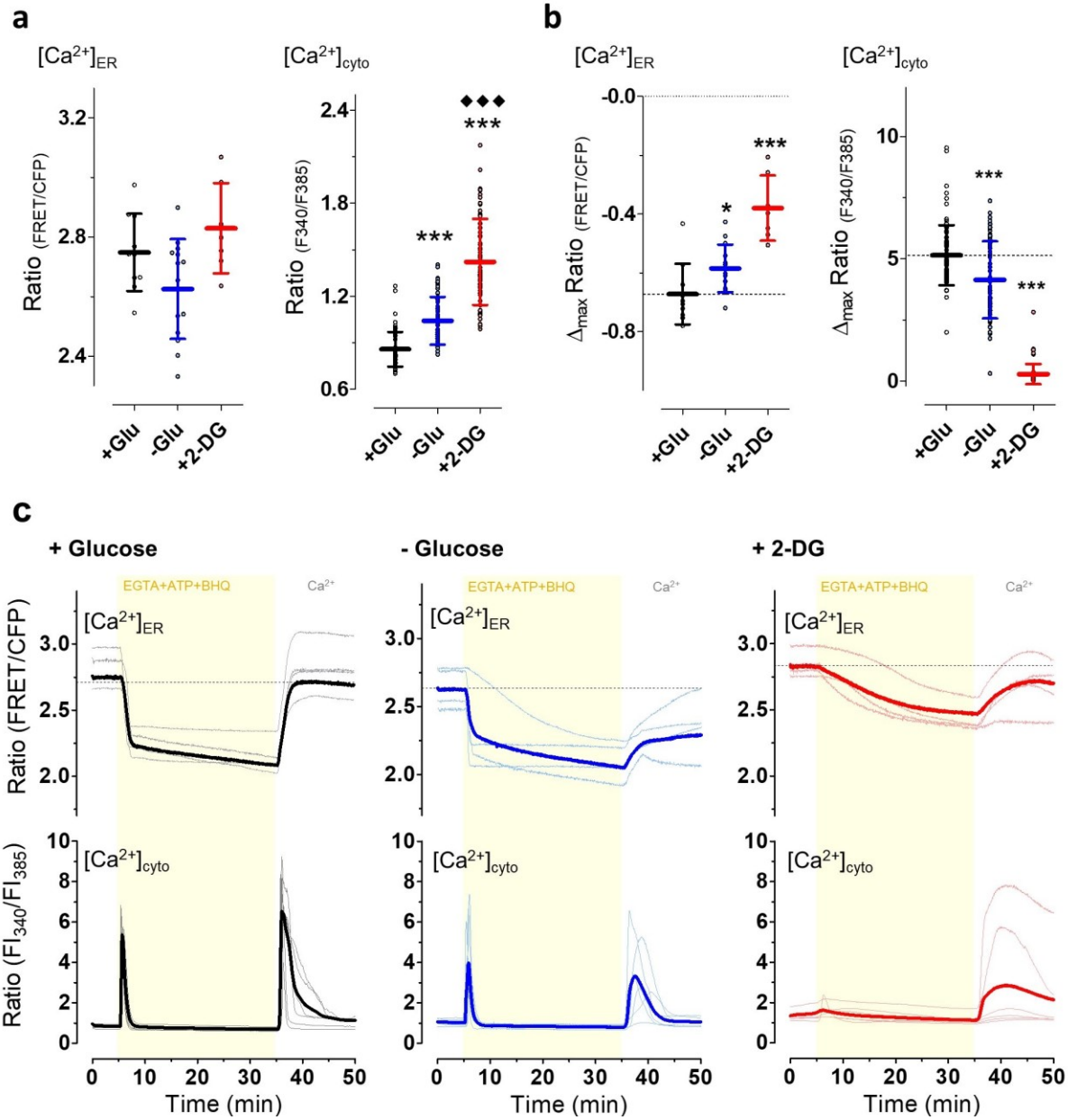

Figure 29: Mild and severe energy depletion affects the cytosolic and ER Ca^{2+} homeostasis. For measurement of cytosolic calcium dynamics HeLa cells were loaded with Fura-2 (+Glu, n = 78 cells from four independent experiments; -Glu, n = 84 cells from three independent experiments, +2-DG n = 73 cells; from four independent experiments), for visualizing ER-calcium HeLa cells expressing D1ER were measured (+Glu, n = 10 cells; -Glu, n = 14 cells, +2-DG n = 7 cells; each from three independent experiments). **(a)** Aligned dot plot and mean ± SD representing FRET ratio values of D1ER (i.e. $[Ca^{2+}]_{ER}$, left) and Fura-2 ratio values (i.e. $[Ca^{2+}]_{cyto}$, right) of unstimulated HeLa cells that were kept in the presence of 10 mM glucose (+ Glu, black), upon glucose starvation for 30 minutes (-Glu, blue) or cell treatment with 10 mM 2-DG for 30 minutes (+2-DG, red). *** significant versus +Glu $p<0.001$, ◆◆◆ significant versus -Glu $p<0.001$; Mann-Whitney-U test. **(b)** Aligned dot plot and means ± SD showing the maximum change in ratio signals of D1ER (left) and Fura-2 (right) upon cell stimulation with ATP (100 µM) and BHQ (15 µM) in the absence of extracellular Ca^{2+} (i.e. EGTA) as also shown in panel c.

* significant versus +Glu $p<0.05$, *** significant versus +Glu $p<0.001$; Mann-Whitney-U test. **(c)** ER (upper panel) and cytosolic (lower panel) Ca^{2+} signals over time in the presence of 10 mM glucose (+Glu control; black, left panels, n_{ER} = 10 cells, n_{cyto} = 78 cells), the absence of glucose (-Glu, blue, middle panels, n_{ER} = 14 cells, n_{cyto} = 84 cells) and upon cell treatment with 10 mM 2-DG (30 minutes prior to imaging experiments, +2-DG red, right panels, n_{ER} = 7 cells, n_{cyto} = 73 cells). As indicated cells were stimulated with a mixture of 100 µM ATP and 15 µM BHQ in the absence of extracellular Ca^{2+} i.e. in the presence of 0.1 mM EGTA. Subsequently ATP and BHQ were removed and 2 mM Ca^{2+} was re-added via a perfusion system. (1) [Figure panel reproduced from Rauter et al., Cells 2020.]

After that, we aimed to assess the impact of the same energy stress conditions on Ca^{2+} dynamics, a key factor in cell signaling and metabolism. For that, the HeLa cells were treated with the inositol 1,4,5-triphosphate (IP_3)-generating agonist ATP and the SERCA-inhibitor 2,5-di-t-butyl-1,4-benzohydroquinone (BHQ) in the complete absence of extracellular Ca^{2+}. The protocol aimed to trigger maximum IP_3-mediated Ca^{2+} release from the ER while preventing backflow from the cytosol by BHQ and then investigate refilling into the ER by re-adding extracellular Ca^{2+} while washing away ATP and BHQ. Under control conditions, i.e. presence of glucose, the treatment led to an immediate drop in ER-Ca^{2+} (**Figure 29b and c**) and consequently triggered a transient peak in $[Ca^{2+}]_{cyto}$ as seen in parallel experiments (**Figure 29c**, left panels). Upon removal of ATP and BHQ and switch to a perfusion buffer with extracellular Ca^{2+}, the ER-Ca^{2+} pool refilled rapidly, largely restoring levels to basal conditions (**Figure 29c**, left panels). Together with another transient peak with a rather fast decrease to almost basal levels in cytosolic Ca^{2+} (**Figure 29c**, left panels) this indicated efficient refilling of $[Ca^{2+}]_{ER}$ under control conditions. There was a rather heterogeneous reaction of glucose-starved cells upon IP_3-mediated Ca^{2+} mobilization, with clearly reduced Ca^{2+} transients upon mobilization and ER Ca^{2+} refilling (**Figure 29c**, middle panels). Under severe energy stress mediated by 2-DG, HeLa cells did not show rapid decreases of $[Ca^{2+}]_{ER}$ but a slow, continuous decline of the ER Ca^{2+} levels over time (**Figure 29c**, right panels), which was also smaller than seen for control and glucose starvation conditions (**Figure 29c**). Accordingly, there was almost no peak in measurements of $[Ca^{2+}]_{cyto}$ when treating the cells with 2-DG (**Figure 29c**, bottom right panel). Moreover, inefficient refilling of ER-Ca^{2+} was observed upon washing out ATP and BHQ and adding extracellular Ca^{2+} under this severe energy stress (**Figure 29c**, right panels). Measurements of the $[Ca^{2+}]_{cyto}$ displayed less pronounced peaks in most cells with some cells triggering strong Ca^{2+} transients, which only decreased slowly again indicating inefficient refilling processes of ER-Ca^{2+} (**Figure 29c**).

As anticipated, these results suggest extensive effects of mild and severe energy stress conditions on the cellular Ca^{2+} homeostasis. Not only do HeLa cells show increased basal

levels of cytosolic Ca^{2+}, they also display significant reductions in Ca^{2+} mobilization ability upon addition of an IP_3-mediating agonist as well as disturbances in refilling the ER Ca^{2+} pool. Strikingly, basal ER Ca^{2+} levels were not affected by glucose starvation or 2-DG treatment.

4.8 Short-term Ca^{2+} stress does not prevent ER-to-Golgi transport

Due to the substantial impact of energy stress induction on subcellular Ca^{2+} concentrations and dynamics in HeLa cells, the impact of Ca^{2+} stress itself on ER-to-Golgi transport efficiency was investigated. Especially elevated $[Ca^{2+}]_{cyto}$ was interesting in this regard since higher levels of cytosolic Ca^{2+} have been shown to massively restrict cellular vesicle movement immediately (109).

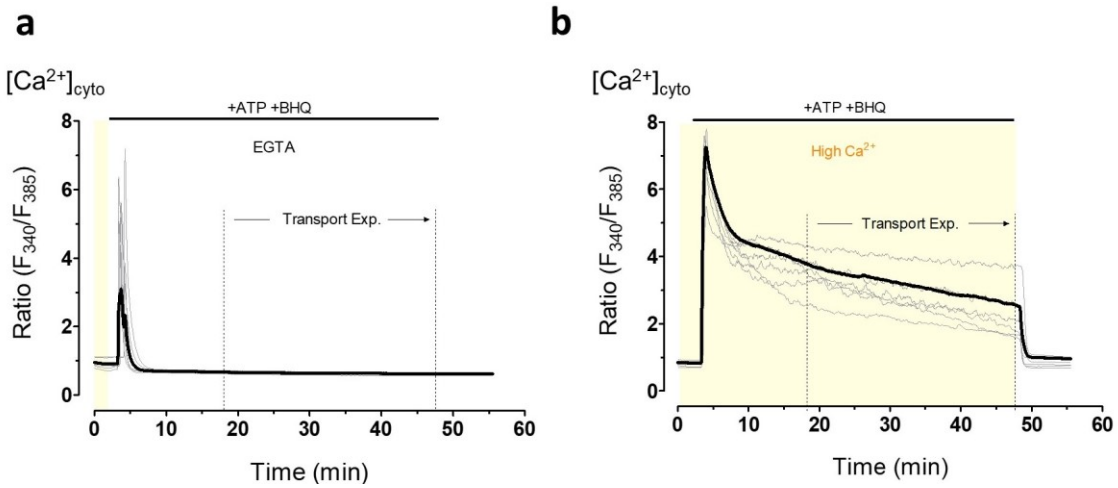

Figure 30: Established Ca^{2+} stress conditions in HeLa cells yield consistently high/low cytosolic Ca^{2+} concentrations. Curves showing changes in Fura-2 ratio (i.e. cytosolic Ca^{2+} concentrations) over time upon Ca^{2+} mobilization using 100 µM ATP and 15 µM BHQ in the absence of extracellular Ca^{2+} (i.e. 0.1 mM EGTA, n = 53 cells from three independent experiments) in **(a)** and presence of 2 mM Ca^{2+} (n = 66 cells from three independent experiments) in **(b)**. The respective time frame after Ca^{2+} mobilization for ER-to-Golgi transport experiments is indicated with dotted lines („Transport Exp."). (1) [Figure panels reproduced from Rauter et al., Cells 2020.]

To investigate this, the ER-Ca^{2+} pool was depleted by applying ATP and BHQ in the complete absence of extracellular Ca^{2+} (plus addition of EGTA) or presence of 2 mM extracellular Ca^{2+}. This led to completely emptied cytosolic Ca^{2+} on the one hand (**Figure 30a**), respectively continuously increased $[Ca^{2+}]_{cyto}$ on the other hand (**Figure 30b**), and

allowed the investigation of the impact of ER Ca^{2+} depletion with a simultaneous elevation in cytosolic Ca^{2+} levels on ER-to-Golgi transport.

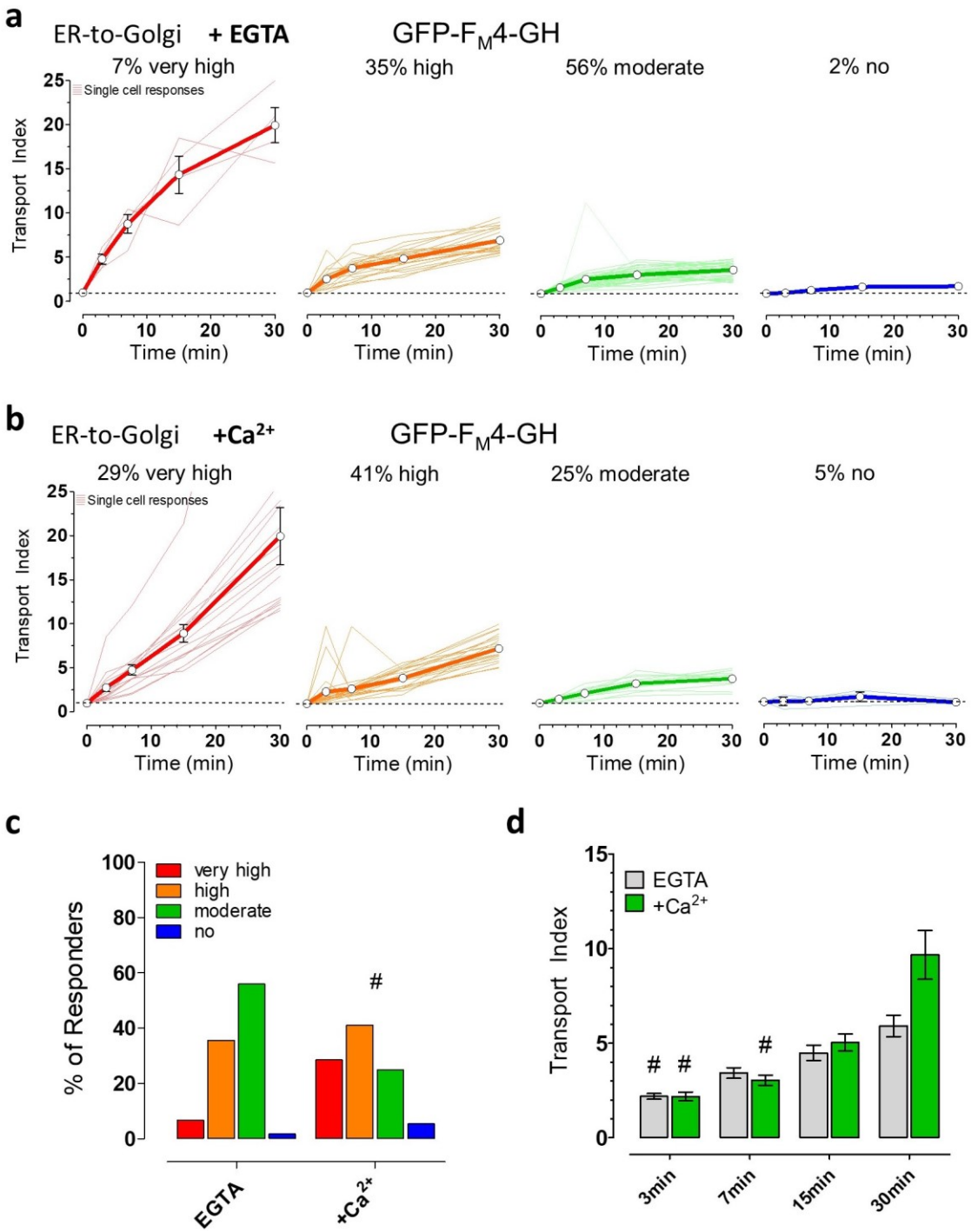

Figure 31: ER-to-Golgi transport of soluble cargo is only minimally affected by short-term Ca^{2+} stresses. (a) Curves represent very high, high, moderate and no ER-to-Golgi transport of GFP-F_M4-GH in single HeLa cells (n = 59 cells from 3 independent experiments) after 15 minutes of Ca^{2+}-mobilization in EGTA. **(b)** ER-to-Golgi transport in single HeLa cells (n = 56 cells from three independent experiments) under conditions of Ca^{2+} mobilization in the presence of Ca^{2+}, as shown in

panel b. **(c)** Bars represent the percentages of different transport efficiencies of the soluble cargo of HeLa cells treated with ATP and BHQ in the absence (i.e. EGTA) or presence (+ 2 mM Ca^{2+}) of extracellular Ca^{2+}. **(d)** Comparison of mean transport index ± SEM in stimulated HeLa cells (100 µM ATP plus 15 µM BHQ) in EGTA (grey bars, n = 59 cells,) or in the presence of 2 mM extracellular Ca^{2+} (green bars, n = 56 cells) at the indicated time points of transport. # significant versus all other time points of the same condition $p<0.05$; Kruskal-Wallis test and Dunn's post hoc test. (1) [Figure panels reproduced from Rauter et al., Cells 2020.]

HeLa cells expressing the soluble, luminal transport construct all showed clear ER-to-Golgi transport upon solubilizer addition, regardless of extracellular Ca^{2+} concentrations (**Figure 31a-d**). Interestingly, there were no significant differences between conditions, yet there was a trend to slightly decreased transport indices after 30 minutes under conditions of low cytosolic Ca^{2+} (**Figure 31a**), despite the known inhibition of vesicle movement under elevated $[Ca^{2+}]_{cyto}$ (109). This trend was also manifested using the arbitrary classification system established above and described in 4.5.3. While there were around 30% fewer cells showing only moderate ER-to-Golgi transport, the group of HeLa cells displaying very high transport efficiency was higher by over 20% (**Figure 31b and c**).

From these results it can be concluded that short-term Ca^{2+} stress does not prevent ER-to-Golgi transport. Non-impaired transport efficiency of protein cargo despite significantly elevated cytosolic Ca^{2+} levels also suggests, that the inhibiting effect of 2-DG on ER-to-Golgi transport is not likely to be mediated by its increasing effect on $[Ca^{2+}]_{cyto}$.

4.9 Cellular vesicle movement is differentially influenced by energy and calcium stresses

Unrestricted movement of vesicular structures in a cell contributes to the proper function of secretory trafficking. While it is known that elevated cytosolic Ca^{2+} levels impair vesicle trafficking (109), ER-to-Golgi transport did not seem to be affected by this (**Figure 31**). However, to better understand if the general movement of vesicular structures is impaired by energy stress further experiments were conducted. We investigated HeLa cells expressing pH-Lemon-GPI, a genetically encoded fluorescent construct located in the cell membrane and vesicular structures within the cell (109). This approach allows the estimation of the impact that energy stress exerts on the movement of GPI-positive vesicular structures and

helps to answer the question if the quantitative visualization of overall vesicle movements in a cell allows concluding on ER-to-Golgi transport.

To capture the fast-paced movements of vesicular structures and quantify their mobility, high-resolution time-lapse imaging was conducted with high frequency (5 images per second) over 2 minutes. After background subtraction and bleaching correction, the image series were analyzed using a custom-made ImageJ algorithm exploiting the TrackMate plugin (143). This allowed tracking single vesicles over time and calculating their speed and displacement. The latter one is hereby understood as the distance between the first and the last point of a track of one vesicle and can be interpreted as directionality in vesicle movement (**Figure 32**).

The observations not only revealed a massive reduction of vesicle movement in HeLa cells upon Ca^{2+} mobilization in the presence of extracellular Ca^{2+}, i.e. elevated cytosolic Ca^{2+} levels, but also a drastic decrease under severe energy stress, i.e. after treatment with the antimetabolite 2-DG. These conclusions can be obtained from looking at the vesicle tracks in representative cells from tested groups, respectively, as compared to glucose controls or cells, in which Ca^{2+} mobilization was triggered in the absence of extracellular Ca^{2+} (**Figure 32a**). The quantification of vesicle movements using the algorithm-based image analysis furthermore allowed an estimation of the restriction of vesicle speed under energy and Ca^{2+} stress. The mean velocity of vesicular structures was found to be slightly reduced upon glucose starvation and 2-DG treatment, while long-distance directional transport was not diminished in glucose-deprived cells (**Figure 32b and c**). 2-DG treated cells, however, displayed immense, highly significant reductions in long-distance transport of GPI-positive vesicles (**Figure 32c**). Both vesicle speed and directional transport over longer distances were strongly decreased after treating cells with the IP_3-generating agonist ATP and SERCA inhibitor BHQ in the presence of extracellular Ca^{2+} (**Figure 32b and c**).

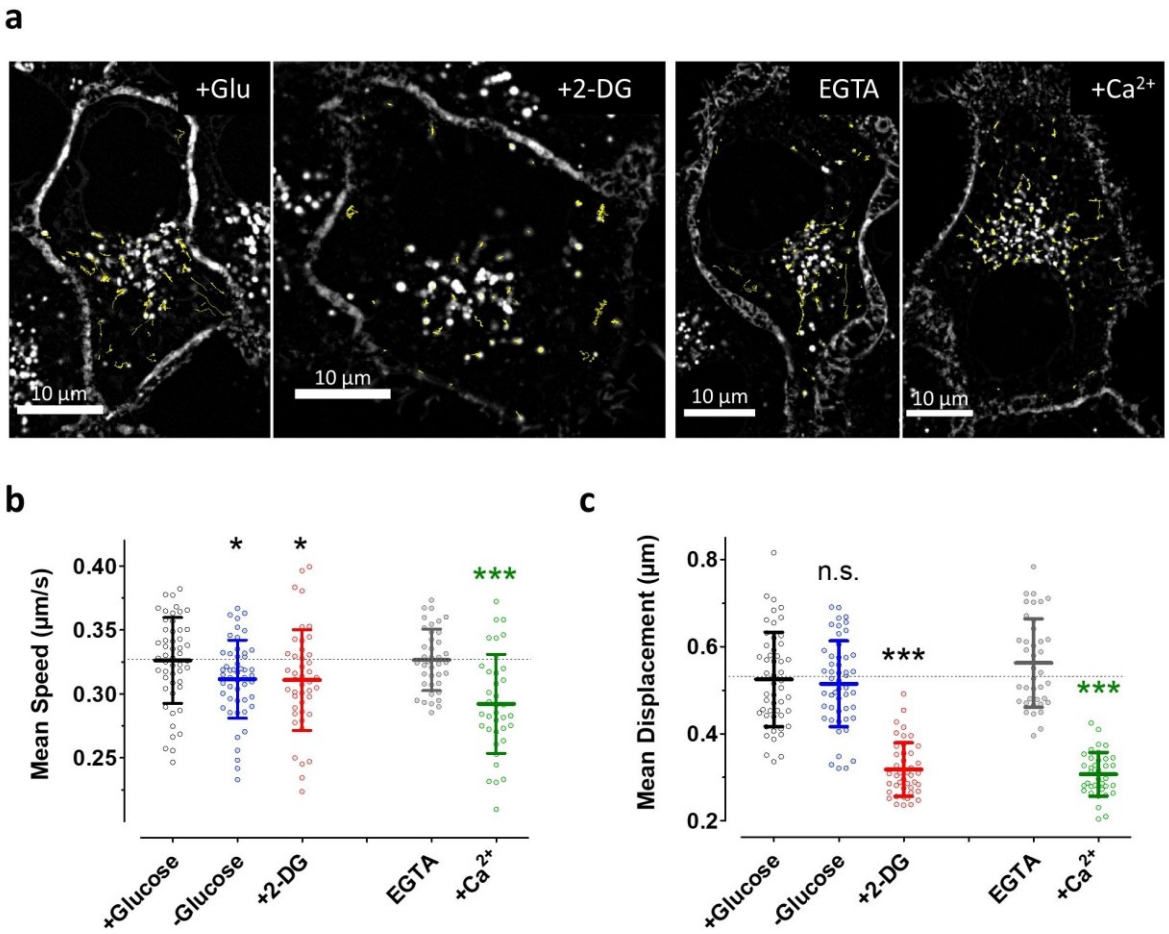

Figure 32: Vesicle motility in HeLa cells is differentially affected by Ca^{2+} and energy stresses. **(a)** Confocal images of HeLa cells stably expressing pH-Lemon-GPI that were used for time-course vesicle movement experiments. The first images in the time courses of representative cells of different treatment conditions (+Glu, +2-DG, both left panel; EGTA, $+Ca^{2+}$, both right panel) are shown. The tracks of all detected moving vesicles in 600 images over 2 minutes for each individual cell are shown in yellow. A 100x magnification objective was used; scale bars represent 10 µm. **(b and c)** Scatter dot plots and mean values ± SD representing Mean Speed (b) and Mean Displacement (c) for each cell measured at different (pre-)treatment conditions: + 10 mM Glucose without any cell stimulation (control: black; n = 51 cells), -Glucose (blue; n = 44), + 10 mM 2-DG (+2-DG: red; n = 50), cell treatment with 100 µM ATP and 15 µM BHQ in EGTA (grey; n = 39) or 2 mM extracellular Ca^{2+} ($+Ca^{2+}$: green; n = 37). n.s. not significant versus +Glucose (control), * significant versus +Glucose (control) $p<0.05$, *** significant versus +Glucose (control) $p<0.001$, *** (green) significant versus EGTA $p<0.001$; unpaired t-test. (1) [Figure panels reproduced from Rauter et al., Cells 2020.]

In conclusion, the motility of vesicular structures in HeLa cells is significantly reduced upon introducing severe energy stress or mobilizing Ca^{2+} yielding increased cytosolic Ca^{2+} levels. While the investigation of a GPI-anchored construct might not necessarily be fully conclusive about the behavior of ER-to-Golgi vesicles themselves, it is striking that ER-to-Golgi

transport can happen uninterruptedly under conditions severely decreasing overall cellular vesicle motility. This is especially remarkable regarding the immense reduction of directional long-distance transport, for which the mechanisms are similarly based on motor proteins and cytoskeleton elements for all vesicular trafficking.

4.10 Novel approaches to monitoring ER-to-Golgi transport via live-cell imaging using the dimerization dependent fluorescent protein technology

Most of the constructs for measuring secretory activity require high-resolution imaging-based readouts. To lay the groundwork for easy large-scale cell population and single-cell analysis of ER-to-Golgi transport alike, a novel approach was developed. The idea was to enable the experimenter to apply a single genetically encoded construct that combines synchronized secretory transport mediated by ligand-sensitivity with the ability to monitor transport efficiency without a high optical resolution fluorescence imaging systems.

4.10.1 Concept of the sensor

The sensor backbone was designed using several well-established technologies. The basis of the construct is the so-called dimerization dependent fluorescent protein (ddFP) technology (131,132). The ddFP constructs are based on a potentially fluorescent monomer A (GA, green fluorescence), which only conveys its fluorescence properties when coming into direct physical contact with a non-fluorescent monomeric counterpart (B) in a non-covalent interaction. To make use of the special properties of this technology, GA was C-terminally fused to a Golgi targeting sequence (GAT, first 243 AA of beta-1,4-galactosyltransferase) followed by a linker (GCCAAGGACCCCCCTGTGGCTACA). After GA, a P2A self-cleavage site was introduced. This was followed by the human growth hormone secretion signal as the start of the second part of the construct, a four-time repeat of the conditional aggregation domain ((125,127); F_M4) and the monomer B (**Figure 33a**).

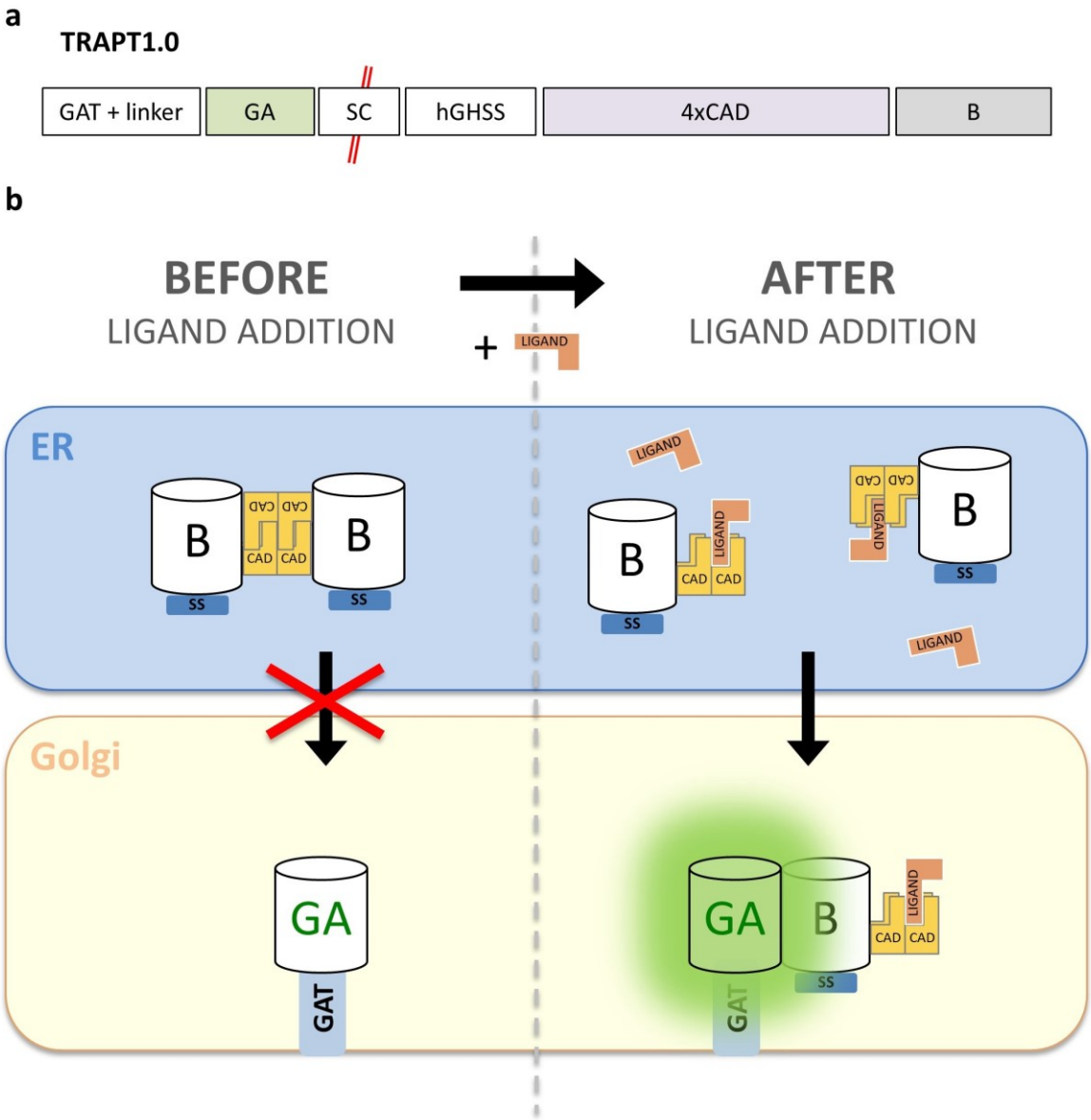

Figure 33: Design and working principle of a novel genetically encoded CAD- and ddFP-based ER-to-Golgi transport sensor. (a) Depiction of the encoded sensor elements: GAT+linker: Golgi anchor plus short amino acid linker; GA: ddFP monomer A; SC: self-cleavage site (P2A); hGHSS: human growth hormone signal sequence/secretion signal; 4xCAD: four repeats of the conditional aggregation domain; B: ddFP monomer B. Cleavage point of the construct during translation highlighted with red lines. **(b)** Sensor working principle. Prior to ligand addition the GA-part resides in the Golgi, while the B part is aggregated in the ER. Ligand (= solubilizer) addition leads to disaggregation of B parts in the ER, transport to the Golgi, thereby initiating fluorescence of GA part in Golgi by direct interaction.

The principle behind the construct was to express it in a cell type of choice and start without any fluorescent signal. Before transport initiation, the GA part would be located in the Golgi and the B part would be aggregated in the ER, unable to be transported further. When the solubilizer was added, ER-to-Golgi transport would be initiated and the monomer B would enter the secretory pathway, thereby meeting part GA in the Golgi, leading to green fluorescence upon successful transport (**Figure 33b**). The sensor was named “TRAPT1.0” (**T**ransport **R**eporter for **A**nalysis of **P**rotein **T**rafficking).

4.10.2 Proof of concept for a novel Transport Reporter for Analysis of Protein Trafficking (TRAPT)

To investigate the functionality of the novel genetically encoded ER-to-Golgi transport sensor TRAPT1.0, HeLa cells were transfected with the construct and investigated via confocal microscopy. First, the sample was screened and, as expected, no fluorescence signal was found. Transport was initiated using high amounts of solubilizer (2 µM) and after 20 minutes the sample was screened again. Unfortunately, only a few cells showing clear but rather low fluorescence intensity in the Golgi apparatus were found (**Figure 34a**), indicating low expression levels.

Due to the lack of reporter fluorescence under starting conditions and supposedly low expression levels based on the few cells found to display fluorescence at time point 20 minutes after solubilizer-mediated transport initiation, it was very hard to find cells to follow over time. General functionality of the construct and low transfection and/or expression levels resulting in low fluorescence intensity levels could be confirmed (**Figure 34b**). However, these factors made analyses of cell populations via plate reader or similar measurements impossible.

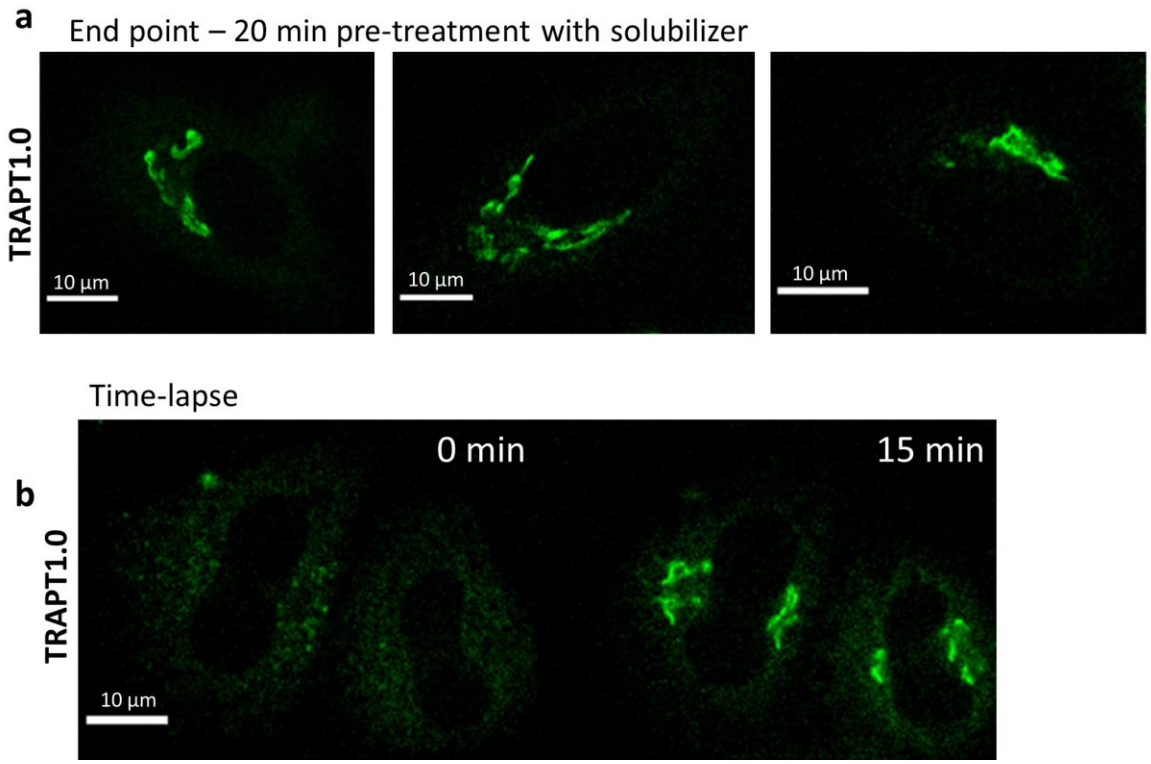

Figure 34: TRAPT1.0 allows quantification of ER-to-Golgi transport by fluorescence increase but shows low expression levels. (a) Representative end point images of HeLa cells expressing TRAPT1.0, taken 20 minutes after solubilizer-addition. **(b)** Time-lapse images of two cells expressing TRAPT1.0 before (0 min) and 10 min after solubilizer addition. Images were scaled with the same parameters to allow comparability of intensities. Scale bars indicate 10 µm.

Because of the size of the TRAPT construct and the P2A self-cleavage element, which has not been used between proteins targeted to the secretory pathway to our knowledge, it is possible that correct expression or targeting is (partially) hindered. Hence, expression and targeting of both protein parts were tested by generating altered constructs carrying fully functional FPs, named TRAPT_SScontrol, TRAPT_GAcontrol, and TRAPT_SIZEcontrol, respectively (**Figure 35a-d**). In cells expressing TRAPT_GAcontrol and TRAPT_SIZEcontrol, we found equally targeted fluorescence signal in the Golgi from the yellow fluorescent protein (CPV) that was inserted for GA in the initial TRAPT construct (**Figure 35b and c**). This indicated that Golgi targeting worked properly and self-cleavage plus a large protein segment at the C-terminus of it does not influence correct targeting and expression. Also, the hGH signal sequence to target the construct part after P2A into the ER and secretory pathway seemed to work properly. When exchanging 4xCAD and monomer B sequences for super folder GFP with a C-terminal nuclear localization sequence (sfGFPnuc; resulting in TRAPT_SScontrol), the high-intensity green fluorescent signal was found in the ER and

partially Golgi structures with no background in the cytosol or the nucleus (**Figure 35d**), suggesting proper co-translational insertion into the ER.

Despite proof of the general principle of the construct, further improvements have to be conducted to optimize it and allow a readout via plate reader measurement in the future. However, the ddFP technology has proven to be a promising variant for the design of advanced fluorescent protein trafficking tools.

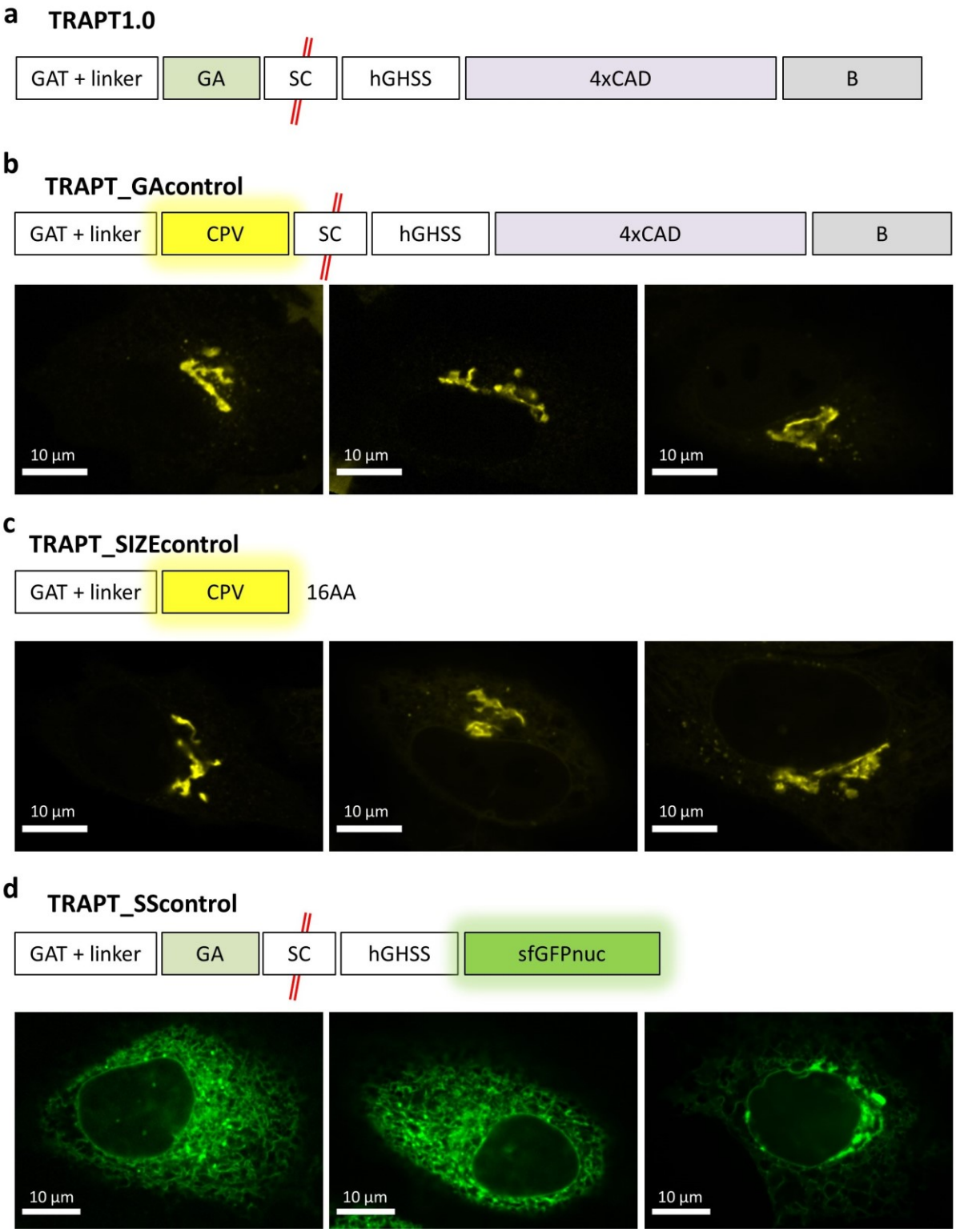

Figure 35: Expression of modified TRAPT1.0-constructs confirms correct targeting of the individual construct parts. All constructs were expressed in HeLa cells. **(a)** Depiction of the encoded sensor elements of TRAPT1.0: GAT+linker: Golgi anchor plus short amino acid linker; GA: ddFP monomer A; SC: self-cleavage site (P2A); hGHSS: human growth hormone signal sequence/secretion

signal; 4xCAD: four repeats of the conditional aggregation domain; B: ddFP monomer B. Cleavage point of the construct during translation highlighted with red lines. **(b)** Illustration of TRAPT_GAcontrol (CPV: circularly permuted Venus, YFP variant) and representative images of TRAPT-GAcontrol (screened n = 118 cells in three independent experiments). **(c)** Depiction of TRAPT_SIZEcontrol with representative images of the construct expressed in cells (screened n = 136 cells in three independent experiments). **(d)** Depiction of TRAPT_SScontrol (sfGFPnuc: super-folder GFP with a C-terminal NLS sequence) and representative images of the construct (screened n = 99 cells in three independent experiments). Scale bars represent 10 µm.

5 Discussion

In this work, an innovative high-resolution fluorescence time-lapse imaging approach for the assessment of ER-to-Golgi transport efficiency in single living cells was refined and exploited to better understand how cell stresses impact the secretory activity. Short-term energy stress conditions were mimicked by glucose deprivation and treatment with the antimetabolite 2-DG and subcellular dynamics of ATP and Ca^{2+} were examined by applying state-of-the-art fluorescence microscopy techniques in combination with established genetically encoded biosensors (136,137). Furthermore, quantitative visualization approaches and the investigation of structural features in living cells in the course of this study significantly improved our understanding of the complex interrelations of metabolic activity and secretory protein trafficking processes in a well-investigated cell model for malignant solid cancer. Finally, novel genetically encoded probes for the visualization of ER-to-Golgi transport were designed, paving the way for assay-based quantification of this process.

This study not only provides new insights into the energy and Ca^{2+} stress resistance of the secretory pathway in the HeLa cancer cell model but also puts the spotlight on how and why these cells can overcome severe ATP depletion and stress to guarantee a functioning secretion of proteins, which might well become an essential focus in future studies investigating the secretory pathway as a therapeutic target in cancer therapy.

5.1 Semi-automated analysis of ER-to-Golgi transport in individual cells over time as an innovative strategy in the research field

To this day, many studies applying genetically encoded, protein-based fluorescent sensors for synchronized ER-to-Golgi transport have not exploited the full potential of these tools. While live-cell imaging of these transport processes has already been performed for some time (47), a large number of publications still use the FP-based reporter only in end point approaches through cell fixation to allow subsequent imaging and quantification (18,45,101,125,127,144–147). Even experiments with novel approaches like the RUSH-system often lay their focus on cell population results, applying granularity-based algorithms and automated imaging of fixed stained cells (126).

However, in my dissertation we have demonstrated high dynamics and heterogeneity in these secretory processes by applying the FP-based tools in intact living cells. Based on these findings, we developed a semi-automated quantification method of the visualized ER-to-Golgi transport over time providing quantifiable time-lapse imaging data for individual cells without the need for cell fixation. We feel that this analysis tool represents an incredibly beneficial addition to the technical repertoire. Thanks to the co-expression of a target organelle marker (or any other desired co-labeling of organelles) dynamic quantification is possible.

Furthermore, the influence of pre-treatments on the Golgi structures can be observed in the very same cells where transport is measured. This opens new possibilities for future experimental approaches including pre-treatment with transport inhibitors (e.g. Brefeldin A (148) or EHT-1864 (149)) or Golgi structure disturbing agents (e.g. Nocodazole, (124)) as well as “online” injection of chemical agents modifying the protein secretion after transport initiation to monitor dynamic changes in the process.

5.2 The cancer cell secretory pathway displays high resilience to energy stress

It has been well established that cancer cells display high efficiency in ER-to-Golgi secretory transport (4). Here, we confirm that HeLa cells have a huge capacity to secrete proteins fast and efficiently, showing similarly strong trafficking efficiency as observed in normal rat kidney (NRK) cells, a cell line with high secretory capacity that is commonly used in secretory pathway studies (101). These observations nicely confirm our understanding of the tumor cell that is strongly dependent on this pathway (4).

Protein secretion is not only known to facilitate cell-extracellular matrix as well as cell-cell communication and protect cancer cells from the immune system (3,4,150,151) but also to relentlessly promote tumor progression and metastasis (4,69–74). The enormous stability of ER-to-Golgi transport as the essential first step in protein secretion (3) in HeLa cells is therefore also in line with the aggressive characteristics of this malignant cervix adenocarcinoma cell line (152).

2-deoxy-D-glucose, or 2-DG for short, is a glucose analog and well-known antimetabolite (153), which blocks the rate-limiting first step of glycolysis (154,155) – the conversion of glucose to glucose-6-phosphate – and thereby causes rapid depletion of subcellular ATP pools ((84) and this study). In this study, we observed that short-term energy stress induced by 2-DG treatment completely abolished ER-to-Golgi transport in HeLa cells suggesting a strong dependence of this process on ATP supply, probably by aerobic glycolysis, the classical cancer cell metabolic setting, well-known as the Warburg effect (92,93).

It has been demonstrated that over longer periods the treatment of cells with 2-DG *in vitro* can also lead to a prevention of cell cycle progression and cytotoxicity eventually resulting in cell death, which has been confirmed in experiments conducted on tumor cells (156). Furthermore, long-term 2-DG treatment might lead to defective protein glycosylation and to the accumulation of un- and misfolded proteins in the ER lumen, resulting in an activation of the unfolded protein response (UPR; (155)). This is a process, which gets switched on upon the accumulation of unfolded proteins in the ER as part of the quality control system in this initial organelle of the secretory pathway (31,32).

Interestingly, 2-DG has been suggested as a potential therapeutic agent in cancer therapy in the past and its effects have been studied in the context of metabolic targeting as an anti-tumor strategy (154–156). Metabolic targeting is seen as a major perspective in therapeutic interventions against cancer (157) with a growing amount of specific targets (158). The effect-enhancing impact of additional 2-DG administration on the efficacy of common therapeutics (Adriamycin/Paclitaxel) has even been tested and confirmed in an *in vivo* xenograft mouse model before (159). Moreover, improved effects of radiotherapy upon additional application of 2-DG have been observed in humans (160). Under the light of this well-founded data and the convincing results gathered in this study, it can be speculated that the anti-tumor effect mediated by 2-DG can at least in part be attributed to its capacity to almost completely prevent cellular secretory transport, which has been established to be an essential feature of cancer cells (4). It therefore stands to reason that the effect of many anti-cancer drugs targeting the metabolic pathway might partially be mediated by restricting secretory transport due to its expected dependence on energy supply.

Given this strong dependence of ER-to-Golgi transport on ATP, it was even more striking to observe that glucose starvation, which differentially decreased cytosolic and mitochondrial ATP levels significantly, did not lower the efficiency of ER-to-Golgi transport in HeLa cells.

Despite these severe reductions in subcellular ATP pools, there was no diminished ER-to-Golgi transport capacity for soluble bulk flow cargo or transmembrane cargo emphasizing the extremely high resilience of this process to energy stress in this cell model for a highly aggressive, malignant cancer. Remarkably, there was even a trend hinting at a facilitation of ER-to-Golgi transport in cells deprived of glucose, which occurred even stronger for actively sorted transmembrane cargo. While this trend, which is nicely reflected in the illustration of distinct ER-to-Golgi transport efficiency groups, has to be interpreted with caution and likely requires further experiments to be confirmed, it fits into the framework of cancer cell life – as will be elaborated in the following paragraphs.

Cancer cells display characteristic physiological hallmarks – collectively known as the Warburg effect (92,93) – which include increased glucose uptake and make glycolysis their prime source of ATP (94). This shift towards anaerobic glycolysis promotes fast and efficient growth and rapid proliferation under conditions of abundant nutrient supply (94). However, tumor cells are much more metabolically flexible than often assumed and are equipped with a whole molecular toolbox to react to certain stress conditions (161).

Glucose deprivation is a state commonly encountered in tumor cells (161), which is why it was chosen as an energy stress condition mimicking certain *in vivo* situations. For instance, missing vascularization in tumors, which can lead to severe acidification of the tumor microenvironment (TME; (162)), hypoxia and importantly severe nutrient shortage (161), is one of the most common obstacles an aggressive, highly proliferating tumor faces (163). The activation of cellular stress pathways through factors like liver kinase B1 (LKB1) or the mTOR complex can lead to sophisticated modifications in the metabolic phenotype to counteract this lack of nutrient abundance (161). On a side note, despite being generally favorable for the patient, tumors successfully adapting to these conditions of insufficient blood supply can emerge highly resistant to anti-tumor therapy based on the crucial drug delivery method via the blood (161).

Interestingly, such metabolic “defense maneuvers” are likely also responsible for the heterogeneous and sometimes oscillatory signals that were observed in this study when measuring ATP over a longer period upon starvation of sample cells by using a measurement buffer completely lacking glucose, amino acids and other compounds utilizable as energy sources. This slow and heterogeneous decrease was quite surprising to us since it is known that cancer cells heavily rely on glycolysis and therefore glucose supply (84). HeLa

cells especially have been shown to require efficient action of hexokinases 1 and 2 (HK-1 and HK-2), which are located at the outer mitochondrial membrane, to phosphorylate glucose using mitochondrial ATP in the first step of glycolysis (84,164). HeLa cells do not express LKB1 lowering the activity of the AMPK pathway (165,166), so they consequently lack some action of the important players mediating the metabolic stress response (161), as mentioned before. However, the AMPK pathway can also be activated via alternative routes like calcium/calmodulin-dependent protein kinase 2 (CaMKK2; (161)). Moreover, transient refilling of the cytosolic ATP resulting in the observed oscillatory signal could also have a different or, most likely, even several underlying causes like a refilling action from the mitochondrial ATP pool or the utilization of metabolic intermediates. Another typical reaction of cells to starvation conditions, for instance, is the activation of autophagy, which is known to play a huge role in cellular energy balance (167).

These counteracting mechanisms favor high resistance of tumor cells under metabolic stress conditions in their local environment (161) and might therefore also provide a framework of sufficient local ATP or GTP levels to maintain a strongly energy-demanding process like the secretory pathway in such a situation (10). Transient peaks in mitochondrial ATP have been detected before upon glucose stress (84) and interestingly also in response to ER-stress (168). As suggested, guaranteeing optimal protein secretion in this state might be absolutely crucial to induce angiogenesis and thereby increase nutrient supply back to the high levels that cancer cells need for optimal growth and proliferation. An essential factor in vasculogenesis – under healthy conditions and in tumors – is the vascular endothelial growth factor (VEGF, (82)). The secretion of such factors has been of great interest and only recently, studies addressed the secretion of the most frequent VEGF isoform VEGF-165, which is mediated by the energy-dependent facilitators Sar1 and Arf1 during its journey from the ER to the Golgi and finally the plasma membrane (169). This need for functioning protein secretion of essential angiogenesis inducers further explains why cancer cells show such a high resilience to energy stress and try to maintain high secretion rates despite significant global ATP depletion.

Another interesting observation in this study was that the effect on ER-to-Golgi transport visualized under glucose starvation was even stronger in the transmembrane cargo construct as compared to the luminal bulk flow construct. The transmembrane cargo based on the vesicular stomatitis virus G protein (VSVG) transmembrane domain, which features an ER export sequence on the cytoplasmic side, is actively sorted into anterograde COPII vesicles

at ER exit sites (141). Therefore, an explanation for this phenomenon would be the increased energy expenditure in ER exit of the transmembrane cargo protein, since these sorting events are dependent on GTP consumption by repeated Sar1 action (170).

5.3 Implications in future cancer therapy

The experimental results of this study confirm the vulnerability of the cancer cell secretory pathway to severe energy stresses like 2-DG treatment and simultaneously underline the resilience of ER-to-Golgi trafficking to significant ATP reductions as they occur under nutrient starvation.

As stated before, the energy dependency of numerous steps during the protein trafficking process (10) together with the importance of the secretory pathway for cancer progression and overall survival (4) might suggest that metabolic targeting as an anti-cancer therapeutic strategy (157) in the past has been successful also due to the blockage of this vital pathway in cancer cell life.

2-DG has not only been shown to efficiently block ER-to-Golgi transport in the cancer cell model applied in this study, it has also been suggested as a metabolic blocker and anticancer therapeutic (154,155,158). However, based on the results gathered in our experiments, less harsh metabolic interferences might allow the cells to escape from death by counteracting nutrient shortage through stress responses and induction of vascularization via secretion of respective factors. This leaves only the induction of very severe energy stress in tumor cells as a potential strategy and gives further reasons for why 2-DG is an effective anti-cancer therapeutic. Moreover, the findings for this cell line are highly interesting for other malignant, solid cancer cell types as well due to the similar metabolic framework (94).

Besides tackling the secretory pathway via interference of the energy household of the cell, there are many other strategies. For instance, it has been suggested to already target proteostasis to alter the proteome (4) and therefore consequently also the secretome of cancer cells. Interestingly, cancer cells usually display aneuploidy as a characteristic feature potentially resulting in multiplied expression of oncogenes or lacking translation of tumor suppressor factors (171). Strikingly, it has also been shown in a much-noticed, high-impact

study that aneuploidy-selective anti-proliferation compounds are targeting this cancer hallmark specifically (172).

In connection to the extensive protein production in cancer cells the quality control system dealing with potentially higher amounts of un- or misfolded proteins has to be constitutively upregulated (173,174). Not only in cancer but also in well-known diseases characterized by specific conformational changes like Creuzfeldt-Jakob or Alzheimer's disease it has been shown that the UPR can be very active (173,175,176). It is also broadly understood that the environment can play a huge role in regulating the ER stress response in cancer and that there is a critical role of insufficient nutrients, hypoxia and acidification in the tumor microenvironment in this regulation (177). Moreover, it is suggested that there is a complex relationship between the hypoxic response and the hypoxia-inducible factor-1alpha (HIF1α) pathway (173) and there is strong evidence that ER stress-mediated autophagy can actively promote tumor growth (178). Overall, tackling the UPR might be a viable option to fight cancer cells (4), not least because it would consequently be accompanied by a decrease in vascularization-inducing factors.

Another interesting aspect of ER stress is its connection to oxidative stress (179). In contrast to the cytosol, the ER provides an oxidizing environment (180) to allow for easy protein folding and disulfide-bridge generation. The role of oxidative stress and reactive oxygen species (ROS) production during these processes could therefore also be a point of attack in cancer therapy approaches, especially considering the essential role of the ER folding environment in cancer development (174). Studies investigating the impact of antioxidants on protein secretion have already been conducted (181).

Interestingly, modulation of pores and channels in the ER membrane by ROS (182,183) is assumed to potentially also influence the cell's Ca^{2+} homeostasis (179). The mechanism and function of ion leakage out of the ER has been an important topic in older as well as more recent publications (184–186). The influence on Ca^{2+}, a complex modulator of protein trafficking (98–100) also connects to the transport experiments under Ca^{2+} stress performed in this dissertation.

A very different approach to target the secretory pathway directly in cancer cells is interfering with microtubule dynamics and stability. Microtubules are known to mediate ER-to-Golgi transport through directed vesicle transport via motor proteins (10,17,19,21). For this reason,

the microtubule network has also been investigated in the course of this study in connection to the severe energy stress condition of 2-DG treatment, which almost completely prevented ER-to-Golgi transport. We could show that protein transport prevention after 2-DG treatment did not originate from restricted microtubule dynamics or degradation. However, this does not implicate that targeting the cytoskeleton leaves ER-to-Golgi transport untouched. In fact, microtubule targeting agents (MTAs) like colchicine or paclitaxel have been utilized to target tubulin polymerization in cancer cells (187) and paclitaxel has even been proven to show increased anti-tumor activity if applied together with the antimetabolite 2-DG (159), as mentioned before.

It is also possible to apply a more general approach to attacking the secretory pathway by using secretion inhibitors like Brefeldin A (BFA, (148)) or EHT-1864 (149). These chemical agents are known to reduce the secretion of VEGF, thereby targeting angiogenesis (70). Their potential as anti-proliferative agents has been demonstrated in a number of studies for different cancer types like breast cancer (188,189), colorectal cancer (190), prostate carcinoma or melanoma cells (191). Such applications have also been suggested to inhibit tumor growth in mouse experiments (70). Despite the success of these approaches on the cellular level, and partially *in vivo*, however, they have not yet been widely used as anti-cancer therapeutics.

In summary, it can be stated that, due to the enormous importance of the secretory pathway in cancer cells (4), protein secretion should remain a focus in anti-cancer strategies. Along with the great variety of potential targets discussed in this chapter, a more general, metabolic or more specific targeting of this pathway represent viable therapeutic options for the future applications.

5.4 The interrelation between Ca^{2+} and ATP as the key to understanding secretory pathway dynamics

Another focus of this study was the estimation of the influence of energy stress on subcellular Ca^{2+} concentrations and dynamics. Surprisingly, even under severe energy stress, introduced by treatment with 2-DG, the basal Ca^{2+} concentrations in the ER remained stable. This is unexpected and particularly fascinating since cells normally rely on the ATP-dependent enzyme SERCA to maintain the Ca^{2+} pool of the ER (142) despite constant

leakage into the cytosol (186) and 2-DG rapidly and efficiently empties subcellular ATP-pools. While further experiments would have to be performed to investigate this phenomenon in detail, it can be speculated that Ca^{2+} efflux from the ER is passively or actively blocked by some kind of, potentially multi-layered, mechanism. This might include modifications of Ca^{2+} channels under energy stress or changes in the ER folding and quality control machinery. An increased demand for Ca^{2+} required for ER-resident chaperones, which are generally known to be Ca^{2+}-dependent (192), resulting from the presence of more misfolded proteins under such conditions, might contribute to this effect. A higher rate of misfolding might be likely caused under conditions of strong ATP depletion. Ca^{2+} leakage through the translocon (186) due to a decline in the strongly energy-dependent process of protein production might also represent a contributing factor.

Moreover, a strong effect of energy stress on IP_3-mediated Ca^{2+} release from the ER as well as refilling of the ER Ca^{2+} pool could be observed. While 2-DG strongly impaired the dynamic Ca^{2+} release, the effect of glucose starvation was still significant, but less pronounced and more heterogenous. This nicely reflects the impact of these two energy stresses on the subcellular ATP pools, where 2-DG led to a complete depletion, while glucose removal also had a decreasing, yet weaker, effect. Naturally, refilling of the ER Ca^{2+} pool after Ca^{2+} readdition without the presence of extracellular ATP or SERCA inhibitors was severely impaired in 2-DG treated cells – most likely due to the strong ATP-dependency of SERCA (142). Paradoxically, the reason for the impaired reaction in Ca^{2+} dynamics in response to ATP as observed in 2-DG treated cells might effectively be a lack of proper trafficking of the respective receptor to the plasma membrane.

Importantly, basal Ca^{2+} concentrations in the cytosol were found to be significantly elevated in 2-DG treated cells. It has been shown that a strong increase of cytosolic Ca^{2+} can lead to a sudden and almost complete stop in vesicle movement (109) and can significantly reduce the motility of mitochondria (193). This prompted us to analyze if this increase in cytosolic Ca^{2+} concentrations might be a substantial factor in the prevention of ER-to-Golgi transport upon 2-DG treatment. It has also been demonstrated that the ER-to-Golgi transport of VSVG can indeed be influenced by continuous Ca^{2+} signaling over a longer time (101).

In this study, we found a similarly striking impact of 2-DG treatment and short-term Ca^{2+} stress induction, yielding strongly elevated cytosolic Ca^{2+} levels, on the movement speed and directional transport of GPI-positive vesicular structures. Speed and long-distance transport

hereby decreased significantly. However, despite this massive impairment of the vesicle motility, ER-to-Golgi transport was only slightly affected under short-term Ca^{2+} stress conditions. These results suggest that increased cytosolic Ca^{2+} levels are not likely to contribute largely to the detrimental effects of 2-DG on ER-to-Golgi transport. This observation is in line with recent reports investigating the impact of Ca^{2+} signaling in a different cell model and experimental setup (101). It is also striking that ER-Ca^{2+} mobilization without the potential for (partial) refilling by removing extracellular Ca^{2+} seemed to have a slightly stronger decreasing effect on ER-to-Golgi transport efficiency, which underlines the importance of luminal Ca^{2+} in the process (98,99).

Overall, because of the complex role of Ca^{2+} in protein trafficking control, it can be speculated that these results are based on more specific, local regulatory actions rather than global Ca^{2+} dynamics.

While this study provided significant data to help understand the interrelation of Ca^{2+} and ATP homeostasis as well as the complex control mechanisms of the secretory pathway by Ca^{2+}, further experiments are needed to answer the many open questions in this fascinating relationship.

5.5 Novel strategies to visualize ER-to-Golgi transport have the potential to complement high-resolution methods

A great strength of the applied high-resolution fluorescence microscopy approach in these particular experiments allowing for the investigation of single living cells in real-time simultaneously represents a certain limitation. The need for high optical resolution might certainly be an obstacle in some cases. For this reason, we already provided proof of concept for a novel and innovative secretory transport construct, that allow easy transport synchronization and visualization without the need for high-resolution detection methods and therefore might well find their way into assay-based plate reader approaches or even *in vivo*-investigations of ER-to-Golgi transport in the future.

In parallel to ddFP approaches (132) it is also imaginable to design constructs based on the splitFP technology (129). The fusion of the small splitFP part (129) to the cargo aggregated in the ER and waiting for ligand-based disaggregation and thereby transport initiation would

have the advantage of less bulky cargos, supposedly leading to more efficient transport. However, it is unclear how the interaction of splitFP parts and the maturation of the functional FP would work sterically in the Golgi.

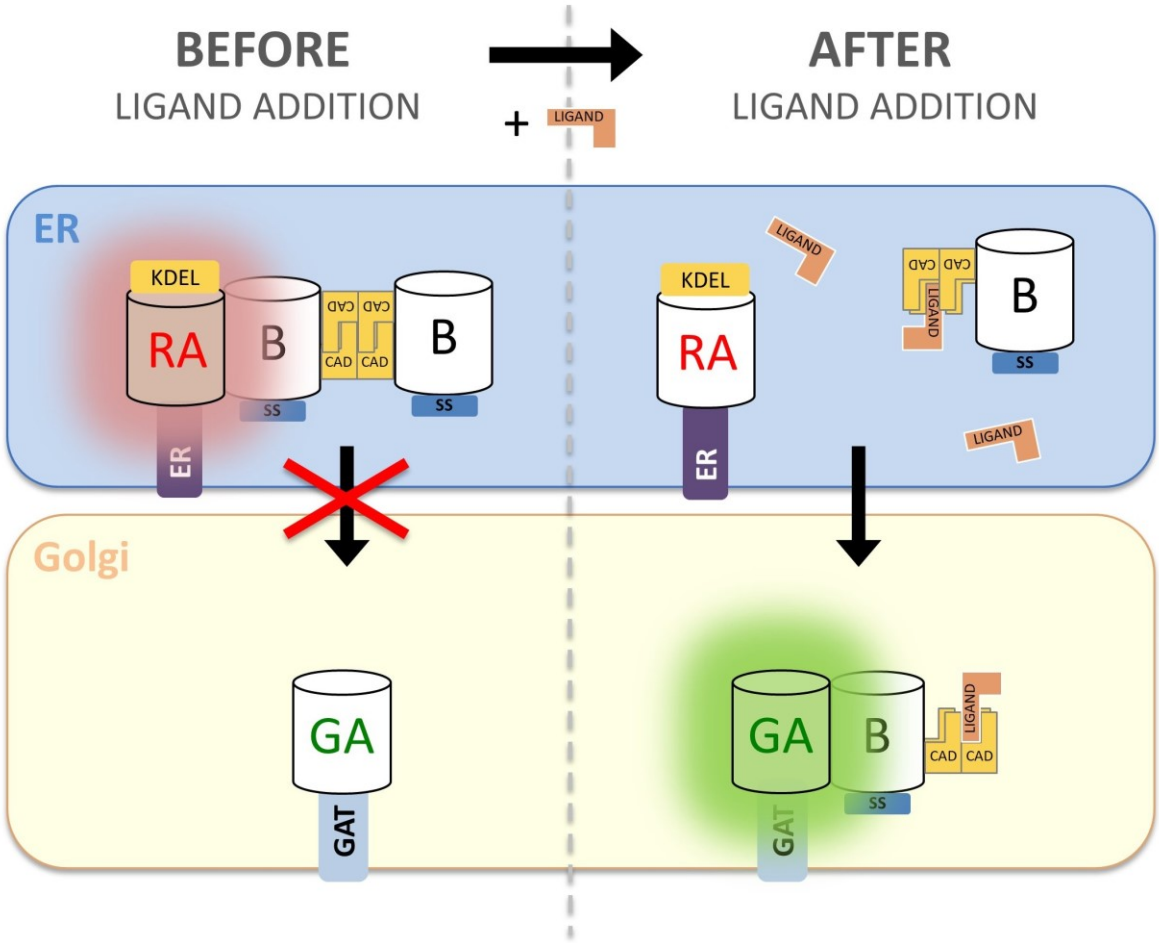

Figure 36: Potential modification of TRAPT1.0 might facilitate measurements and make quantification independent from expression levels. Red monomer A (RA) resides in ER due to calreticulin signal sequence (ER, purple) and KDEL retrieval signal, where it interacts with aggregated monomer B (B) yielding red fluorescence. Upon solubilizer addition (LIGAND) B disaggregates and is trafficking to the Golgi through its hGH secretion signal (SS), where it interacts with green monomer A (GA) waiting in the Golgi because of its Golgi anchor (GAT), leading to an increase in green fluorescence and parallel decrease in red fluorescence.

A potential modification of the current ddFP approach would be the addition of a second FP with different fluorescence properties. The introduction of a second FP, this time conveying red fluorescence, in the ER could represent a potential improvement (**Figure 36**). The advantage hereby would be that this red FP (RA), fused to an ER targeting sequence like the calreticulin signal sequence and equipped with a KDEL sequence to promote ER retention

and retrieval, could interact with the non-fluorescent FP (B), which resides in the ER in an aggregated form (via CAD) at the beginning of the experiment. This would yield a red fluorescence signal before ligand-addition (**Figure 36**). After transport initiation, the interaction of RA and B would decrease since B-CAD is transported to the Golgi, where it would interact with GA yielding green fluorescence (**Figure 36**). Successful transport could therefore be expressed as a ratio between green and red fluorescence making the concept independent from expression levels. This is particularly important because poor expression levels might be a serious problem due to the rather large size of the construct. Furthermore, it is unclear how cells handle transport constructs of this size in their secretory pathway.

In summary, this study shows that the implemented ddFP approach represents an innovative and promising strategy to complement high-resolution methods in research investigating ER-to-Golgi transport.

5.6 Concluding remarks

The connection between metabolic activity and secretory rates, especially in cancer cells, is frequently discussed in the literature, and the applied state-of-the-art techniques for the first time allow a closer look into this fascinating interrelation. The novel approach taken in this study opens the door for a great number of experiments addressing this crucial topic in the future.

Furthermore, this study shows yet unseen stability of secretory transport under significant energy stress and ATP depletion mimicking conditions of nutrient starvation that tumor cells can encounter during their life. This potentiates the importance of the secretory pathway in cancer cell life and underlines the efficiency of energy supply in these cells. The antimetabolite 2-DG, a compound used in the past to support cancer therapy (160), was found to be highly effective in hampering ER-to-Golgi transport and its, thus far, unknown impact on the (sub)cellular Ca^{2+} homeostasis, a crucial component in secretory transport regulation, was revealed. However, short-term Ca^{2+} stress alone proved to not majorly contribute to the diminishing effect of 2-DG on secretory trafficking. Strikingly, the correlation of severe energy stress mediated by 2-DG with the structural integrity of the ER and microtubule network showed no effect of the antimetabolite.

Finally, a novel design for a genetically-encoded sensor based on ddFPs and utilizing self-cleavage and conditional aggregation domains as demonstrated in this study opens up new possibilities to complement high-resolution fluorescence imaging methods.

The results gathered in this study by applying refined innovative methodical approaches overall demonstrated a highly stress-resistant secretory pathway in the cancer cell model. New insights into the efficiency of ER-to-Golgi transport under energy and Ca^{2+} stress further emphasized the importance of the secretory pathway as a potential target in cancer therapy.

References

1. Rauter T, Burgstaller S, Gottschalk B, Ramadani-Muja J, Bischof H, Hay JC, et al. ER-to-Golgi Transport in HeLa Cells Displays High Resilience to Ca^{2+} and Energy Stresses. Cells. 2020 Oct;9(10):2311.

2. Farhan H, Rabouille C. Signalling to and from the secretory pathway. J Cell Sci. 2011 Jan 15;124(2):171–80.

3. Yarwood R, Hellicar J, Woodman PG, Lowe M. Membrane trafficking in health and disease. Dis Model Mech. 2020 Apr 1;13(4):dmm043448.

4. Dejeans N, Manié S, Hetz C, Bard F, Hupp T, Agostinis P, et al. Addicted to secrete – novel concepts and targets in cancer therapy. Trends in Molecular Medicine. 2014 May;20(5):242–50.

5. Wang B, Stanford KR, Kundu M. ER-to-Golgi Trafficking and Its Implication in Neurological Diseases. Cells. 2020 Feb 11;9(2):408.

6. Luini A, Mavelli G, Jung J, Cancino J. Control systems and coordination protocols of the secretory pathway. F1000Prime Rep [Internet]. 2014 Oct 1 [cited 2020 Aug 5];6(88). Available from: https://www.ncbi.nlm.nih.gov/pmc/articles/PMC4191269/

7. Levine CG, Mitra D, Sharma A, Smith CL, Hegde RS. The Efficiency of Protein Compartmentalization into the Secretory Pathway□D. Molecular Biology of the Cell. 2005;16:16.

8. Dancourt J, Barlowe C. Protein Sorting Receptors in the Early Secretory Pathway. Annu Rev Biochem. 2010 Jun 7;79(1):777–802.

9. Kanapin A, Batalov S, Davis MJ, Gough J, Grimmond S, Kawaji H, et al. Mouse Proteome Analysis. Genome Res. 2003 Jan 6;13(6b):1335–44.

10. Martínez J, Marmisolle I, Tarallo D, Quijano C. Mitochondrial Bioenergetics and Dynamics in Secretion Processes. Front Endocrinol. 2020;11:319.

11. Molinari M, Sitia R. The Secretory Capacity of a Cell Depends on the Efficiency of Endoplasmic Reticulum-Associated Degradation. In: Wiertz E, Kikkert M, editors. Dislocation and Degradation of Proteins from the Endoplasmic Reticulum [Internet]. Berlin, Heidelberg: Springer; 2005 [cited 2020 Aug 5]. p. 1–15. (Current Topics in Microbiology and Immunology). Available from: https://doi.org/10.1007/3-540-28007-3_1

12. Kirk SJ, Cliff JM, Thomas JA, Ward TH. Biogenesis of secretory organelles during B cell differentiation. Journal of Leukocyte Biology. 2010;87(2):245–55.

13. Jensen D, Schekman R. COPII-mediated vesicle formation at a glance. Journal of Cell Science. 2011 Jan 1;124(1):1–4.

14. Budnik A, Stephens DJ. ER exit sites – Localization and control of COPII vesicle formation. FEBS Letters. 2009;583(23):3796–803.

15. Bannykh SI, Rowe T, Balch WE. The organization of endoplasmic reticulum export complexes. J Cell Biol. 1996 Oct 1;135(1):19–35.

16. Appenzeller-Herzog C, Hauri H-P. The ER-Golgi intermediate compartment (ERGIC): in search of its identity and function. Journal of Cell Science. 2006 Jun 1;119(11):2173–83.

17. Saraste J, Svensson K. Distribution of the intermediate elements operating in ER to Golgi transport. J Cell Sci. 1991 Nov;100 (Pt 3):415–30.

18. Scales SJ, Pepperkok R, Kreis TE. Visualization of ER-to-Golgi Transport in Living Cells Reveals a Sequential Mode of Action for COPII and COPI. Cell. 1997 Sep 19;90(6):1137–48.

19. Murshid A, Presley JF. ER-to-Golgi transport and cytoskeletal interactions in animal cells. CMLS, Cell Mol Life Sci. 2004 Jan 1;61(2):133–45.

20. Stalder D, Gershlick DC. Direct trafficking pathways from the Golgi apparatus to the plasma membrane. Semin Cell Dev Biol [Internet]. 2020 Apr 13 [cited 2020 Aug 6]; Available from: https://www.ncbi.nlm.nih.gov/pmc/articles/PMC7152905/

21. Ben-Tekaya H, Miura K, Pepperkok R, Hauri H-P. Live imaging of bidirectional traffic from the ERGIC. Journal of Cell Science. 2005 Jan 15;118(2):357–67.

22. Lynes EM, Simmen T. Urban planning of the endoplasmic reticulum (ER): How diverse mechanisms segregate the many functions of the ER. Biochimica et Biophysica Acta (BBA) - Molecular Cell Research. 2011 Oct 1;1813(10):1893–905.

23. Dallner G, Orrenius S, Bergstrand A. ISOLATION AND PROPERTIES OF ROUGH AND SMOOTH VESICLES FROM RAT LIVER. Journal of Cell Biology. 1963 Feb 1;16(2):426–30.

24. Walter P, Lingappa VR. Mechanism of Protein Translocation Across the Endoplasmic Reticulum Membrane. Annual Review of Cell Biology. 1986;2(1):499–516.

25. Mandon EC, Trueman SF, Gilmore R. Protein Translocation across the Rough Endoplasmic Reticulum. Cold Spring Harb Perspect Biol. 2013 Jan 2;5(2):a013342.

26. Lodish H, Berk A, Zipursky SL, Matsudaira P, Baltimore D, Darnell J. Post-Translational Modifications and Quality Control in the Rough ER. Molecular Cell Biology 4th edition [Internet]. 2000 [cited 2021 Feb 25]; Available from: https://www.ncbi.nlm.nih.gov/books/NBK21741/

27. Lewis MJ, Pelham HRB. Ligand-induced redistribution of a human KDEL receptor from the Golgi complex to the endoplasmic reticulum. Cell. 1992 Jan 24;68(2):353–64.

28. Beck R, Ravet M, Wieland FT, Cassel D. The COPI system: Molecular mechanisms and function. FEBS Letters. 2009;583(17):2701–9.

29. Barlowe C, Helenius A. Cargo Capture and Bulk Flow in the Early Secretory Pathway. Annu Rev Cell Dev Biol. 2016 Oct 6;32(1):197–222.

30. Meusser B, Hirsch C, Jarosch E, Sommer T. ERAD: the long road to destruction. Nature Cell Biology. 2005 Aug;7(8):766–72.

31. Hetz C, Zhang K, Kaufman RJ. Mechanisms, regulation and functions of the unfolded protein response. Nature Reviews Molecular Cell Biology. 2020 Aug;21(8):421–38.

32. Hwang J, Qi L. Quality Control in the Endoplasmic Reticulum: Crosstalk between ERAD and UPR pathways. Trends in Biochemical Sciences. 2018 Aug 1;43(8):593–605.

33. Cole NB, Ellenberg J, Song J, DiEuliis D, Lippincott-Schwartz J. Retrograde Transport of Golgi-localized Proteins to the ER. J Cell Biol. 1998 Jan 12;140(1):1–15.

34. Thor F, Gautschi M, Geiger R, Helenius A. Bulk flow revisited: transport of a soluble protein in the secretory pathway. Traffic. 2009 Dec;10(12):1819–30.

35. Fries E, Lindström I. The effects of low temperatures on intracellular transport of newly synthesized albumin and haptoglobin in rat hepatocytes. Biochemical Journal. 1986 Jul 1;237(1):33–9.

36. Geiger R, Gautschi M, Thor F, Hayer A, Helenius A. Folding, Quality Control, and Secretion of Pancreatic Ribonuclease in Live Cells*,. Journal of Biological Chemistry. 2011 Feb 18;286(7):5813–22.

37. Wieland FT, Gleason ML, Serafini TA, Rothman JE. The rate of bulk flow from the endoplasmic reticulum to the cell surface. Cell. 1987 Jul 17;50(2):289–300.

38. Losev E, Reinke CA, Jellen J, Strongin DE, Bevis BJ, Glick BS. Golgi maturation visualized in living yeast. Nature. 2006 Jun 22;441(7096):1002–6.

39. Bonifacino JS, Glick BS. The Mechanisms of Vesicle Budding and Fusion. Cell. 2004 Jan 23;116(2):153–66.

40. Miller EA, Beilharz TH, Malkus PN, Lee MCS, Hamamoto S, Orci L, et al. Multiple Cargo Binding Sites on the COPII Subunit Sec24p Ensure Capture of Diverse Membrane Proteins into Transport Vesicles. Cell. 2003 Aug 22;114(4):497–509.

41. Mossessova E, Bickford LC, Goldberg J. SNARE Selectivity of the COPII Coat. Cell. 2003 Aug 22;114(4):483–95.

42. Castillon GA, Aguilera-Romero A, Manzano-Lopez J, Epstein S, Kajiwara K, Funato K, et al. The yeast p24 complex regulates GPI-anchored protein transport and quality control by monitoring anchor remodeling. MBoC. 2011 Jun 16;22(16):2924–36.

43. Barlowe CK, Miller EA. Secretory Protein Biogenesis and Traffic in the Early Secretory Pathway. Genetics. 2013 Feb;193(2):383–410.

44. Martínez-Menárguez JA, Geuze HJ, Slot JW, Klumperman J. Vesicular Tubular Clusters between the ER and Golgi Mediate Concentration of Soluble Secretory Proteins by Exclusion from COPI-Coated Vesicles. Cell. 1999 Jul 9;98(1):81–90.

45. Helm JR, Bentley M, Thorsen KD, Wang T, Foltz L, Oorschot V, et al. Apoptosis-linked gene-2 (ALG-2)/Sec31 interactions regulate endoplasmic reticulum (ER)-to-Golgi transport: a potential effector pathway for luminal calcium. J Biol Chem. 2014 Aug 22;289(34):23609–28.

46. Xu D, Hay JC. Reconstitution of COPII vesicle fusion to generate a pre-Golgi intermediate compartment. J Cell Biol. 2004 Dec 20;167(6):997–1003.

47. Presley JF, Cole NB, Schroer TA, Hirschberg K, Zaal KJM, Lippincott-Schwartz J. ER-to-Golgi transport visualized in living cells. Nature. 1997 Sep;389(6646):81–5.

48. Johnson A, Bhattacharya N, Hanna M, Pennington JG, Schuh AL, Wang L, et al. TFG clusters COPII-coated transport carriers and promotes early secretory pathway organization. The EMBO Journal. 2015 Mar 12;34(6):811–27.

49. Cai H, Yu S, Menon S, Cai Y, Lazarova D, Fu C, et al. TRAPPI tethers COPII vesicles by binding the coat subunit Sec23. Nature. 2007 Feb;445(7130):941–4.

50. Brandizzi F, Barlowe C. Organization of the ER–Golgi interface for membrane traffic control. Nature Reviews Molecular Cell Biology. 2013 Jun;14(6):382–92.

51. Allan BB, Moyer BD, Balch WE. Rab1 Recruitment of p115 into a cis-SNARE Complex: Programming Budding COPII Vesicles for Fusion. Science. 2000 Jul 21;289(5478):444–8.

52. Hay JC, Klumperman J, Oorschot V, Steegmaier M, Kuo CS, Scheller RH. Localization, Dynamics, and Protein Interactions Reveal Distinct Roles for ER and Golgi SNAREs. J Cell Biol. 1998 Jun 29;141(7):1489–502.

53. McNew JA, Parlati F, Fukuda R, Johnston RJ, Paz K, Paumet F, et al. Compartmental specificity of cellular membrane fusion encoded in SNARE proteins. Nature. 2000 Sep;407(6801):153–9.

54. Reynders E, Foulquier F, Annaert W, Matthijs G. How Golgi glycosylation meets and needs trafficking: the case of the COG complex. Glycobiology. 2011 Jul 1;21(7):853–63.

55. Agrawal GK, Jwa N-S, Lebrun M-H, Job D, Rakwal R. Plant secretome: Unlocking secrets of the secreted proteins. PROTEOMICS. 2010;10(4):799–827.

56. Prudovsky I, Tarantini F, Landriscina M, Neivandt D, Soldi R, Kirov A, et al. Secretion without Golgi. Journal of Cellular Biochemistry. 2008;103(5):1327–43.

57. Nickel W. Unconventional secretory routes: direct protein export across the plasma membrane of mammalian cells. Traffic. 2005 Aug;6(8):607–14.

58. Tarantini F, Micucci I, Bellum S, Landriscina M, Garfinkel S, Prudovsky I, et al. The Precursor but Not the Mature Form of IL1α Blocks the Release of FGF1 in Response to Heat Shock*. Journal of Biological Chemistry. 2001 Feb 16;276(7):5147–51.

59. Andrei C, Dazzi C, Lotti L, Torrisi MR, Chimini G, Rubartelli A. The Secretory Route of the Leaderless Protein Interleukin 1β Involves Exocytosis of Endolysosome-related Vesicles. MBoC. 1999 May 1;10(5):1463–75.

60. Jackson A, Friedman S, Zhan X, Engleka KA, Forough R, Maciag T. Heat shock induces the release of fibroblast growth factor 1 from NIH 3T3 cells. PNAS. 1992 Nov 15;89(22):10691–5.

61. Mambula SS, Calderwood SK. Heat Shock Protein 70 Is Secreted from Tumor Cells by a Nonclassical Pathway Involving Lysosomal Endosomes. The Journal of Immunology. 2006 Dec 1;177(11):7849–57.

62. Chapman LP, Epton MJ, Buckingham JC, Morris JF, Christian HC. Evidence for a Role of the Adenosine 5′-Triphosphate-Binding Cassette Transporter A1 in the Externalization of Annexin I from Pituitary Folliculo-Stellate Cells. Endocrinology. 2003 Mar 1;144(3):1062–73.

63. Ancellin N, Colmont C, Su J, Li Q, Mittereder N, Chae S-S, et al. Extracellular Export of Sphingosine Kinase-1 Enzyme: SPHINGOSINE 1-PHOSPHATE GENERATION AND THE INDUCTION OF ANGIOGENIC VASCULAR MATURATION*. Journal of Biological Chemistry. 2002 Feb 22;277(8):6667–75.

64. Villarreal L, Méndez O, Salvans C, Gregori J, Baselga J, Villanueva J. Unconventional Secretion is a Major Contributor of Cancer Cell Line Secretomes. Mol Cell Proteomics. 2013 May;12(5):1046–60.

65. Hetz C, Glimcher LH. Protein homeostasis networks in physiology and disease. Current Opinion in Cell Biology. 2011 Apr 1;23(2):123–5.

66. Chow J, Rahman J, Achermann JC, Dattani MT, Rahman S. Mitochondrial disease and endocrine dysfunction. Nat Rev Endocrinol. 2017;13(2):92–104.

67. Devine MJ, Kittler JT. Mitochondria at the neuronal presynapse in health and disease. Nature Reviews Neuroscience. 2018 Feb;19(2):63–80.

68. Haythorne E, Rohm M, van de Bunt M, Brereton MF, Tarasov AI, Blacker TS, et al. Diabetes causes marked inhibition of mitochondrial metabolism in pancreatic β-cells. Nat Commun. 2019 Jun 6;10(1):1–17.

69. Lodish H, Berk A, Zipursky SL, Matsudaira P, Baltimore D, Darnell J. Tumor Cells and the Onset of Cancer. Molecular Cell Biology 4th edition [Internet]. 2000 [cited 2020 Aug 7]; Available from: https://www.ncbi.nlm.nih.gov/books/NBK21590/

70. Bonnin DAA, Havrda MC, Israel MA. Glioma Cell Secretion: A Driver of Tumor Progression and a Potential Therapeutic Target. Cancer Res. 2018 Nov 1;78(21):6031–9.

71. Short B. Determining the dynamics of cancer cell secretion. J Gen Physiol. 2019 Dec 2;151(12):1333–1333.

72. Karagiannis GS, Pavlou MP, Diamandis EP. Cancer secretomics reveal pathophysiological pathways in cancer molecular oncology. Molecular Oncology. 2010 Dec 1;4(6):496–510.

73. Mueller MM, Fusenig NE. Friends or foes — bipolar effects of the tumour stroma in cancer. Nature Reviews Cancer. 2004 Nov;4(11):839–49.

74. Kano A. Tumor cell secretion of soluble factor(s) for specific immunosuppression. Scientific Reports. 2015 Mar 9;5(1):8913.

75. Stephens DC, Osunsanmi N, Sochacki KA, Powell TW, Taraska JW, Harris DA. Spatiotemporal organization and protein dynamics involved in regulated exocytosis of MMP-9 in breast cancer cells. J Gen Physiol. 2019 Dec 2;151(12):1386–403.

76. Lubbe WJ, Zhou ZY, Fu W, Zuzga D, Schulz S, Fridman R, et al. Tumor epithelial cell matrix metalloproteinase 9 is a target for antimetastatic therapy in colorectal cancer. Clin Cancer Res. 2006 Mar 15;12(6):1876–82.

77. Chien M-H, Lin C-W, Cheng C-W, Wen Y-C, Yang S-F. Matrix metalloproteinase-2 as a target for head and neck cancer therapy. Expert Opin Ther Targets. 2013 Feb;17(2):203–16.

78. Dufour A, Overall CM. Missing the target: matrix metalloproteinase antitargets in inflammation and cancer. Trends Pharmacol Sci. 2013 Apr;34(4):233–42.

79. Abdelmoneim AH, Mustafa MI, Abdelmageed MI, Murshed NS, Dawoud E dk, Ahmed EM, et al. Immunoinformatics design of multiepitopes peptide-based universal cancer vaccine using matrix metalloproteinase-9 protein as a target. Immunological Medicine. 2020 Jul 21;0(0):1–18.

80. Alos HC, Billones JB, Vasquez RD, Castillo AL. Antiangiogenesis Potential of Alpinumisoflavone as an Inhibitor of Matrix Metalloproteinase-9 (MMP-9) and Vascular Endothelial Growth Factor Receptor-2 (VEGFR-2). Current Enzyme Inhibition. 2019 Dec 1;15(3):159–78.

81. Rodríguez D, Morrison CJ, Overall CM. Matrix metalloproteinases: What do they not do? New substrates and biological roles identified by murine models and proteomics. Biochimica et Biophysica Acta (BBA) - Molecular Cell Research. 2010 Jan 1;1803(1):39–54.

82. Ferrara N. VEGF-A: a critical regulator of blood vessel growth. European Cytokine Network. 2009 Dec;20(4):158–63.

83. Contessa JN, Bhojani MS, Freeze HH, Rehemtulla A, Lawrence TS. Inhibition of N-linked glycosylation disrupts receptor tyrosine kinase signaling in tumor cells. Cancer Res. 2008 May 15;68(10):3803–9.

84. Depaoli MR, Karsten F, Madreiter-Sokolowski CT, Klec C, Gottschalk B, Bischof H, et al. Real-Time Imaging of Mitochondrial ATP Dynamics Reveals the Metabolic Setting of Single Cells. Cell Reports. 2018 Oct;25(2):501-512.e3.

85. Klein M-C, Zimmermann K, Schorr S, Landini M, Klemens PAW, Altensell J, et al. AXER is an ATP/ADP exchanger in the membrane of the endoplasmic reticulum. Nature Communications. 2018 Aug 28;9(1):3489.

86. Dorner AJ, Wasley LC, Kaufman RJ. Protein dissociation from GRP78 and secretion are blocked by depletion of cellular ATP levels. Proceedings of the National Academy of Sciences. 1990 Oct 1;87(19):7429–32.

87. Dorner AJ, Kaufman RJ. The Levels of Endoplasmic Reticulum Proteins and ATP Affect Folding and Secretion of Selective Proteins. Biologicals. 1994 Jun;22(2):103–12.

88. Antoine JC, Jouanne C. Multiple effects of the phenylhydrazone derivative FCCP on the secretory pathway in rat plasma cells. Eur J Cell Biol. 1986 Oct;42(1):68–73.

89. Argon Y, Burkhardt JK, Leeds JM, Milstein C. Two steps in the intracellular transport of IgD are sensitive to energy depletion. J Immunol. 1989 Jan 15;142(2):554–61.

90. Depaoli MR, Bischof H, Eroglu E, Burgstaller S, Ramadani-Muja J, Rauter T, et al. Live cell imaging of signaling and metabolic activities. Pharmacol Ther. 2019;202:98–119.

91. Depaoli MR, Hay JC, Graier WF, Malli R. The enigmatic ATP supply of the endoplasmic reticulum. Biol Rev Camb Philos Soc. 2019;94(2):610–28.

92. Warburg O, Posener K, Negelein E. The metabolism of cancer cells. Biochem Z. 1924;152:319–44.

93. Liberti MV, Locasale JW. The Warburg Effect: How Does it Benefit Cancer Cells? Trends Biochem Sci. 2016 Mar;41(3):211–8.

94. Vander Heiden MG, Cantley LC, Thompson CB. Understanding the Warburg effect: the metabolic requirements of cell proliferation. Science. 2009 May 22;324(5930):1029–33.

95. Rauter T, Depaoli MR, Bischof H, Graier WF, Malli R. Metabolic Profiling of Single Cancer Cells Using Mitochondrial ATP Probes. STAR Protocols. 2020 Sep 18;1(2):100048.

96. Roomi MW, Monterrey JC, Kalinovsky T, Rath M, Niedzwiecki A. In vitro modulation of MMP-2 and MMP-9 in human cervical and ovarian cancer cell lines by cytokines, inducers and inhibitors. Oncology Reports. 2010 Mar 1;23(3):605–14.

97. Nishida N, Yano H, Nishida T, Kamura T, Kojiro M. Angiogenesis in Cancer. Vasc Health Risk Manag. 2006 Sep;2(3):213–9.

98. Bentley M, Nycz DC, Joglekar A, Fertschai I, Malli R, Graier WF, et al. Vesicular Calcium Regulates Coat Retention, Fusogenicity, and Size of Pre-Golgi Intermediates. MBoC. 2010 Jan 20;21(6):1033–46.

99. Hay JC. Calcium: a fundamental regulator of intracellular membrane fusion? EMBO Rep. 2007 Mar;8(3):236–40.

100. Chen J-L, Ahluwalia JP, Stamnes M. Selective Effects of Calcium Chelators on Anterograde and Retrograde Protein Transport in the Cell*. Journal of Biological Chemistry. 2002 Sep 20;277(38):35682–7.

101. Sargeant J, Costain T, Madreiter-Sokolowski C, Gordon DE, Peden AA, Mali R, et al. Calcium Sensors ALG-2 and Peflin Bind ER Exit Sites in Alternate States to Modulate Secretion in Response to Calcium Signaling. bioRxiv. 2020 Feb 22;2020.02.22.944264.

102. Burgoyne RD, Clague MJ. Calcium and calmodulin in membrane fusion. Biochimica et Biophysica Acta (BBA) - Molecular Cell Research. 2003 Aug 18;1641(2):137–43.

103. SHIBATA H, INUZUKA T, YOSHIDA H, SUGIURA H, WADA I, MAKI M. The ALG-2 Binding Site in Sec31A Influences the Retention Kinetics of Sec31A at the Endoplasmic Reticulum Exit Sites as Revealed by Live-Cell Time-Lapse Imaging. Bioscience, Biotechnology, and Biochemistry. 2010 Sep 23;74(9):1819–26.

104. Shibata H, Suzuki H, Yoshida H, Maki M. ALG-2 directly binds Sec31A and localizes at endoplasmic reticulum exit sites in a Ca^{2+}-dependent manner. Biochemical and Biophysical Research Communications. 2007 Feb 16;353(3):756–63.

105. Adamíková L, Straube A, Schulz I, Steinberg G. Calcium Signaling Is Involved in Dynein-dependent Microtubule Organization. Mol Biol Cell. 2004 Apr;15(4):1969–80.

106. Hepler PK. The Cytoskeleton and Its Regulation by Calcium and Protons. Plant Physiol. 2016 Jan;170(1):3–22.

107. Vinogradova MV, Malanina GG, Reddy ASN, Fletterick RJ. Structure of the complex of a mitotic kinesin with its calcium binding regulator. PNAS. 2009 May 19;106(20):8175–9.

108. Sakato M, King SM. Calcium Regulates ATP-sensitive Microtubule Binding by Chlamydomonas Outer Arm Dynein *. Journal of Biological Chemistry. 2003 Oct 31;278(44):43571–9.

109. Burgstaller S, Bischof H, Gensch T, Stryeck S, Gottschalk B, Ramadani-Muja J, et al. pH-Lemon, a Fluorescent Protein-Based pH Reporter for Acidic Compartments. ACS Sens. 2019 Apr 26;4(4):883–91.

110. Petersen OH, Verkhratsky A. Calcium and ATP control multiple vital functions. Phil Trans R Soc B. 2016 Aug 5;371(1700):20150418.

111. McCoy CE, Selvaggio AM, Alexander EA, Schwartz JH. Adenosine triphosphate depletion induces a rise in cytosolic free calcium in canine renal epithelial cells. J Clin Invest. 1988 Oct 1;82(4):1326–32.

112. Lee C, Chen LB. Dynamic behavior of endoplasmic reticulum in living cells. Cell. 1988 Jul 1;54(1):37–46.

113. Jamieson JD, Palade GE. INTRACELLULAR TRANSPORT OF SECRETORY PROTEINS IN THE PANCREATIC EXOCRINE CELL : I. Role of the Peripheral Elements of the Golgi Complex. Journal of Cell Biology. 1967 Aug 1;34(2):577–96.

114. Jamieson JD, Palade GE. INTRACELLULAR TRANSPORT OF SECRETORY PROTEINS IN THE PANCREATIC EXOCRINE CELL : III. Dissociation of Intracellular Transport from Protein Synthesis. Journal of Cell Biology. 1968 Dec 1;39(3):580–8.

115. Fries E, Rothman JE. Transport of vesicular stomatitis virus glycoprotein in a cell-free extract. PNAS. 1980 Jul 1;77(7):3870–4.

116. Barlowe C, Orci L, Yeung T, Hosobuchi M, Hamamoto S, Salama N, et al. COPII: A membrane coat formed by Sec proteins that drive vesicle budding from the endoplasmic reticulum. Cell. 1994 Jun 17;77(6):895–907.

117. Presley JF. Imaging the secretory pathway: The past and future impact of live cell optical techniques. Biochimica et Biophysica Acta (BBA) - Molecular Cell Research. 2005 Jul 10;1744(3):259–72.

118. Chalfie M, Tu Y, Euskirchen G, Ward WW, Prasher DC. Green fluorescent protein as a marker for gene expression. Science. 1994 Feb 11;263(5148):802–5.

119. Verissimo F, Pepperkok R. Imaging ER-to-Golgi transport: towards a systems view. Journal of Cell Science. 2013 Nov 15;126(22):5091–100.

120. Mironov AA, Mironov AA, Beznoussenko GV, Trucco A, Lupetti P, Smith JD, et al. ER-to-Golgi Carriers Arise through Direct En Bloc Protrusion and Multistage Maturation of Specialized ER Exit Domains. Developmental Cell. 2003 Oct 1;5(4):583–94.

121. Forster R, Weiss M, Zimmermann T, Reynaud EG, Verissimo F, Stephens DJ, et al. Secretory cargo regulates the turnover of COPII subunits at single ER exit sites. Curr Biol. 2006 Jan 24;16(2):173–9.

122. Boncompain G, Perez F. Chapter 11 - Fluorescence-Based Analysis of Trafficking in Mammalian Cells. In: Perez F, Stephens DJ, editors. Methods in Cell Biology [Internet]. Academic Press; 2013 [cited 2020 Aug 6]. p. 179–94. (Methods for Analysis of Golgi Complex Function; vol. 118). Available from: http://www.sciencedirect.com/science/article/pii/B9780124171640000112

123. Lafay F. Envelope Proteins of Vesicular Stomatitis Virus: Effect of Temperature-Sensitive Mutations in Complementation Groups III and V. Journal of Virology. 1974 Nov 1;14(5):1220–8.

124. Tie HC, Mahajan D, Chen B, Cheng L, VanDongen AMJ, Lu L. A novel imaging method for quantitative Golgi localization reveals differential intra-Golgi trafficking of secretory cargoes. MBoC. 2016 Jan 13;27(5):848–61.

125. Rollins CT, Rivera VM, Woolfson DN, Keenan T, Hatada M, Adams SE, et al. A ligand-reversible dimerization system for controlling protein–protein interactions. Proc Natl Acad Sci U S A. 2000 Jun 20;97(13):7096–101.

126. Boncompain G, Divoux S, Gareil N, de Forges H, Lescure A, Latreche L, et al. Synchronization of secretory protein traffic in populations of cells. Nature Methods. 2012 May;9(5):493–8.

127. Rivera VM. Regulation of Protein Secretion Through Controlled Aggregation in the Endoplasmic Reticulum. Science. 2000 Feb 4;287(5454):826–30.

128. Chen D, Gibson ES, Kennedy MJ. A light-triggered protein secretion system. Journal of Cell Biology. 2013 May 13;201(4):631–40.

129. Kamiyama D, Sekine S, Barsi-Rhyne B, Hu J, Chen B, Gilbert LA, et al. Versatile protein tagging in cells with split fluorescent protein. Nature Communications. 2016 Mar 18;7(1):11046.

130. Ramadani-Muja J, Gottschalk B, Pfeil K, Burgstaller S, Rauter T, Bischof H, et al. Visualization of Sirtuin 4 Distribution between Mitochondria and the Nucleus, Based on Bimolecular Fluorescence Self-Complementation. Cells. 2019 Dec;8(12):1583.

131. Alford SC, Ding Y, Simmen T, Campbell RE. Dimerization-Dependent Green and Yellow Fluorescent Proteins. ACS Synth Biol. 2012 Dec 21;1(12):569–75.

132. Ding Y, Li J, Enterina JR, Shen Y, Zhang I, Tewson PH, et al. Ratiometric biosensors based on dimerization-dependent fluorescent protein exchange. Nature Methods. 2015 Mar;12(3):195–8.

133. Bischof H, Rehberg M, Stryeck S, Artinger K, Eroglu E, Waldeck-Weiermair M, et al. Novel genetically encoded fluorescent probes enable real-time detection of potassium in vitro and in vivo. Nature Communications. 2017 Nov 10;8(1):1422.

134. Liu Z, Chen O, Wall JBJ, Zheng M, Zhou Y, Wang L, et al. Systematic comparison of 2A peptides for cloning multi-genes in a polycistronic vector. Sci Rep. 2017 May 19;7(1):1–9.

135. Eroglu E, Gottschalk B, Charoensin S, Blass S, Bischof H, Rost R, et al. Development of novel FP-based probes for live-cell imaging of nitric oxide dynamics. Nature Communications. 2016 Feb 4;7(1):10623.

136. Imamura H, Nhat KPH, Togawa H, Saito K, Iino R, Kato-Yamada Y, et al. Visualization of ATP levels inside single living cells with fluorescence resonance energy transfer-based genetically encoded indicators. PNAS. 2009 Sep 15;106(37):15651–6.

137. Palmer AE, Jin C, Reed JC, Tsien RY. Bcl-2-mediated alterations in endoplasmic reticulum Ca^{2+} analyzed with an improved genetically encoded fluorescent sensor. Proc Natl Acad Sci USA. 2004 Dec 14;101(50):17404–9.

138. Bianchi-Smiraglia A, Rana MS, Foley CE, Paul LM, Lipchick BC, Moparthy S, et al. Internally ratiometric fluorescent sensors for evaluation of intracellular GTP levels and distribution. Nat Methods. 2017 Oct;14(10):1003–9.

139. Goedhart J, van Weeren L, Hink MA, Vischer NOE, Jalink K, Gadella TWJ. Bright cyan fluorescent protein variants identified by fluorescence lifetime screening. Nat Methods. 2010 Feb;7(2):137–9.

140. Spinelli JB, Haigis MC. The multifaceted contributions of mitochondria to cellular metabolism. Nat Cell Biol. 2018 Jul;20(7):745–54.

141. Sevier CS, Weisz OA, Davis M, Machamer CE. Efficient Export of the Vesicular Stomatitis Virus G Protein from the Endoplasmic Reticulum Requires a Signal in the Cytoplasmic Tail That Includes Both Tyrosine-based and Di-acidic Motifs. Mol Biol Cell. 2000 Jan;11(1):13–22.

142. Primeau JO, Armanious GP, Fisher ME, Young HS. The SarcoEndoplasmic Reticulum Calcium ATPase. In: Harris JR, Boekema EJ, editors. Membrane Protein Complexes: Structure and Function [Internet]. Singapore: Springer; 2018 [cited 2020 Aug 5]. p. 229–58. (Subcellular Biochemistry). Available from: https://doi.org/10.1007/978-981-10-7757-9_8

143. Tinevez J-Y, Perry N, Schindelin J, Hoopes GM, Reynolds GD, Laplantine E, et al. TrackMate: An open and extensible platform for single-particle tracking. Methods. 2017 Feb 15;115:80–90.

144. Sawyer GW, Ehlert FJ, Hart JP. Determination of the rate of muscarinic M1 receptor plasma membrane delivery using a regulated secretion/aggregation system. Journal of Pharmacological and Toxicological Methods. 2006 May 1;53(3):219–33.

145. Volchuk A, Amherdt M, Ravazzola M, Brügger B, Rivera VM, Clackson T, et al. Megavesicles Implicated in the Rapid Transport of Intracisternal Aggregates across the Golgi Stack. Cell. 2000 Aug 4;102(3):335–48.

146. Jaiswal JK, Rivera VM, Simon SM. Exocytosis of Post-Golgi Vesicles Is Regulated by Components of the Endocytic Machinery. Cell. 2009 Jun 26;137(7):1308–19.

147. Gordon DE, Bond LM, Sahlender DA, Peden AA. A Targeted siRNA Screen to Identify SNAREs Required for Constitutive Secretion in Mammalian Cells. Traffic. 2010;11(9):1191–204.

148. Misumi Y, Misumi Y, Miki K, Takatsuki A, Tamura G, Ikehara Y. Novel blockade by brefeldin A of intracellular transport of secretory proteins in cultured rat hepatocytes. J Biol Chem. 1986 Aug 25;261(24):11398–403.

149. Shutes A, Onesto C, Picard V, Leblond B, Schweighoffer F, Der CJ. Specificity and Mechanism of Action of EHT 1864, a Novel Small Molecule Inhibitor of Rac Family Small GTPases. J Biol Chem. 2007 Jul 12;282(49):35666–78.

150. Sevenich L, Joyce JA. Pericellular proteolysis in cancer. Genes Dev. 2014 Nov 1;28(21):2331–47.

151. Mason SD, Joyce JA. Proteolytic Networks in Cancer. Trends Cell Biol. 2011 Apr;21(4):228–37.

152. Lucey BP, Nelson-Rees WA, Hutchins GM. Henrietta Lacks, HeLa Cells, and Cell Culture Contamination. Archives of Pathology & Laboratory Medicine. 2009 Sep 1;133(9):1463–7.

153. Wick AN, Drury DR, Nakada HI, Wolfe JB, Britton B, Grabowski R. LOCALIZATION OF THE PRIMARY METABOLIC BLOCK PRODUCED BY 2-DEOXYGLUCOSE. Journal of Biological Chemistry. 1957 Feb 1;224(2):963–9.

154. Pelicano H, Martin DS, Xu R-H, Huang P. Glycolysis inhibition for anticancer treatment. Oncogene. 2006 Aug;25(34):4633–46.

155. Kang HT, Hwang ES. 2-Deoxyglucose: An anticancer and antiviral therapeutic, but not any more a low glucose mimetic. Life Sciences. 2006 Feb 16;78(12):1392–9.

156. Maher JC, Krishan A, Lampidis TJ. Greater cell cycle inhibition and cytotoxicity induced by 2-deoxy-d-glucose in tumor cells treated under hypoxic vs aerobic conditions. Cancer Chemother Pharmacol. 2004 Feb 1;53(2):116–22.

157. Pan JG, Mak TW. Metabolic Targeting as an Anticancer Strategy: Dawn of a New Era? Sci STKE. 2007 Apr 10;2007(381):pe14–pe14.

158. Zhao Y, Liu H, Riker AI, Fodstad O, Ledoux SP, Wilson GL, et al. Emerging Metabolic Targets in Cancer Therapy. Front Biosci. 2011 Jan 1;16:1844–60.

159. Maschek G, Savaraj N, Priebe W, Braunschweiger P, Hamilton K, Tidmarsh GF, et al. 2-Deoxy-d-glucose Increases the Efficacy of Adriamycin and Paclitaxel in Human Osteosarcoma and Non-Small Cell Lung Cancers In Vivo. Cancer Res. 2004 Jan 1;64(1):31–4.

160. Mohanti BK, Rath GK, Anantha N, Kannan V, Das BS, Chandramouli BAR, et al. Improving cancer radiotherapy with 2-deoxy-d-glucose: phase I/II clinical trials on human cerebral gliomas. International Journal of Radiation Oncology*Biology*Physics. 1996 Apr 1;35(1):103–11.

161. Kreuzaler P, Panina Y, Segal J, Yuneva M. Adapt and conquer: Metabolic flexibility in cancer growth, invasion and evasion. Molecular Metabolism. 2020 Mar 1;33:83–101.

162. Corbet C, Feron O. Tumour acidosis: from the passenger to the driver's seat. Nature Reviews Cancer. 2017 Oct;17(10):577–93.

163. De Palma M, Biziato D, Petrova TV. Microenvironmental regulation of tumour angiogenesis. Nature Reviews Cancer. 2017 Aug;17(8):457–74.

164. Tseng P-L, Chen C-W, Hu K-H, Cheng H-C, Lin Y-H, Tsai W-H, et al. The decrease of glycolytic enzyme hexokinase 1 accelerates tumor malignancy via deregulating energy metabolism but sensitizes cancer cells to 2-deoxyglucose inhibition. Oncotarget. 2018 Apr 10;9(27):18949–69.

165. Zhang X, Chen H, Wang X, Zhao W, Chen JJ. Expression and transcriptional profiling of the LKB1 tumor suppressor in cervical cancer cells. Gynecol Oncol. 2014 Aug;134(2):372–8.

166. Shaw RJ, Kosmatka M, Bardeesy N, Hurley RL, Witters LA, DePinho RA, et al. The tumor suppressor LKB1 kinase directly activates AMP-activated kinase and regulates apoptosis in response to energy stress. Proceedings of the National Academy of Sciences. 2004 Mar 9;101(10):3329–35.

167. Singh R, Cuervo AM. Autophagy in the Cellular Energetic Balance. Cell Metab. 2011 May 4;13(5):495–504.

168. Bravo R, Vicencio JM, Parra V, Troncoso R, Munoz JP, Bui M, et al. Increased ER–mitochondrial coupling promotes mitochondrial respiration and bioenergetics during early phases of ER stress. J Cell Sci. 2011 Jul 1;124(13):2143–52.

169. Guzmán-Hernández ML, Potter G, Egervári K, Kiss JZ, Balla T. Secretion of VEGF-165 has unique characteristics, including shedding from the plasma membrane. Mol Biol Cell. 2014 Apr;25(7):1061–72.

170. Sato K, Nakano A. Dissection of COPII subunit-cargo assembly and disassembly kinetics during Sar1p-GTP hydrolysis. Nat Struct Mol Biol. 2005 Feb;12(2):167–74.

171. Lengauer C, Kinzler KW, Vogelstein B. Genetic instabilities in human cancers. Nature. 1998 Dec;396(6712):643–9.

172. Tang Y-C, Williams BR, Siegel JJ, Amon A. Identification of Aneuploidy-Selective Antiproliferation Compounds. Cell. 2011 Feb 18;144(4):499–512.

173. Ma Y, Hendershot LM. The role of the unfolded protein response in tumour development: friend or foe? Nature Reviews Cancer. 2004 Dec;4(12):966–77.

174. Wang M, Kaufman RJ. The impact of the endoplasmic reticulum protein-folding environment on cancer development. Nature Reviews Cancer. 2014 Sep;14(9):581–97.

175. Imaizumi K, Miyoshi K, Katayama T, Yoneda T, Taniguchi M, Kudo T, et al. The unfolded protein response and Alzheimer's disease. Biochimica et Biophysica Acta (BBA) - Molecular Basis of Disease. 2001 May 31;1536(2):85–96.

176. Hetz C, Russelakis-Carneiro M, Maundrell K, Castilla J, Soto C. Caspase-12 and endoplasmic reticulum stress mediate neurotoxicity of pathological prion protein. The EMBO Journal. 2003 Oct 15;22(20):5435–45.

177. Moenner M, Pluquet O, Bouchecareilh M, Chevet E. Integrated Endoplasmic Reticulum Stress Responses in Cancer. Cancer Res. 2007 Nov 15;67(22):10631–4.

178. Hart LS, Cunningham JT, Datta T, Dey S, Tameire F, Lehman SL, et al. ER stress–mediated autophagy promotes Myc-dependent transformation and tumor growth. J Clin Invest. 2012 Dec 3;122(12):4621–34.

179. Malhotra JD, Kaufman RJ. Endoplasmic Reticulum Stress and Oxidative Stress: A Vicious Cycle or a Double-Edged Sword? Antioxidants & Redox Signaling. 2007 Nov 2;9(12):2277–94.

180. van der Vlies D, Makkinje M, Jansens A, Braakman I, Verkleij AJ, Wirtz KWA, et al. Oxidation of ER Resident Proteins Upon Oxidative Stress: Effects of Altering Cellular Redox/Antioxidant Status and Implications for Protein Maturation. Antioxidants & Redox Signaling. 2003 Aug 1;5(4):381–7.

181. Malhotra JD, Miao H, Zhang K, Wolfson A, Pennathur S, Pipe SW, et al. Antioxidants reduce endoplasmic reticulum stress and improve protein secretion. Proceedings of the National Academy of Sciences. 2008 Nov 25;105(47):18525–30.

182. Görlach A, Klappa P, Kietzmann DrT. The Endoplasmic Reticulum: Folding, Calcium Homeostasis, Signaling, and Redox Control. Antioxidants & Redox Signaling. 2006 Sep 1;8(9–10):1391–418.

183. Berridge MJ, Bootman MD, Roderick HL. Calcium signalling: dynamics, homeostasis and remodelling. Nature Reviews Molecular Cell Biology. 2003 Jul;4(7):517–29.

184. Leon-Aparicio D, Chavez-Reyes J, Guerrero-Hernandez A. Activation of endoplasmic reticulum calcium leak by 2-APB depends on the luminal calcium concentration. Cell Calcium. 2017 Jul;65:80–90.

185. Klec C, Madreiter-Sokolowski CT, Ziomek G, Stryeck S, Sachdev V, Duta-Mare M, et al. Presenilin-1 Established ER-Ca^{2+} Leak: a Follow Up on Its Importance for the Initial Insulin Secretion in Pancreatic Islets and β-Cells Upon Elevated Glucose | Cell Physiol Biochem. Cellular Physiology & Biochemistry. 2019 Sep 18;53(3):573–86.

186. Camello C, Lomax R, Petersen OH, Tepikin AV. Calcium leak from intracellular stores--the enigma of calcium signalling. Cell Calcium. 2002 Dec;32(5–6):355–61.

187. Hasanpourghadi M, Karthikeyan C, Pandurangan AK, Looi CY, Trivedi P, Kobayashi K, et al. Targeting of tubulin polymerization and induction of mitotic blockage by Methyl 2-(5-fluoro-2-hydroxyphenyl)-1H-benzo[d]imidazole-5-carboxylate (MBIC) in human cervical cancer HeLa cell. Journal of Experimental & Clinical Cancer Research. 2016 Mar 31;35(1):58.

188. Hampsch RA, Shee K, Bates D, Lewis LD, Désiré L, Leblond B, et al. Therapeutic sensitivity to Rac GTPase inhibition requires consequential suppression of mTORC1, AKT, and MEK signaling in breast cancer. Oncotarget. 2017 Feb 21;8(13):21806–17.

189. Tseng C-N, Hong Y-R, Chang H-W, Yu T-J, Hung T-W, Hou M-F, et al. Brefeldin A Reduces Anchorage-Independent Survival, Cancer Stem Cell Potential and Migration of MDA-MB-231 Human Breast Cancer Cells. Molecules. 2014 Nov;19(11):17464–77.

190. Tseng C-N, Huang C-F, Cho C-L, Chang H-W, Huang C-W, Chiu C-C, et al. Brefeldin A Effectively Inhibits Cancer Stem Cell-Like Properties and MMP-9 Activity in Human Colorectal Cancer Colo 205 Cells. Molecules. 2013 Sep;18(9):10242–53.

191. Sausville EA, Duncan KL, Senderowicz A, Plowman J, Randazzo PA, Kahn R, et al. Antiproliferative effect in vitro and antitumor activity in vivo of brefeldin A. Cancer J Sci Am. 1996 Feb;2(1):52–8.

192. Coe H, Michalak M. Calcium binding chaperones of the endoplasmic reticulum. Gen Physiol Biophys. 2009;28 Spec No Focus:F96–103.

193. Yi M, Weaver D, Hajnóczky G. Control of mitochondrial motility and distribution by the calcium signal. Journal of Cell Biology. 2004 Nov 22;167(4):661–72.